

Research Paper

Virtual Prototyping, Multibody Dynamics, and Control Design of an Adaptive Lift Table for Material Handling

Carmine Maria Pappalardo¹, Timoteo Magaldi², Lorenzo Masucci³, Rosario La Regina⁴, Alessandro Naddeo⁵

¹Department of Industrial Engineering, University of Salerno, Via Giovanni Paolo II 132, 84084 Fisciano, Italy, Email: cpappalardo@unisa.it

²Department of Industrial Engineering, University of Salerno, Via Giovanni Paolo II 132, 84084 Fisciano, Italy, Email: t.magaldi@studenti.unisa.it

³Department of Industrial Engineering, University of Salerno, Via Giovanni Paolo II 132, 84084 Fisciano, Italy, Email: l.masucci5@studenti.unisa.it

⁴Department of Industrial Engineering, University of Salerno, Via Giovanni Paolo II 132, 84084 Fisciano, Italy, Email: r.laregina2@studenti.unisa.it

⁵Department of Industrial Engineering, University of Salerno, Via Giovanni Paolo II 132, 84084 Fisciano, Italy, Email: anaddeo@unisa.it

Received November 16 2023; Revised April 05 2024; Accepted for publication April 06 2024.

Corresponding author: Carmine Maria Pappalardo (cpappalardo@unisa.it)

© 2024 Published by Shahid Chamran University of Ahvaz

Abstract. This paper is devoted to presenting the results of the computer-aided design, the multibody dynamic analysis, and the proportional-derivative control synthesis of an adaptive mechanism serving as a lifting table. More specifically, the first part of the manuscript deals with the methodological approach and the mathematical background employed in the entire research work, whereas the second part of the present paper is focused on the model development and the numerical experiments carried out in this investigation. The analytical derivations presented herein demonstrate that the desired adaptive behavior can be successfully obtained for the virtual prototype of the lift mechanism devised in this investigation. Furthermore, a detailed CAD model of the proposed design was constructed in this investigation using SOLIDWORKS. To this end, particular attention was paid to the actual assembly and disassembly of each mechanical component, in conjunction with the choice of the actuators and sensors that are necessary for the proper functioning of the lifting mechanism. Then, a three-dimensional multibody model was developed starting from the CAD model of the virtual prototype devised in this investigation. The resulting multibody model, following appropriate simplifications, was subsequently imported into the MATLAB virtual environment, thereby allowing for readily performing kinematic and dynamic simulations of the nonlinear behavior of the mechanical system under study by using the SIMSCAPE MULTIBODY computational software. By doing so, the development of an appropriate control strategy, as well as the analysis of its behavior under loading and unloading goods conditions, was carried out and tested in the case of four different scenarios considered as the case study. For this purpose, the applicative scenarios considered are: 1) an impulsive loading scenario; 2) a progressive loading scenario; 3) an impulsive unloading scenario; 4) and a progressive unloading scenario. The performance of the feedforward plus feedback control strategy devised in this study was discussed based on several computer simulations. Numerical simulations demonstrate that the desired adaptive behavior is successfully obtained for the virtual prototype of the lift table designed in this study.

Keywords: Computer-Aided Design, Ergonomics, Manual Material Handling, Adaptive Mechanism, Multibody Dynamic Analysis, Feedforward and Feedback Control Design.

1. Introduction

1.1 General Background and Main Significance of the Present Research Work

This paper deals with the virtual prototyping of an articulated mechanical system serving as an adaptive lifting platform for ergonomically enhancing the heavy material handling carried out by human operators. In the remaining parts of this section, the background of the research topic, the definition of the problem of interest for this research work, a discussion of the literature concerning the issues at hand, the contributions of the present research, and the organization of the entire manuscript are reported.

In modern industrial engineering applications, the synergistic use of Computer-Aided Design (CAD) programs and Computer-Aided Engineering (CAE) software represents a problem of paramount importance [1, 2]. In this vein, the Integration of Computer-Aided Design and Analysis (I-CAD-A) is playing a fundamental role in the general field of mechanical engineering [3]. To address this complex problem, the multibody approach to the kinematic and dynamic analysis of articulated mechanical systems turned out to be an effectively viable solution. In this paper, therefore, the multibody approach to the analysis of constrained mechanical systems is adopted [4–6]. The analysis of the mechanical system considered as the case study of this work was carried out in the MATLAB computational framework by using the software called SIMSCAPE MULTIBODY, which has a 3D simulation environment capable of modeling articulated mechanical systems. In the dynamic analysis of multibody mechanical systems, the complex task of automatically deriving the differential-algebraic equations of motion starts from the CAD design of the system of interest [7, 8]. In this



vein, geometric modeling is achieved by using computer-aided design programs, which are specifically devised to ease the creation of complex geometric forms that are mathematically based on the NURBS (Non-Uniform Rational Basis-Splines) representation [9, 10]. Thus, it is clear that, in mechanical engineering applications, the synergy between computer-aided design and analysis tools has a fundamental role [11, 12].

In this investigation, the controller architecture used to control the analyzed system is of the Proportional Derivative (PD) type. In the research and development of novel control systems in general, the use of benchmark problems is fundamental for analyzing the quality of any newly proposed control strategy. Besides, this allows for comparison with other existing solutions for control systems. Furthermore, because of their simple structure, ease of implementation, and active research in the parameters tuning, most of the control systems that are implemented to date in engineering systems employ Proportional-Integral-Derivative (PID) control schemes [13, 14]. Typically, the original technology for industrial PID controllers features a very simple interface for manually tuning the parameters of the controller. The PID tuner was indeed known to have a process control interface comprising three simple dials marked with P, I, and D, respectively. This reflected the fact that, for many of the simple processes found in the mechanical industries, a manual procedure for tuning the parameters of the PID controller was often quite adequate. One of the great strengths of the PID controllers is that, for simple plants, there are straightforward correlations between the system responses and the adjustment of the three terms in the controller.

In the process of the design and synthesis of a PID controller, the tuning procedure is composed of two fundamental steps. The first step deals with the selection of the structure of the PID controller, that is, which terms should be included in the controller. The second step is focused on the proper definition of the numerical values of the PID control parameters, which must be suitable for tuning the functioning of the control system. As expected, when using and tuning PID controllers, the key aspect is related to the second step mentioned before, namely the proper definition of its control coefficients. This problem can be empirically solved by a skilled human operator, who should be able to leverage his/her knowledge, experience, and intuition to identify the proper set of parameters of the PID controller. However, this is a nontrivial task and, therefore, some aiding tools are necessary to address this issue. A general and viable criterion useful for this purpose is represented by the well-known Ziegler-Nichols technique, which offers a method for iteratively determining the parameters of the PID controller [15]. The literature on the selection of the proper parameters of PID controllers is very wide, and the methods used are mainly semi-empirical [16].

When computers appeared, together with them came Programmable Logic Controllers (PLCs), Supervisory Control And Data Acquisition (SCADA) systems, and Distributed Control Systems (DCSs). Thus, automated tuning or autotuning methods for PID controllers were introduced [17, 18]. The autotuning techniques implemented in the systems mentioned before were devised to adjust the parameters of a PID controller in an automatic mode featuring probing influences, either once or upon the specific request of the operator. Usually, the probing influences interfere with the regular operating condition of the Control Object (CO). As a result, the autotuning process actually takes place during the remaining short time that has been set aside for it, that is, when the operation with the current PID controller becomes impossible or when the processor boots up. However, the optimal control parameters of many COs are nonstationary and tend to drift over time [19, 20]. Consequently, the main goal of the regulation system cannot be achieved by the implementation of a controller that was tuned only once during the full CO operation. In order to properly adjust the CO parameters in a way that the control objective is always accomplished over time, one must tune the coefficients of a PID controller continuously or, at least, periodically. To solve this important issue, the adaptive control strategy can be adopted. Depending on the specific approach used in this strategy, adaptive control algorithms require to implementation of constant or periodic modifications to the PID controller coefficients, which can be also performed in conjunction with the use of applied system identification methods necessary for refining the mathematical model of the dynamical system to be controlled.

In this work, the fundamental idea that stands behind the adaptive control approach mentioned before is employed. Thus, to guarantee proper guidance of the motion of the lifting mechanism in different scenarios of engineering interest, multiple sets of optimal or refined control parameters are devised.

1.2 Formulation of the Specific Problem of Interest for this Investigation

In industrial applications, the scissor lift mechanism is a mechanical system commonly used for several standard and nonstandard applications. This is the ideal tool for lifting goods and people with the smallest footprint occupied [21, 22]. This mechanical system consists of a horizontal platform that lifts vertically with ease, thereby allowing for reaching raised floors, or, as in the case considered in this paper, facilitating access to the desired objects without loading problems. Therefore, analysis of the scissor lift mechanism and the design of an adaptive lift table is the object of the present research work. A short discussion concerning the industrial use of this mechanical system, as well as the computer-aided design and analysis methods useful for modeling and simulating this type of system, is provided herein.

Multibody System Dynamics (MBD) is grounded in a large body of knowledge of research of engineering interest [4, 23, 24]. This scientific discipline deals with the development of analytical and computational methods for describing rigid and flexible mechanical systems, their application to the analysis and synthesis of articulated systems, and the implementation of experimental procedures necessary to validate their theoretical foundations [7, 8]. In modern engineering applications, multibody systems have been used to simulate a vast number of physical systems, such as robots, mechanisms, chains, cables, space structures, and biomechanical systems [25, 26].

Multibody systems are articulated mechanical systems composed of collections of rigid and/or deformable bodies, kinematic joints and/or driving constraints, force elements and/or force fields, and external actions and/or control inputs [27, 28]. From both the kinematic and dynamic points of view, multibody mechanical systems exhibit complex behavior [14, 29]. This is due to the presence of high nonlinearities in the kinematic and dynamic equations describing the motion of this family of mechanical systems. The nonlinear nature of the multibody equations of motion is induced by the capacity of capturing large reference displacements and large finite rotations [6, 30, 31]. Consequently, general analysis approaches are required to be able of describing the dynamic behavior of a general multibody mechanical system such as the articulated lifting mechanism analyzed in this paper [32, 33].

As can be intuitively imagined, the problem of the dynamic analysis of rigid-flexible multibody systems is strongly related to the design of proper control strategies for this category of mechanical systems [34–36]. To solve the optimal control, estimation, and identification problems associated with machines and mechanisms of engineering interest, it is crucial to correctly formulate the dynamic equations that characterize the nonlinear behavior of multibody systems [37–39]. In this respect, it is well-known that the conventional algorithms based on the linearization of the equations of motion are inappropriate for controlling the nonlinear behavior of multibody systems [40, 41]. As a result, more sophisticated design methods, estimation procedures, and control strategies must be employed to address this issue. In recent mechanical engineering applications, various studies focused on the active and passive control problems of machines and structures have appeared. For instance, considering the mathematical techniques developed in the field of system identification and optimal control, several studies can be found in the literature [42–45].

In the design of proper control actions for guiding the motion of nonlinear mechanical systems, specific formulation procedures and computational strategies must be employed [46, 47]. The solution to the guidance and control problem, which can be separated into the two categories of regulation and tracking control, is particularly challenging in the case of rigid and flexible multibody sys-



tems. Before trying to develop a new control policy for an articulated mechanical system, one first needs to construct a reliable dynamic model of the system of interest, which must be intrinsically capable of mathematically describing its nonlinear physical features. By using the analytical approaches and computational methodologies available in the literature, the control design process associated with the regulation and tracking problems of the nonlinear mechanical system of interest can be addressed and solved [48, 49].

1.3 Literature Review and Comparative Study

Lifting tables are commonly used in industry for facilitating heavy material handling. Geometrically, these mechanisms are constructed by employing a scissor topology, in which the purpose of the cross bars is to transform a horizontal motion of the actuator into a vertical motion of the table. A concise literature survey about the issues associated with the design and analysis of this kind of mechanical system is reported below together with a comparative discussion on the principal solutions found in the literature.

In the literature, the discussion about several engineering problems related to the proper design, functioning, and control of this type of articulated mechanical system can be found. In [50], Momin et al. analyzed the design and manufacturing processes of hydraulic scissor lift systems, in which the desired displacement is indeed achieved by employing hydraulic or pneumatic actuators. As shown in the work of Ismael et al. [51], which is concerned with electrical lifting tables, ball-screw motor transmissions are also used to guide the motion of scissor lift tables. Mainly focusing on CAD modeling, Hongyu and Ziyi designed a new scissor table for ensuring the stability and safety of human workers during the operation of this mechanical system, which could turn out to be potentially dangerous [52]. In [53], Akgun et al. proposed a finite element analysis of the spatial scissor-hinge structural mechanism designed in their work to improve the structural reliability of this system, which can hardly be obtained by adopting only simple geometric considerations. Following the same line, Mohan and Zech analyzed the main characteristics of worker accidents due to the instability of scissor lift tables. Liu and Sun performed several dynamical simulations using SIMULINK to reach the optimal and stable design of a scissor-lifting mechanism [54]. In [55], Olenin addressed the design of hydraulic scissor lifting tables focusing on the modulation of the actuation force to ensure system stability and safety. Li et al. analyzed the influence of the clearance present between the parts, the friction forces, and the contact reactions in the context of the dynamic analysis of lifting tables [56]. While several interesting research studies concerning the robust design and functional optimization of lift tables can be found in the literature, the attention paid to the human-machine interaction from an ergonomic viewpoint is quite restricted to a few cases.

Industrial jobs that require Manual Materials Handling (MMH), especially the lifting of loads carried out by human operators, have an increased incidence of back injury cases [57]. Overexertion injuries are usually linked to occupational risk factors such as moving large, heavy, and bulky goods from the ground or lifting products repeatedly and frequently [58, 59]. For years, the risk of Low Back Disorders (LBDs) has been associated with a combination of five measures representing both workplace and trunk motion factors [60], which are occupationally related. In particular, the load moment and the lifting frequency are the principal workplace factors. On the other hand, the lateral trunk velocity, the twisting trunk velocity, and the sagittal flexion angle are the main trunk motion factors, where a variation of the sagittal flexion angle takes place in the case of trunk flexion [61]. Consequently, as the magnitude of each of these variables increases, the accident and injury risks increase as well. In addition, another prominent problem comes from the random distribution of loads on uneven surfaces on working sites [62], leading to account for a lot of fatal accidents due to lifting tip-over. To solve this issue, there are control systems that can be added to the current control mechanism using an Inertial Measurement Unit (IMU) to measure the tilt angles of the platform, and relays for signal conditioning [36, 63]. However, the problem of proper material handling aided by specifically designed mechanical systems is still an object of research in the ergonomic literature [64]. This issue represents the main research question to be addressed in this work.

In all fields where the lifting of objects is required, the human operator could potentially suffer from serious problems [65]. Therefore, this is also true for the specific case study analyzed in the current paper, which deals with the loading and unloading of pallets using a scissor mechanism forming a lift table [66]. The solution devised in this work to avoid back pain is to adopt a self-leveling mechanism, which allows for keeping the pallet at a constant and ergonomically correct height [58]. This solution must prove to be suitable for the material handling carried out by the operator [60]. When compared to the traditional pallet manipulation on the floor and nonadjustable pallet tables, which do not guarantee an ergonomic posture for the operator, previous studies provided evidence that the use of self-leveling scissor lift tables for handling pallets is highly effective at reducing spine loading during depalletizing/palletizing tasks [67]. Despite all the high risks for the human operator adopting an incorrect posture in MMH operations, and even though this practice is very widespread in the industry, the scientific literature concerning this ergonomic issue is very limited. This is also the case with the specific problem of palletizing/depalletizing goods using a scissor lift mechanism, as well as the biomechanical research that aims to improve the effectiveness of this device [61]. This paper, therefore, tries to fill this gap in the literature.

The behavior of the articulated mechanism serving a lift table, which is analyzed in this investigation, is kinematically and dynamically nonlinear. As shown in several research works in different areas of structural and mechanical engineering, the study of the mechanical behavior of dynamical systems having a nonlinear nature represents an important topic [68, 69]. Many different scissor lifters are available in the market. Thus, regarding the design of the CAD model of the virtual prototype developed in this study, several aspects were analyzed, paying attention to the shapes, dimensions, configuration of the components, transmission mechanism, and actuation systems [50, 54, 70]. Most lifters use a hydraulic actuator and, to the best of the authors' knowledge, in no case was employed a rack and pinion transmission mechanism. Consequently, such a system was chosen in this work. This design solution was also adopted in this study to facilitate the subsequent development of the control system, which can directly operate on the electric motors connected to the arms of the lift table by the mechanical transmission. Additionally, in the analysis of the literature, as well as by observing the final products actually available in the market, a distinction was made between the mechanical components that are quite significantly different from one model to another and those that are more or less identical.

As far as the long-term damages caused to the workers are concerned, the research studies made in the industrial field of material handling employing lift tables are quite limited [71]. To reduce the spine loads, Ramsey et al. proposed a self-leveling pallet machine designed to position the loads vertically and horizontally, as well as an adjustable cart specifically designed to raise loads vertically at the destination [67]. The principle to reduce the stresses on the backbone of the human operator is to hold the object as close to the body as possible [72]. Since Low Back Pain (LBP) is generally associated with lifting, the solution adopted by self-leveling pallet carousels together with skid positioners is to automatically raise the pallet by using pneumatic air bladders or coil springs. The basic concept of this lifter, which is only adjustable through the calibration of the base springs, is similar to that adopted for the realization of the scissor lift control system designed in this paper. However, the main difference between the proposed solution and what is already available in the literature is that, while in the pallet carousel springs and pneumatic air bladders are used to adjust the height, and, consequently, the system is not fully adjustable without modifying the lifting mechanism, the adaptive system designed in this work is much more flexible and can be easily adapted to different operating configurations.



1.4 Scope and Contributions of this Study

In this investigation, the virtual prototype of a new adaptive mechanism serving as a lift table is developed by leveraging the integration of modern computer-aided design, analysis, and control tools [73, 74]. The CAD model of the new scissor mechanism developed in this investigation is represented in Figure 1.



Fig. 1. CAD exploded view of the adaptive scissor lift mechanism representing the case study of this investigation.

Since the lifting of goods is required in several industrial applications, the principal design goal of the mechanical system devised in this study is to improve the working conditions of human operators in such a way as to ensure proper ergonomics. In effect, the ability to adaptively adjust the height of the lifting mechanism analyzed in this investigation is aimed at ensuring a constant platform height for the operator. In particular, the main idea is to keep a safe and ergonomically correct posture during the manual materials handling of the goods. To achieve this fundamental goal, the first step is to carry out the development of a high-fidelity computer model of the system of interest. This objective can be readily achieved by using the multibody approach to the analysis of articulated mechanical systems, as shown in this work. Additionally, in the synthesis of the control system of the lifting table, a proportional-derivative control architecture is used in this paper. More specifically, adaptivity is achieved by modulating the height of the lift table according to the actual payload collocated on the platform. Thus, when the desired amounts of goods are loaded onto the platform, the lift table lowers. Vice versa, when the goods are unloaded, the lift table rises.

The main idea is to devise an adaptive loading platform. More specifically, this paper proposes a solution to ensure ergonomics in lifting operations to avoid low back disorders for the operator during manual material handling. The goal of the design process is to create an ergonomic lifting system that, according to the actual operating conditions, must be able to position the packages at the right height. Standard industrial scissor tables are designed to comply with a height that comes out of a statistical discourse of the 5th and 95th percentiles from the height of 0.8 (m) to 1.1 (m), namely for an adult woman and man [75]. Differently from the conventional approach, the principal innovation of the proposed solution lies in the fact that this new system, instead of positioning itself at a predetermined height, adapts itself to current conditions by reading the total weight of the platform. As discussed in detail above, from the literature survey carried out in this work, the proposed smart system turns out to be one of the first self-adaptive lifters, which automatically adapts its operating configuration to the needs of the operator and the current loading conditions. Furthermore, the main features of the proposed adaptive mechanism can also be tailored to the characteristics of the individual operator since it is sufficient to change only some reference parameters to adapt the height of the lifter to the one suitable for the current operator.

For performing dynamic simulations of the case study considered in the paper, four scenarios are considered, namely 1) an impulsive loading, 2) a progressive loading, 3) an impulsive unloading, and 4) a progressive unloading. As discussed in the manuscript, for the four scenarios taken into account, the four height steps and loading conditions mentioned before were thoroughly analyzed, which are reported in the paper together with the controller parameters and the control torques (or the equivalent control forces) corresponding to the different height steps. In particular, the worst scenario, which is the heaviest in terms of loads, is discussed in more detail in the paper and is used as a reference for the others. This choice is induced by the fact that the nominal motor power shows its peak in the heaviest case, as this represents an important numerical value that is needed for dimensioning the mechanical system in general. For each loading step, the correct positioning of the platform at the nominal values of the defined height is guaranteed by the feedforward control torque. The determination of the magnitude of the feedforward control torque was, in turn, performed by using an inverse dynamics approach. Additionally, between each step, the law of motion of the platform is, instead, regulated by the PD controller serving as a feedback system in such a way as to guarantee a sufficiently smooth movement.



This paper proposes the description of the general methodology adopted in this investigation, that is, the procedure employed for the CAD modeling, with a focus on the model import interface from SOLIDWORKS to SIMSCAPE MULTIBODY, the systematic multibody approach used for modeling articulated mechanical systems, as well as their implementation in the MATLAB computational environment, and the strategy for the design of feedforward-feedback controllers, with an emphasis on the related methods that justify the choices made in the paper regarding the control parameters [74, 76]. By using a CAD model developed employing SOLIDWORKS, which was constructed respecting the design constraints in terms of height, the paper aims to analyze, first, from a design viewpoint, the construction of the proposed scissor lift table, paying particular attention to joint elements, the assembly and disassembly processes, and the effective manufacturing of the components [77]. Then, the subsequent analysis is focused on exporting a properly simplified version of the CAD model of the proposed mechanism in the MATLAB environment. To this end, a multibody model of the mechanical system at hand is developed by using SIMSCAPE MULTIBODY. Therefore, the paper presents first the development of a detailed full-size three-dimensional CAD model for the system geometry using SOLIDWORKS [78, 79].

As a design requirement, the virtual prototype of the adaptive mechanism must allow for an elevation change of one meter for the working platform. For the mechanical system under study, on the other hand, the multibody model and the control actions were developed by exploiting the MATLAB simulation environment and by using the SIMSCAPE MULTIBODY suite. For this purpose, to improve the quality of the work of the operator in the phase of loading and unloading goods, the dynamic behavior of the virtual prototype was simulated by importing its CAD model from SOLIDWORKS to SIMSCAPE MULTIBODY. Subsequently, to increase the ergonomics of this machine, a proper set of control laws was developed for the scissor lift system in the MATLAB environment. To this end, the synthesis of the control system of this adaptive mechanism was carried out considering four different platform height steps, at four different loading conditions, with trends in the rate of changes of the control actions that are inversely proportional to the final height to be attained. In other words, to maintain a constant grip height for the operator, the platform is raised as the load decreases and lowered as the load increases [80]. On the other hand, the determination of the feedback control torques was performed by using a direct dynamics approach, thereby calibrating and/or refining the values of the controller parameters by performing several numerical experiments.

To summarize the approach followed in this investigation, as well as the scope and the contributions of the work done, a synthetic flowchart is reported in Figure 2.

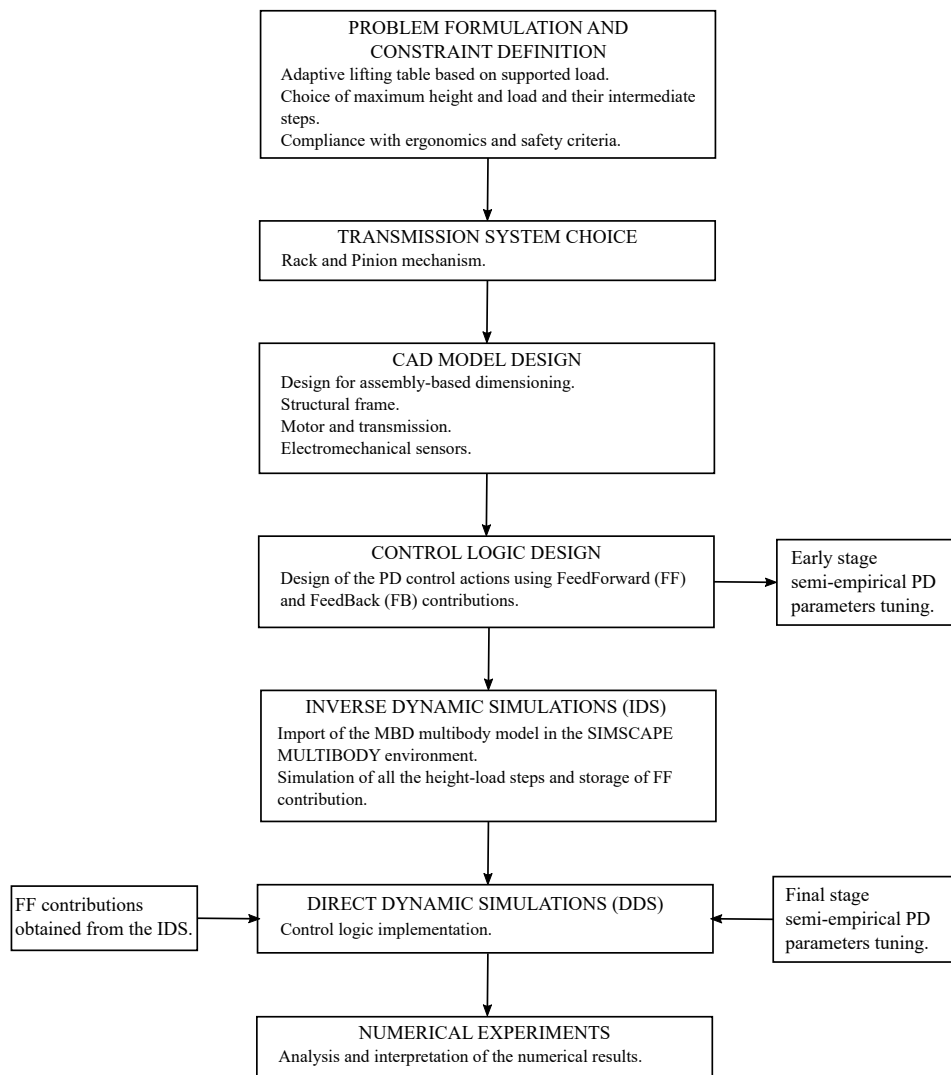


Fig. 2. Conceptual flowchart of the approach proposed and followed in the paper to perform the virtual prototyping, the multibody dynamic analysis, and the controller design for the adaptive lift table serving for industrial material handling considered as the case study of this investigation.

1.5 Organization of the Manuscript

Apart from the current introduction section, this paper is organized according to the following structure. In Section 2., the systematic procedure based on the multibody approach for the mathematical modeling of articulated mechanical systems is recalled.



Section 3. describes the key points involved in the design of nonlinear controllers suitable for guiding the spatial motion of multibody mechanical systems. In Section 4., the principal aspects of the CAD model of the proposed adaptive lifting mechanism constructed by using SOLIDWORKS are described, thereby devoting a special focus to the assembly and disassembly characteristics of the system geometric model, as well as on the functional analysis of its mechanical components. In Section 5., the main features of the dynamical model of the adaptive lift table developed using SIMSCAPE MULTIBODY are illustrated, paying particular attention to the simplifications and modifications made in the transition from the CAD model to the multibody model implemented in MATLAB. Section 6. presents the numerical analysis together with the dynamical simulations of the virtual prototype constructed in this work, the formulation of the laws of motion of the platform height for the respective case studies, and the definition of the parameters used for the control system. Finally, Section 7. contains the summary of the paper, the conclusions reached in this investigation, and some ideas for future research works.

2. Mathematical Modeling of Articulated Mechanical Systems

2.1 Kinematics of Multibody Systems

The mechanical components forming a given multibody system may experience significant relative translational and rotational displacements. To be able to define an arbitrary configuration of a generic body in a multibody system, one must be able to identify the collocation of the material points pertaining to that body in relation to a chosen inertial frame of reference [81]. To achieve this goal, it is convenient to assign to each body of the multibody system a body-fixed reference frame that facilitates the definition of the relative position vectors of the material points [82]. The position vectors of these points can then be found in other coordinate systems, such as the inertial coordinate system, by simply defining the relative position and orientation of the body coordinate system with respect to the other coordinate systems taken into consideration [83]. For a generic rigid body deployed in a three-dimensional space, the definition of the position and orientation of one coordinate system with respect to another coordinate system can be expressed using six variables, three of which define the relative translational motion between the two coordinate systems and the remaining three specify the orientation of one coordinate system with respect to the other. In general, the three-dimensional displacement of an arbitrary body labeled with the integer i that belongs to the multibody system can be described by a rotation plus a translation [84]. By denoting with $d = 3$ the space dimension, the position vector $\bar{\mathbf{u}}^i(P^i)$ having dimensions $d \times 1$ of an arbitrary point P^i on the rigid body i of the multibody system has constant components in the body-fixed coordinate system. If this rigid body undergoes pure rotation, the position vector of point P^i in the global frame of reference is defined by the vector $\mathbf{u}^i(P^i)$ and can be determined according to the following equation:

$$\mathbf{u}^i(P^i) = \mathbf{A}^i \bar{\mathbf{u}}^i(P^i) \quad (1)$$

being:

$$\mathbf{A}^i = \begin{bmatrix} \boldsymbol{\alpha}^i & \boldsymbol{\beta}^i & \boldsymbol{\gamma}^i \end{bmatrix} \quad (2)$$

where \mathbf{A}^i is the rotation matrix of dimensions $d \times d$ that defines the orientation of the body-fixed reference frame with respect to the absolute coordinate system, whereas $\boldsymbol{\alpha}^i$, $\boldsymbol{\beta}^i$, and $\boldsymbol{\gamma}^i$ respectively represent the global unit vectors of dimensions $d \times 1$ associated with the directions of the \bar{x}^i , \bar{y}^i , and \bar{z}^i axes of the local frame of reference. If the body translates in addition to the rotation, its general motion can be described by using the translation of a reference point and the rotation of the body-fixed frame along the axis of rotation. More specifically, the translation of the body can then be described by the position vector of the origin of the body-fixed reference frame, and this position vector of dimensions $d \times 1$ is denoted as \mathbf{R}^i . Thus, in a three-dimensional space, one can write:

$$\mathbf{R}^i = \begin{bmatrix} x^i & y^i & z^i \end{bmatrix}^T \quad (3)$$

where x^i , y^i , and z^i denote the global Cartesian coordinates of the body-fixed reference point \bar{O}^i taken into consideration for the rigid body i . In the multibody literature, this approach is commonly referred to as the Reference Point Coordinate Formulation (RPCF) [83].

When planar (spatial) rigid bodies are considered, the configuration of a generic body can be completely described by using three (six) independent geometric coordinates serving as generalized coordinates. By denoting with n_b the number of generalized coordinates of a given rigid body modeled in a space of dimension equal to d , the general formula for determining the number of independent coordinates is $n_b = 3(d - 1)$. Considering a three-dimensional space, three generalized coordinates are needed as translational coordinates to identify the position of the reference point serving as the origin of the body-fixed frame of reference with respect to the global reference system, while three generalized coordinates are required as rotational coordinates to define the orientation of the body-fixed frame of reference with respect to the global reference system. By doing so, considering a generic rigid body identified with the discrete number i , the body translational coordinates are embedded in the reference point position vector \mathbf{R}^i of dimensions $d \times 1$, whereas the body rotational coordinates are embedded in the vector $\boldsymbol{\theta}^i$ of dimensions $d \times 1$, which is necessary for constructing the rotation matrix of the rigid body i . The rotation matrix \mathbf{A}^i is, therefore, a function of the set of rotational coordinates contained in the vector $\boldsymbol{\theta}^i$. In the spatial analysis, the rotational coordinate vector $\boldsymbol{\theta}^i$ can have three or four elements depending on whether Euler angles, Rodriguez parameters, or Euler parameters are employed. However, in this work, it is assumed that the set of rotational coordinates is formed by the typical sequence of Euler angles employed in applied mechanics, that is, a first angular displacement denoted with ϕ^i about the current \bar{x}^i axis (corresponding to the roll of the rigid body i), a second angular displacement denoted with ϑ^i about the current \bar{y}^i axis (corresponding to the pitch of the rigid body i), and a third angular displacement denoted with ψ^i about the current \bar{z}^i axis (corresponding to the yaw of the rigid body i). The rotational coordinate vector used in this study is, therefore, given by:

$$\boldsymbol{\theta}^i = \begin{bmatrix} \phi^i & \vartheta^i & \psi^i \end{bmatrix}^T \quad (4)$$

By assuming this hypothesis, one can readily calculate the rotation matrix \mathbf{A}^i of the rigid body i as follows:

$$\mathbf{A}^i = \mathbf{A}_x^i \mathbf{A}_y^i \mathbf{A}_z^i \quad (5)$$

being:

$$\mathbf{A}_x^i = \begin{bmatrix} 1 & 0 & 0 \\ 0 & C_\phi^i & -S_\phi^i \\ 0 & S_\phi^i & C_\phi^i \end{bmatrix}, \quad \mathbf{A}_y^i = \begin{bmatrix} C_\vartheta^i & 0 & S_\vartheta^i \\ 0 & 1 & 0 \\ -S_\vartheta^i & 0 & C_\vartheta^i \end{bmatrix}, \quad \mathbf{A}_z^i = \begin{bmatrix} C_\psi^i & -S_\psi^i & 0 \\ S_\psi^i & C_\psi^i & 0 \\ 0 & 0 & 1 \end{bmatrix} \quad (6)$$



where α^i is a generic angle associated with the rigid body i , while the abbreviations $C_\alpha^i = \cos(\alpha^i)$ and $S_\alpha^i = \sin(\alpha^i)$ were used because of space limitations. By using the set of Euler angles introduced before, one can readily prove the following two identities:

$$\dot{\tilde{\omega}}^i = \dot{A}^i (A^i)^T, \quad \tilde{\omega}^i = (A^i)^T \dot{A}^i \quad (7)$$

where the dot symbol stands for the first time derivative, whereas $\tilde{\omega}^i$ and $\dot{\tilde{\omega}}^i$ respectively represent the skew-symmetric matrices of the cross product associated with the global and local angular velocity vectors ω^i and $\bar{\omega}^i$. These matrices are respectively defined as follows:

$$\tilde{\omega}^i = \begin{bmatrix} 0 & -\omega_z^i & \omega_y^i \\ \omega_z^i & 0 & -\omega_x^i \\ -\omega_y^i & \omega_x^i & 0 \end{bmatrix}, \quad \tilde{\bar{\omega}}^i = \begin{bmatrix} 0 & -\bar{\omega}_z^i & \bar{\omega}_y^i \\ \bar{\omega}_z^i & 0 & -\bar{\omega}_x^i \\ -\bar{\omega}_y^i & \bar{\omega}_x^i & 0 \end{bmatrix} \quad (8)$$

where:

$$\omega^i = \begin{bmatrix} \omega_x^i \\ \omega_y^i \\ \omega_z^i \end{bmatrix}, \quad \bar{\omega}^i = \begin{bmatrix} \bar{\omega}_x^i \\ \bar{\omega}_y^i \\ \bar{\omega}_z^i \end{bmatrix} \quad (9)$$

The global and local angular velocity vectors ω^i and $\bar{\omega}^i$ are nonlinear functions of the rotational coordinate vector θ^i and linear functions of its time derivative $\dot{\theta}^i$. By exploiting this important property of the angular velocity vectors of a generic rigid body i , one can write:

$$\omega^i = G^i \dot{\theta}^i, \quad \bar{\omega}^i = \bar{G}^i \dot{\theta}^i \quad (10)$$

being:

$$G^i = \begin{bmatrix} 1 & 0 & S_\psi^i \\ 0 & C_\phi^i & -S_\phi^i C_\psi^i \\ 0 & S_\phi^i & C_\phi^i C_\psi^i \end{bmatrix}, \quad \bar{G}^i = \begin{bmatrix} C_\psi^i C_\phi^i & S_\psi^i & 0 \\ -C_\psi^i S_\phi^i & C_\phi^i & 0 \\ S_\psi^i & 0 & 1 \end{bmatrix} \quad (11)$$

where G^i and \bar{G}^i represent two linear transformation matrices of dimensions $d \times d$ that allow for readily computing the global and local angular velocity vectors ω^i and $\bar{\omega}^i$ of a rigid body i starting from the body rotational coordinate vector θ^i and its time derivative $\dot{\theta}^i$. Consequently, through the analytical definition of the translational and rotational coordinates R^i and θ^i of the body reference, the configuration of the rigid body is completely identified. Additionally, the global position vector of an arbitrary point P^i on the rigid body i can be expressed in terms of the translation and rotation of the body by the vector $r^i(P^i)$ of dimension $d \times 1$ given by:

$$r^i(P^i) = R^i + u^i(P^i) = R^i + A^i \bar{u}^i(P^i) \quad (12)$$

where the three-dimensional vector $r^i(P^i)$ identifies the position field of the rigid body i . This basic equation is referred to as the fundamental formula of rigid kinematics since it can be used as the fundamental building block of the position, velocity, acceleration, and jerk analysis of multibody systems consisting of interconnected rigid bodies.

The global velocity vector of a material point P^i of the rigid body i is a vector of dimensions $d \times 1$ denoted with $v^i(P^i)$ that can be determined by a direct time differentiation as $v^i(P^i) = \dot{r}^i(P^i)$. By doing so, one obtains the following mathematical expression of the velocity field of the rigid body i :

$$v^i(P^i) = \dot{R}^i + \omega^i \times u^i(P^i) = \dot{R}^i + A^i (\bar{\omega}^i \times \bar{u}^i(P^i)) \quad (13)$$

where ω^i and $\bar{\omega}^i$ are two vectors of dimensions $d \times 1$ that respectively represent the global and local angular velocity vectors of the rigid body i related to each other by the equation $\omega^i = A^i \bar{\omega}^i$.

The global acceleration vector of a material point P^i of the rigid body i is a vector of dimensions $d \times 1$ denoted with $a^i(P^i)$ that can be determined by a direct time differentiation as $a^i(P^i) = \dot{v}^i(P^i) = \ddot{r}^i(P^i)$. By doing so, one obtains:

$$\begin{aligned} a^i(P^i) &= \ddot{R}^i + \dot{\omega}^i \times u^i(P^i) + \omega^i \times (\omega^i \times u^i(P^i)) \\ &= \ddot{R}^i + A^i (\dot{\bar{\omega}}^i \times \bar{u}^i(P^i)) + A^i (\bar{\omega}^i \times (\bar{\omega}^i \times \bar{u}^i(P^i))) \end{aligned} \quad (14)$$

where the three-dimensional vector $a^i(P^i)$ identifies the acceleration field of the rigid body i .

Finally, the global jerk vector of a material point P^i of the rigid body i is a vector of dimensions $d \times 1$ denoted with $j^i(P^i)$ that can be determined by a direct time differentiation as $j^i(P^i) = \dot{a}^i(P^i) = \ddot{v}^i(P^i) = \ddot{r}^i(P^i)$. By doing so, one obtains:

$$\begin{aligned} j^i(P^i) &= \ddot{\ddot{R}}^i + \ddot{\omega}^i \times u^i(P^i) + 2\dot{\omega}^i \times (\omega^i \times u^i(P^i)) \\ &\quad + \omega^i \times (\dot{\omega}^i \times u^i(P^i)) + \omega^i \times (\omega^i \times (\omega^i \times u^i(P^i))) \\ &= \ddot{\ddot{R}}^i + A^i (\ddot{\bar{\omega}}^i \times \bar{u}^i(P^i)) + A^i (\dot{\bar{\omega}}^i \times (\bar{\omega}^i \times \bar{u}^i(P^i))) \\ &\quad + 2A^i (\bar{\omega}^i \times (\dot{\bar{\omega}}^i \times \bar{u}^i(P^i))) + A^i (\bar{\omega}^i \times (\bar{\omega}^i \times (\bar{\omega}^i \times \bar{u}^i(P^i)))) \end{aligned} \quad (15)$$

where the three-dimensional vector $j^i(P^i)$ identifies the jerk field of the rigid body i .

As discussed above, the global position, velocity, acceleration, and jerk fields of any material points on the rigid body of interest can be described in terms of the system set of generalized coordinates once they have been determined. For convenience, the generalized coordinate vector q_b^i of dimensions $n_b \times 1$ is used to denote the generalized coordinates of the body reference, that is:

$$q_b^i = \begin{bmatrix} R^i \\ \theta^i \end{bmatrix} \quad (16)$$

where R^i and θ^i respectively represent the translational and rotational coordinates of the rigid body i introduced before. On the other hand, considering the entire multibody system composed of a total number of N_b rigid bodies, one can identify the total



number of the system generalized coordinates as $n_q = N_b n_b$. Thus, the system generalized coordinate vector is denoted with the vector \mathbf{q} of dimensions $n_q \times 1$ and can be immediately assembled as follows:

$$\mathbf{q} = \begin{bmatrix} (\mathbf{q}_b^1)^T & (\mathbf{q}_b^2)^T & \dots & (\mathbf{q}_b^{N_b})^T \end{bmatrix}^T \quad (17)$$

where the generalized coordinate vector \mathbf{q}_b^i associated with the generic rigid body i can be readily recovered from the total generalized coordinate vector of the multibody system \mathbf{q} by using a proper Boolean matrix \mathbf{B}_b^i of dimensions $n_b \times n_q$ through the simple equation $\mathbf{q}_b^i = \mathbf{B}_b^i \mathbf{q}$.

2.2 Dynamics of Multibody Systems

The correct formulation of the kinematic equations describing the geometric features of a given rigid body represents a fundamental preliminary step for the subsequent derivation of the equations of motion of the multibody system considered as a whole [85]. To achieve this goal, the analyst can conveniently start from the set of Newton-Euler equations that represent one of the basic principles of classical mechanics [86]. In this vein, one can readily write the cardinal equations of dynamics for a given rigid body i as the following:

$$\begin{cases} m^i \ddot{\mathbf{R}}^i = \mathbf{F}_e^i + \mathbf{F}_c^i \\ \bar{\mathbf{I}}_{G^i} \dot{\bar{\boldsymbol{\omega}}}^i + \bar{\boldsymbol{\omega}}^i \times (\bar{\mathbf{I}}_{G^i} \bar{\boldsymbol{\omega}}^i) = \bar{\mathbf{T}}_{G^i,e}^i + \bar{\mathbf{T}}_{G^i,c}^i \end{cases} \quad (18)$$

where the point G^i identifies the center of mass of the rigid body i , m^i is the mass of the rigid body i , the matrix $\bar{\mathbf{I}}_{G^i}$ of dimensions $d \times d$ denotes the local inertia matrix of the rigid body i referred to the center of mass G^i , \mathbf{F}_e^i and \mathbf{F}_c^i are two global vectors of dimensions $d \times 1$ respectively representing the external and constraint force vectors applied on the rigid body i , while $\bar{\mathbf{T}}_{G^i,e}^i$ and $\bar{\mathbf{T}}_{G^i,c}^i$ are two local vectors of dimensions $d \times 1$ respectively representing the external and constraint torque vectors referred to the center of mass G^i of the rigid body i . The Newton-Euler equations introduced above are valid for all the rigid bodies that form the multibody system and are based on the assumption that the body-fixed frame of reference is chosen such that its origin \bar{O}^i is coincident with the center of mass G^i of the rigid body i , that is, the reference point of each rigid body i is indeed its center of mass.

Apart from the basic geometric assumptions recalled previously, the Newton-Euler equations are quite general in the sense that they can be used for describing both unconstrained and constrained multibody mechanical systems. More precisely, in the dynamic analysis of multibody mechanical systems, two general approaches can be utilized, namely a Minimal Coordinate Formulation (MCF) and a Redundant Coordinate Formulation (RCF). By denoting with n_f the number of degrees of freedom of the multibody system of interest, the MCF assumes that $n_q = n_f$, that is, the system configuration is described by a number of generalized coordinates that is equal to the number of the system degrees of freedom. In the RCF, on the other hand, it is assumed that $n_q > n_f$, that is, the system configuration is described by a number of generalized coordinates that is greater than the number of the system degrees of freedom. Consequently, the generalized forces associated with the presence of algebraic constraints disappear from the equations of motion obtained using the MCF, while they are present in the mathematical formulation based on the RCF. This means that the net constraint forces and torques \mathbf{F}_c^i and $\bar{\mathbf{T}}_{G^i,c}^i$ vanish from the Newton-Euler equations when the MCF is used, whereas these mechanical actions are nonzero vector quantities in the case of the representation based on the RCF described before. To keep as general as possible the mathematical derivation of the multibody equations of motion presented herein, the latter case is taken into consideration.

Another important aspect to be analyzed concerns the mathematical form of the multibody equations of motion, which are based on the cardinal equations of rigid body dynamics deduced from the Newton-Euler principle. This additional step is necessary for transforming the equations of motion of the multibody system of interest into a form that is more convenient from an analytical and computational point of view. This is because the original form of the Newton-Euler equations cannot be readily implemented in a computer program devised for solving Ordinary Differential Equations (ODEs) or Differential-Algebraic Equations (DAEs). Incidentally, the main cause of this problem is that the angular velocity vector is not the time derivative of any vector or vector function. To solve this issue, a proper coordinate transformation must be used. The desired coordinate transformation must be able to relate the conventional definition of the generalized coordinate vector of a rigid body i , denoted with the vector \mathbf{q}_b^i having dimensions $n_b \times 1$, with the pseudo-coordinate vector of the same body, denoted with the vector \mathbf{p}_b^i having dimensions $2d \times 1$, which naturally appears in the Newton-Euler equations. The latter vector is given by:

$$\mathbf{p}_b^i = \begin{bmatrix} \dot{\mathbf{R}}^i \\ \bar{\boldsymbol{\omega}}^i \end{bmatrix} \quad (19)$$

By employing the definition of the pseudo-coordinate vector given above, the Newton-Euler equations can be rewritten in the following equivalent matrix form:

$$\begin{bmatrix} m^i \mathbf{I} & \mathbf{O} \\ \mathbf{O} & \bar{\mathbf{I}}_{G^i} \end{bmatrix} \begin{bmatrix} \ddot{\mathbf{R}}^i \\ \dot{\bar{\boldsymbol{\omega}}}^i \end{bmatrix} = \begin{bmatrix} \mathbf{0} \\ (\bar{\boldsymbol{\omega}}^i)^T \bar{\mathbf{I}}_{G^i} \bar{\boldsymbol{\omega}}^i \end{bmatrix} + \begin{bmatrix} \mathbf{F}_e^i \\ \bar{\mathbf{T}}_{G^i,e}^i \end{bmatrix} + \begin{bmatrix} \mathbf{F}_c^i \\ \bar{\mathbf{T}}_{G^i,c}^i \end{bmatrix} \quad (20)$$

or:

$$\mathbf{I}_b^i \dot{\mathbf{p}}_b^i = \mathbf{P}_v^i + \mathbf{P}_e^i + \mathbf{P}_c^i \quad (21)$$

where:

$$\mathbf{I}_b^i = \begin{bmatrix} m^i \mathbf{I} & \mathbf{O} \\ \mathbf{O} & \bar{\mathbf{I}}_{G^i} \end{bmatrix}, \quad \mathbf{P}_v^i = \begin{bmatrix} \mathbf{0} \\ (\bar{\boldsymbol{\omega}}^i)^T \bar{\mathbf{I}}_{G^i} \bar{\boldsymbol{\omega}}^i \end{bmatrix}, \quad \mathbf{P}_e^i = \begin{bmatrix} \mathbf{F}_e^i \\ \bar{\mathbf{T}}_{G^i,e}^i \end{bmatrix}, \quad \mathbf{P}_c^i = \begin{bmatrix} \mathbf{F}_c^i \\ \bar{\mathbf{T}}_{G^i,c}^i \end{bmatrix} \quad (22)$$

where \mathbf{I} is the $d \times d$ identity matrix, \mathbf{I}_b^i is the augmented inertia matrix of the rigid body i having dimensions $2d \times 2d$, \mathbf{P}_v^i is a vector of mechanical actions associated with the centrifugal and Coriolis inertia forces having dimensions $2d \times 1$, \mathbf{P}_e^i is a vector of mechanical actions associated with the external forces having dimensions $2d \times 1$, and \mathbf{P}_c^i is a vector of mechanical actions associated with the constraint forces having dimensions $2d \times 1$. In robotics and automation engineering, the vector \mathbf{p}_b^i is referred to as the twist vector, the matrix \mathbf{I}_b^i is called the spatial generalized inertia matrix, whereas the vectors \mathbf{P}_v^i , \mathbf{P}_e^i , and \mathbf{P}_c^i are respectively identified as the inertial, external, and constraint wrench vectors [87].



Starting from the matrix formulation obtained above, the velocity transformation of interest can be directly expressed by exploiting the linear transformation used for defining the angular velocity vector as follows:

$$\begin{bmatrix} \dot{\mathbf{R}}^i \\ \dot{\boldsymbol{\omega}}^i \end{bmatrix} = \begin{bmatrix} \dot{\mathbf{R}}^i \\ \bar{\mathbf{G}}^i \dot{\boldsymbol{\theta}}^i \end{bmatrix} = \begin{bmatrix} \mathbf{I} & \mathbf{O} \\ \mathbf{O} & \bar{\mathbf{G}}^i \end{bmatrix} \begin{bmatrix} \dot{\mathbf{R}}^i \\ \dot{\boldsymbol{\theta}}^i \end{bmatrix} \Leftrightarrow \mathbf{p}_b^i = \mathbf{V}_b^i \dot{\mathbf{q}}_b^i \quad (23)$$

being:

$$\mathbf{V}_b^i = \begin{bmatrix} \mathbf{I} & \mathbf{O} \\ \mathbf{O} & \bar{\mathbf{G}}^i \end{bmatrix} \quad (24)$$

where the matrix \mathbf{V}_b^i having dimensions $2d \times n_b$ is the velocity transformation matrix of interest that is necessary for transforming the equations of motion of a generic rigid body i from the Newton-Euler form used in classical mechanics to the Lagrangian form used in applied mechanics. It immediately follows that:

$$\mathbf{p}_b^i = \mathbf{V}_b^i \dot{\mathbf{q}}_b^i \Rightarrow \dot{\mathbf{p}}_b^i = \mathbf{V}_b^i \ddot{\mathbf{q}}_b^i + \dot{\mathbf{V}}_b^i \dot{\mathbf{q}}_b^i \quad (25)$$

By substituting the velocity transformation so found in the matrix form of the Newton-Euler equations, one obtains:

$$\mathbf{I}_b^i \mathbf{V}_b^i \ddot{\mathbf{q}}_b^i + \mathbf{I}_b^i \dot{\mathbf{V}}_b^i \dot{\mathbf{q}}_b^i = \mathbf{P}_v^i + \mathbf{P}_e^i + \mathbf{P}_c^i \quad (26)$$

The pre-multiplication of both the left and right-hand sides of the previous matrix equation with the transpose of the velocity transformation matrix yields:

$$(\mathbf{V}_b^i)^T \mathbf{I}_b^i \mathbf{V}_b^i \ddot{\mathbf{q}}_b^i = (\mathbf{V}_b^i)^T (\mathbf{P}_v^i - \mathbf{I}_b^i \dot{\mathbf{V}}_b^i \dot{\mathbf{q}}_b^i) + (\mathbf{V}_b^i)^T \mathbf{P}_e^i + (\mathbf{V}_b^i)^T \mathbf{P}_c^i \quad (27)$$

or:

$$\mathbf{M}^i \ddot{\mathbf{q}}_b^i = \mathbf{Q}_v^i + \mathbf{Q}_e^i + \mathbf{Q}_c^i \quad (28)$$

being:

$$\mathbf{M}^i = (\mathbf{V}_b^i)^T \mathbf{I}_b^i \mathbf{V}_b^i = \begin{bmatrix} m^i \mathbf{I} & \mathbf{O} \\ \mathbf{O} & (\bar{\mathbf{G}}^i)^T \bar{\mathbf{I}}_{G^i} \bar{\mathbf{G}}^i \end{bmatrix} \quad (29)$$

$$\mathbf{Q}_v^i = (\mathbf{V}_b^i)^T (\mathbf{P}_v^i - \mathbf{I}_b^i \dot{\mathbf{V}}_b^i \dot{\mathbf{q}}_b^i) = \begin{bmatrix} \mathbf{0} \\ -(\bar{\mathbf{G}}^i)^T (\dot{\boldsymbol{\omega}}^i \bar{\mathbf{I}}_{G^i} \boldsymbol{\omega}^i + \bar{\mathbf{I}}_{G^i} \dot{\bar{\mathbf{G}}^i} \dot{\boldsymbol{\theta}}^i) \end{bmatrix} \quad (30)$$

$$\mathbf{Q}_e^i = (\mathbf{V}_b^i)^T \mathbf{P}_e^i = \begin{bmatrix} \mathbf{F}_e^i \\ (\bar{\mathbf{G}}^i)^T \bar{\mathbf{T}}_{G^i, e}^i \end{bmatrix}, \quad \mathbf{Q}_c^i = (\mathbf{V}_b^i)^T \mathbf{P}_c^i = \begin{bmatrix} \mathbf{F}_c^i \\ (\bar{\mathbf{G}}^i)^T \bar{\mathbf{T}}_{G^i, c}^i \end{bmatrix} \quad (31)$$

where \mathbf{M}^i represents the mass matrix of the generic rigid body i having dimensions $n_b \times n_b$, \mathbf{Q}_v^i identifies the inertia generalized force vector of the body i having dimensions $n_b \times 1$ which absorbs the generalized forces that are quadratic in the generalized velocities, \mathbf{Q}_e^i denotes the external generalized force vector of the body i having dimensions $n_b \times 1$, and \mathbf{Q}_c^i indicates the constraint generalized force vector of the body i having dimensions $n_b \times 1$.

By adopting a standard assembly process, the total set of equations of motion of the multibody system of interest can be constructed leading to the following matrix form:

$$\mathbf{M} \ddot{\mathbf{q}} = \mathbf{Q}_b + \mathbf{Q}_e, \quad \mathbf{Q}_b = \mathbf{Q}_v + \mathbf{Q}_e \quad (32)$$

where:

$$\mathbf{M} = \underset{i=1}{\overset{N_b}{\mathbf{A}}} \mathbf{M}^i = \begin{bmatrix} \mathbf{M}^1 & \mathbf{O} & \mathbf{O} & \mathbf{O} \\ \mathbf{O} & \mathbf{M}^2 & \mathbf{O} & \mathbf{O} \\ \mathbf{O} & \mathbf{O} & \ddots & \mathbf{O} \\ \mathbf{O} & \mathbf{O} & \mathbf{O} & \mathbf{M}^{N_b} \end{bmatrix}, \quad \mathbf{Q}_v = \underset{i=1}{\overset{N_b}{\mathbf{A}}} \mathbf{Q}_v^i = \begin{bmatrix} \mathbf{Q}_v^1 \\ \mathbf{Q}_v^2 \\ \vdots \\ \mathbf{Q}_v^{N_b} \end{bmatrix} \quad (33)$$

and

$$\mathbf{Q}_e = \underset{i=1}{\overset{N_b}{\mathbf{A}}} \mathbf{Q}_e^i = \begin{bmatrix} \mathbf{Q}_e^1 \\ \mathbf{Q}_e^2 \\ \vdots \\ \mathbf{Q}_e^{N_b} \end{bmatrix}, \quad \mathbf{Q}_c = \underset{i=1}{\overset{N_b}{\mathbf{A}}} \mathbf{Q}_c^i = \begin{bmatrix} \mathbf{Q}_c^1 \\ \mathbf{Q}_c^2 \\ \vdots \\ \mathbf{Q}_c^{N_b} \end{bmatrix} \quad (34)$$

where \mathbf{M} represents the mass matrix of the multibody system having dimensions $n_q \times n_q$, \mathbf{Q}_v identifies the inertia generalized force vector of the multibody system having dimensions $n_q \times 1$ which absorbs the generalized forces that are quadratic in the generalized velocities, \mathbf{Q}_e denotes the external generalized force vector of the multibody system having dimensions $n_q \times 1$, \mathbf{Q}_c indicates the constraint generalized force vector of the multibody system having dimensions $n_q \times 1$, and \mathbf{Q}_b is the total generalized force vector of the multibody system having dimensions $n_q \times 1$.

As discussed in detail below, to complete the mathematical description of the mechanical model of a given multibody system considering a total number of algebraic equations equal to n_c , a proper set of constraint equations grouped in the vector \mathbf{C} of dimensions $n_c \times 1$ must be appended to the equations of motion, thereby leading to the following differential-algebraic set of dynamic equations:

$$\begin{cases} \mathbf{M} \ddot{\mathbf{q}} = \mathbf{Q}_b + \mathbf{Q}_c \\ \mathbf{C} = \mathbf{0} \end{cases} \quad (35)$$



This is referred to as the index-3 form of the differential-algebraic equations describing the dynamic behavior of multibody mechanical systems. By adopting the analytical technique of Lagrange multipliers, the constraint generalized force vector Q_c can be written by using a vector of additional unknowns, which are called Lagrange multipliers and are grouped in the vector λ having dimensions $n_c \times 1$. By doing so, one can write $Q_c = -C_q^T \lambda$, where C_q is a rectangular matrix having dimensions $n_c \times n_q$ that represents the Jacobian matrix of the constraint vector C computed with respect to the generalized coordinate vector q . It follows that the multibody equations of motion can be conveniently expressed in the following equivalent form:

$$\begin{cases} M\ddot{q} = Q_b - C_q^T \lambda \\ C = 0 \end{cases} \quad (36)$$

It is well-known that, to obtain a numerical solution of the multibody equations of motion that is physically consistent and mathematically stable, one must enforce the constraint equations at the position, velocity, and acceleration levels in correspondence of each time step of the dynamical simulation [88]. To achieve this goal, the constraint equations must be preliminary formulated at the velocity and acceleration levels by performing the direct integration process summarized below:

$$C = 0 \Rightarrow \dot{C} = 0 \Rightarrow \ddot{C} = 0 \quad (37)$$

being:

$$\dot{C} = C_q \dot{q} + C_t = 0 \Leftrightarrow C_q \dot{q} = -C_t \quad (38)$$

and

$$\ddot{C} = C_q \ddot{q} - Q_d = 0 \Leftrightarrow C_q \ddot{q} = Q_d \quad (39)$$

where C_t is a vector of dimensions $n_c \times 1$ representing the first partial time derivative of the constraint vector and Q_d is a vector of dimensions $n_c \times 1$ which absorbs the terms that are quadratic in the generalized velocities. By replacing the constraint vector with its second time derivative in the differential-algebraic form of the equations of motion, one obtains the so-called index-1 form of the multibody equations given by:

$$\begin{cases} M\ddot{q} = Q_b - C_q^T \lambda \\ C_q \ddot{q} = Q_d \end{cases} \Leftrightarrow \begin{cases} M\ddot{q} + C_q^T \lambda = Q_b \\ C_q \ddot{q} = Q_d \end{cases} \quad (40)$$

or:

$$\begin{bmatrix} M & C_q^T \\ C_q & O \end{bmatrix} \begin{bmatrix} \ddot{q} \\ \lambda \end{bmatrix} = \begin{bmatrix} Q_b \\ Q_d \end{bmatrix} \Leftrightarrow M_a q_a = Q_a \quad (41)$$

being:

$$q_a = \begin{bmatrix} \ddot{q} \\ \lambda \end{bmatrix}, \quad M_a = \begin{bmatrix} M & C_q^T \\ C_q & O \end{bmatrix}, \quad Q_a = \begin{bmatrix} Q_b \\ Q_d \end{bmatrix} \quad (42)$$

where $n_a = n_q + n_c$ is the total number of augmented coordinates, q_a denotes the augmented coordinate vector of the multibody system having dimensions $n_a \times 1$, M_a is the augmented mass matrix of the multibody system having dimensions $n_a \times n_a$, and Q_a is the augmented generalized force vector of the multibody system having dimensions $n_a \times 1$. By numerically solving the linear system of algebraic equations formulated above, one can obtain at each time step of the dynamical simulation the system generalized acceleration vector \ddot{q} and the system Lagrange multipliers vector λ , which, in turns, can be respectively employed to march forward the numerical solution of the equations of motion on the time grid and to calculate the constraint generalized force vector necessary for determining the mechanical actions of the joint constraints.

The numerical procedure described so far is referred to as the augmented formulation. From a wider perspective, the solution of the equations of motion obtained using the augmented Lagrangian formulation, which presents a solid theoretical foundation [89], requires the solution of a system of differential-algebraic equations [90]. In multibody systems, kinematic constraint equations come into play because of the presence of mechanical joints or specified motion trajectories. In general, two procedures can be followed to analytically formulate and numerically solve the dynamic equations of constrained multibody systems. These procedures are referred to as the embedding technique and the augmented formulation [91]. In the embedding technique, the system dynamic equations are formulated in terms of the degrees of freedom. This technique leads to a minimum set of dynamic equations that do not contain any constraint forces. Therefore, when using the embedding technique, there are $n_q = n_f$ equations for n_q unknowns, where n_q is the number of generalized coordinates and n_f are the degrees of freedom of the multibody system. The numerical solution of the multibody equations obtained using the embedding technique requires only the integration of a system of differential equations [92].

As mentioned before, by using the embedding technique, the constraint forces are systematically eliminated and a number of equations of motion equal to the number of the system degrees of freedom are found [93]. To obtain this minimum set of differential equations, it is necessary to use a proper velocity transformation matrix specifically devised for this purpose, which can be systematically determined when the total vector of the system generalized coordinates is expressed in terms of the independent generalized coordinates [94]. In the augmented formulation, on the other hand, the dynamic equations are formulated in terms of a set of redundant coordinates. As a consequence, the resulting equations are expressed in terms of dependent and independent generalized coordinates, as well as in terms of the constraint generalized forces. Therefore, when using the augmented formulation, there are $n_a = n_q + n_c$ equations for n_a unknowns, where n_q is the number of generalized coordinates that include both independent and dependent generalized coordinates, while n_c is the total number of the algebraic constraints involved in the mathematical model of the multibody system. In particular, the latter approach is the one adopted in this paper in conjunction with a proper constraint stabilization method based on the generalized coordinate partitioning procedure [91].

2.3 Algebraic Constraints Classification

One of the most fundamental aspects of the development of a multibody model of a given articulated mechanical system is represented by the proper mathematical modeling of the constraint equations applied to it [95]. From a general perspective, algebraic constraints are classified according to the mathematical structure and physical meaning of the equations that represent them [96]. A short summary of the constraint classification methods is, therefore, presented herein.

First, algebraic constraints can be classified into unilateral and bilateral constraints. A bilateral constraint is described by one or more constraint equations. A unilateral constraint is described by one or more constraint inequalities. An example of a bilateral constraint is a material point constrained to move on the surface of a sphere. An example of a unilateral constraint is a material



point constrained to move within a cube. The mechanical joints of interest for the present study are exclusively modeled as bilateral constraints.

A second constraint classification can be made to distinguish between holonomic and nonholonomic constraints. A holonomic constraint is described by one or more algebraic equations formulated exclusively in terms of the generalized coordinates of the system. A holonomic constraint acts on the space of generalized positions of the multibody system subjected to it by placing geometric limits on the feasible motion. Consequently, a holonomic constraint removes degrees of freedom from the mechanical system it acts on. On the other hand, a nonholonomic constraint is described by one or more algebraic equations formulated in terms of the generalized coordinates and/or the generalized velocities and/or generalized accelerations of the mechanical system. However, to be effectively nonholonomic, these equations must not be integrable, that is, they must be not ascribable to an equivalent mathematical form in which only generalized coordinates appear. The mechanical joints of interest for this work are exclusively described by holonomic constraints.

A third constraint classification is the distinction between scleronomic and rheonomic constraints. A rheonomic constraint is described by one or more algebraic equations in which the time dependence explicitly appears. A scleronomic constraint is described by one or more algebraic equations in which the time dependence does not explicitly appear. Examples of rheonomic constraints are the trajectory imposed on the end effector of a robotic manipulator or the time law of the angular velocity imposed on an axis of a rotor. An example of a scleronomic constraint is the linear guide between a seat and the chassis of a road vehicle. The mechanical joints of interest for the present study are exclusively modeled as scleronomic constraints.

A fourth constraint classification encompasses ideal and real constraints. An ideal constraint, referred to as a smooth or perfect, or frictionless constraint, is a constraint that presents a virtual work of its generalized constraint reaction forces equal to zero. Therefore, there is no resistance offered by the constraint in the motions that occur along the linear or angular directions not impeded by the shapes of the kinematic surfaces. On the other hand, a real constraint, referred to as a rough or imperfect, or frictional constraint, is a constraint that presents a virtual work of its generalized constraint reaction forces different from zero. An example of an ideal constraint is a piston of an internal combustion engine that moves in a cylinder whose surface is perfectly smooth. An example of a real constraint is a piston of an internal combustion engine that moves in a cylinder whose surface has significant surface asperities and, therefore, presents a resistant friction force on the piston itself. The mechanical joints of interest for this work are described by ideal constraints.

A fifth and final classification of the algebraic constraint equations identifies intrinsic and extrinsic constraints. Intrinsic constraints are mathematically described by algebraic equations that schematize the normalization conditions of the rotational coordinates used in the description of the kinematics of the rigid body. Physically, they correspond to the rigidity condition of a rigid body. An example of an intrinsic constraint is the normalization condition of the Euler parameters that describe the orientation of a rigid body in space. Extrinsic constraints, on the other hand, are mathematically described by algebraic equations that consider the coupling conditions between the various rigid bodies that form a multibody mechanical system. For convenience, although they should be formally classified as extrinsic constraints, the constraints that impose a certain dynamic behavior on the system, such as the pure rolling condition, are excluded from this category. Physically, extrinsic constraints correspond to the kinematic pairs present in the joints of the multibody mechanical system. An example of an extrinsic constraint is the cylindrical joint between a piston and a cylinder of an internal combustion engine. Additionally, as mentioned before, the imposed motion constraints can be conveniently grouped in a separate category even if they physically represent extrinsic constraints. An example of an imposed motion constraint is the angular displacement rate assigned to the crank of the slider-crank mechanism of an internal combustion engine.

Formally, it is possible to represent the set of intrinsic constraint equations as the vector $\Phi \equiv \Phi(q, t)$ having dimensions $n_{c,\Phi} \times 1$, where $n_{c,\Phi}$ is the total number of intrinsic constraint equations. Also, it is possible to represent the set of the algebraic constraint equations modeling imposed motions as the vector $\Theta \equiv \Theta(q, t)$ having dimensions $n_{c,\Theta} \times 1$, where $n_{c,\Theta}$ is the total number of imposed motion equations. Similarly, it is possible to represent the set of extrinsic constraint equations as the vector $\Psi \equiv \Psi(q, t)$ having dimensions $n_{c,\Psi} \times 1$, where $n_{c,\Psi}$ is the total number of extrinsic constraint equations. By combining all the previous constraint vectors in one vector function denoted with $C \equiv C(q, t)$ of dimensions $n_c \times 1$, where $n_c = n_{c,\Phi} + n_{c,\Theta} + n_{c,\Psi}$ is the total number of algebraic constraint equations, one obtains the following formal expression of the constraint equations:

$$C = \begin{bmatrix} \Phi \\ \Theta \\ \Psi \end{bmatrix} \quad (43)$$

where the corresponding Jacobian matrix is given by:

$$C_q = \begin{bmatrix} \Phi_q \\ \Theta_q \\ \Psi_q \end{bmatrix} \quad (44)$$

The mechanical joints of interest for the present study are exclusively modeled as extrinsic constraints.

2.4 Mechanical Joints Modeling

As discussed above, the kinematic constraints can be distinguished into mechanical joints and driving joints. Mechanical joints define the connectivity between the rigid bodies forming the multibody system, whereas driving joints describe the motion trajectories that are specified for the components of the mechanical system [97]. When using absolute coordinates in the analysis of multibody mechanical systems, the formulation of the kinematic constraints that describe a joint between two arbitrary rigid bodies in the multibody system can be made independent of the topological structure of the system [98]. This is because identical sets of coordinates are used to describe the motion of all the bodies that compose the multibody system under analysis.

In this subsection, the mathematical formulation of the algebraic equations of the mechanical joints used in spatial multibody systems is discussed, with particular emphasis on the description of the mechanical joints encountered in the multibody analysis of the case study considered in this work. In particular, to simplify the kinematic and dynamic analysis of the adaptive mechanism serving as a lifting table assumed as the case study of this investigation, only three types of kinematic joints are considered, namely revolute joints, prismatic joints, and planar joints. The mathematical formulation of the algebraic constraint equations associated with these three general joint constraints is analyzed in detail below.

Before analyzing in detail the development of the algebraic constraint equations, which serve for the mathematical modeling of the mechanical joints, it is convenient to recall the expression of the position, velocity, acceleration, and jerk fields of a generic rigid body i in a compact matrix form, which is commonly employed in the framework of the Lagrangian formulation assumed in



multibody dynamics. For this purpose, one can write:

$$\begin{cases} \mathbf{r}^i(P^i) = \mathbf{R}^i + \mathbf{A}^i \bar{\mathbf{u}}^i(P^i) \\ \dot{\mathbf{r}}^i(P^i) = \mathbf{L}^i(P^i) \dot{\mathbf{q}}^i \\ \ddot{\mathbf{r}}^i(P^i) = \mathbf{L}^i(P^i) \ddot{\mathbf{q}}^i + \dot{\mathbf{L}}^i(P^i) \dot{\mathbf{q}}^i \\ \ddot{\mathbf{r}}^i(P^i) = \mathbf{L}^i(P^i) \ddot{\mathbf{q}}^i + 2\dot{\mathbf{L}}^i(P^i) \dot{\mathbf{q}}^i + \ddot{\mathbf{L}}^i(P^i) \mathbf{q}^i \end{cases} \quad (45)$$

being:

$$\mathbf{L}^i(P^i) = \begin{bmatrix} \mathbf{I} & \mathbf{A}^i(\bar{\mathbf{u}}^i(P^i))^T \bar{\mathbf{G}}^i \end{bmatrix} \quad (46)$$

where $\mathbf{L}^i(P^i)$ is a rectangular matrix having dimensions $d \times n_b$ that represents the Jacobian matrix of the position field $\mathbf{r}^i(P^i)$ describing the rigid body i computed with respect to the generalized coordinate vector \mathbf{q}_b^i of the same generic body.

Let the discrete index k be the identifier of a generic kinematic pair describing a mechanical joint that connects two rigid bodies of the multibody system, which are respectively identified with the integers i_k and j_k . The collocation points of the kinematic joint k on the two bodies i_k and j_k are respectively denoted with P^{i_k} and P^{j_k} , while their local position vectors of dimensions $d \times 1$ are respectively indicated as $\bar{\mathbf{u}}^{i_k}(P^{i_k})$ and $\bar{\mathbf{u}}^{j_k}(P^{j_k})$. Additionally, to identify the joint axis of a given kinematic pair k as seen by the two rigid bodies i_k and j_k , it is necessary to specify two local direction vectors of dimensions $d \times 1$, which are respectively denoted as $\bar{\mathbf{v}}_1^{i_k}$ and $\bar{\mathbf{v}}_1^{j_k}$. The local direction vectors of the joint axis k denoted with $\bar{\mathbf{v}}_1^{i_k}$ and $\bar{\mathbf{v}}_1^{j_k}$ can be readily employed to construct two orthogonal triads necessary for the subsequent definition of the algebraic equations modeling the kinematic joint k . To this end, one can readily determine the local unit vectors $\bar{\mathbf{v}}_2^{i_k}$ and $\bar{\mathbf{v}}_3^{i_k}$ starting from the direction vector $\bar{\mathbf{v}}_1^{i_k}$, as well as the local unit vectors $\bar{\mathbf{v}}_2^{j_k}$ and $\bar{\mathbf{v}}_3^{j_k}$ starting from the direction vector $\bar{\mathbf{v}}_1^{j_k}$. By doing so, the following properties of mutual orthonormality are satisfied:

$$\begin{cases} \begin{pmatrix} \bar{\mathbf{v}}_1^{i_k} \\ \bar{\mathbf{v}}_2^{i_k} \\ \bar{\mathbf{v}}_3^{i_k} \end{pmatrix}^T \begin{pmatrix} \bar{\mathbf{v}}_1^{i_k} \\ \bar{\mathbf{v}}_2^{i_k} \\ \bar{\mathbf{v}}_3^{i_k} \end{pmatrix} - \mathbf{1} = 0 \\ \begin{pmatrix} \bar{\mathbf{v}}_1^{i_k} \\ \bar{\mathbf{v}}_2^{i_k} \\ \bar{\mathbf{v}}_3^{i_k} \end{pmatrix}^T \begin{pmatrix} \bar{\mathbf{v}}_2^{i_k} \\ \bar{\mathbf{v}}_3^{i_k} \end{pmatrix} = 0 \\ \begin{pmatrix} \bar{\mathbf{v}}_1^{i_k} \\ \bar{\mathbf{v}}_2^{i_k} \\ \bar{\mathbf{v}}_3^{i_k} \end{pmatrix}^T \begin{pmatrix} \bar{\mathbf{v}}_3^{i_k} \end{pmatrix} = 0 \end{cases}, \quad \begin{cases} \begin{pmatrix} \bar{\mathbf{v}}_1^{j_k} \\ \bar{\mathbf{v}}_2^{j_k} \\ \bar{\mathbf{v}}_3^{j_k} \end{pmatrix}^T \begin{pmatrix} \bar{\mathbf{v}}_1^{j_k} \\ \bar{\mathbf{v}}_2^{j_k} \\ \bar{\mathbf{v}}_3^{j_k} \end{pmatrix} - \mathbf{1} = 0 \\ \begin{pmatrix} \bar{\mathbf{v}}_1^{j_k} \\ \bar{\mathbf{v}}_2^{j_k} \\ \bar{\mathbf{v}}_3^{j_k} \end{pmatrix}^T \begin{pmatrix} \bar{\mathbf{v}}_2^{j_k} \\ \bar{\mathbf{v}}_3^{j_k} \end{pmatrix} = 0 \\ \begin{pmatrix} \bar{\mathbf{v}}_1^{j_k} \\ \bar{\mathbf{v}}_2^{j_k} \\ \bar{\mathbf{v}}_3^{j_k} \end{pmatrix}^T \begin{pmatrix} \bar{\mathbf{v}}_3^{j_k} \end{pmatrix} = 0 \end{cases} \quad (47)$$

Furthermore, by considering the rotation matrices \mathbf{A}^{i_k} and \mathbf{A}^{j_k} respectively associated with the rigid bodies i_k and j_k , it is possible to express the direction vectors introduced before with respect to the global reference system, thereby being able to write the absolute geometric relationships that define the mathematical structure of the mechanical joint k of interest. By doing so, it follows that:

$$\begin{cases} \mathbf{v}_1^{i_k} = \mathbf{A}^{i_k} \bar{\mathbf{v}}_1^{i_k} \\ \mathbf{v}_2^{i_k} = \mathbf{A}^{i_k} \bar{\mathbf{v}}_2^{i_k} \\ \mathbf{v}_3^{i_k} = \mathbf{A}^{i_k} \bar{\mathbf{v}}_3^{i_k} \end{cases}, \quad \begin{cases} \mathbf{v}_1^{j_k} = \mathbf{A}^{j_k} \bar{\mathbf{v}}_1^{j_k} \\ \mathbf{v}_2^{j_k} = \mathbf{A}^{j_k} \bar{\mathbf{v}}_2^{j_k} \\ \mathbf{v}_3^{j_k} = \mathbf{A}^{j_k} \bar{\mathbf{v}}_3^{j_k} \end{cases} \quad (48)$$

Consequently, it is now possible to define an arbitrary direction vector associated with the kinematic joint k with respect to both the rigid bodies i_k and j_k involved in the kinematic pair. In this vein, by denoting with \mathbf{w}^{i_k} and \mathbf{w}^{j_k} the two arbitrary direction vectors of dimensions $d \times 1$ mentioned before, one can write:

$$\mathbf{w}^{i_k} = a^{i_k} \mathbf{v}_1^{i_k} + b^{i_k} \mathbf{v}_2^{i_k} + c^{i_k} \mathbf{v}_3^{i_k}, \quad \mathbf{w}^{j_k} = a^{j_k} \mathbf{v}_1^{j_k} + b^{j_k} \mathbf{v}_2^{j_k} + c^{j_k} \mathbf{v}_3^{j_k} \quad (49)$$

where a^{i_k} , b^{i_k} , c^{i_k} , a^{j_k} , b^{j_k} , and c^{j_k} are arbitrary scalar quantities necessary for identifying the generic direction vectors of interest, while the dot product between the global vectors \mathbf{w}^{i_k} and \mathbf{w}^{j_k} is a constant scalar quantity denoted as $d^{i_k, j_k} = (\mathbf{w}^{i_k})^T \mathbf{w}^{j_k}$. Additionally, the following useful identities can be easily proved:

$$\begin{cases} \dot{\mathbf{v}}_1^{i_k} = \mathbf{D}_1^{i_k} \dot{\mathbf{q}}^{i_k} \\ \dot{\mathbf{v}}_2^{i_k} = \mathbf{D}_2^{i_k} \dot{\mathbf{q}}^{i_k} \\ \dot{\mathbf{v}}_3^{i_k} = \mathbf{D}_3^{i_k} \dot{\mathbf{q}}^{i_k} \end{cases}, \quad \begin{cases} \dot{\mathbf{v}}_1^{j_k} = \mathbf{D}_1^{j_k} \dot{\mathbf{q}}^{j_k} \\ \dot{\mathbf{v}}_2^{j_k} = \mathbf{D}_2^{j_k} \dot{\mathbf{q}}^{j_k} \\ \dot{\mathbf{v}}_3^{j_k} = \mathbf{D}_3^{j_k} \dot{\mathbf{q}}^{j_k} \end{cases} \quad (50)$$

where:

$$\begin{cases} \mathbf{D}_1^{i_k} = \begin{bmatrix} \mathbf{O} & \mathbf{A}^{i_k} (\bar{\mathbf{v}}_1^{i_k})^T \bar{\mathbf{G}}^{i_k} \end{bmatrix} \\ \mathbf{D}_2^{i_k} = \begin{bmatrix} \mathbf{O} & \mathbf{A}^{i_k} (\bar{\mathbf{v}}_2^{i_k})^T \bar{\mathbf{G}}^{i_k} \end{bmatrix} \\ \mathbf{D}_3^{i_k} = \begin{bmatrix} \mathbf{O} & \mathbf{A}^{i_k} (\bar{\mathbf{v}}_3^{i_k})^T \bar{\mathbf{G}}^{i_k} \end{bmatrix} \end{cases}, \quad \begin{cases} \mathbf{D}_1^{j_k} = \begin{bmatrix} \mathbf{O} & \mathbf{A}^{j_k} (\bar{\mathbf{v}}_1^{j_k})^T \bar{\mathbf{G}}^{j_k} \end{bmatrix} \\ \mathbf{D}_2^{j_k} = \begin{bmatrix} \mathbf{O} & \mathbf{A}^{j_k} (\bar{\mathbf{v}}_2^{j_k})^T \bar{\mathbf{G}}^{j_k} \end{bmatrix} \\ \mathbf{D}_3^{j_k} = \begin{bmatrix} \mathbf{O} & \mathbf{A}^{j_k} (\bar{\mathbf{v}}_3^{j_k})^T \bar{\mathbf{G}}^{j_k} \end{bmatrix} \end{cases} \quad (51)$$

A generic revolute joint k is described by $n_{c, \Psi}^k = 5$ algebraic equations. In the geometric description of a generic revolute joint k , the unit vectors $\bar{\mathbf{v}}_1^{i_k}$ and $\bar{\mathbf{v}}_1^{j_k}$ define the direction vectors of the revolute joint axis and are respectively expressed with respect to the rigid bodies i_k and j_k that form the kinematic pair k . For a revolute joint k that connects the rigid bodies i_k and j_k of the multibody system, the following vector of extrinsic constraint equations can be assembled:

$$\Psi^k = \begin{bmatrix} \mathbf{r}^{i_k}(P^{i_k}) - \mathbf{r}^{j_k}(P^{j_k}) \\ \begin{pmatrix} \mathbf{v}_2^{i_k} \\ \mathbf{v}_3^{i_k} \end{pmatrix}^T \mathbf{v}_1^{j_k} \\ \begin{pmatrix} \mathbf{v}_2^{j_k} \\ \mathbf{v}_3^{j_k} \end{pmatrix}^T \mathbf{v}_1^{i_k} \end{bmatrix} \quad (52)$$



The Jacobian matrix of the constraint equations associated with the revolute joint k can be written as:

$$\Psi_{q^k}^k = \begin{bmatrix} \Psi_{q^{i_k}}^k & \Psi_{q^{j_k}}^k \end{bmatrix} \quad (53)$$

where:

$$\Psi_{q^{i_k}}^k = \begin{bmatrix} \mathbf{L}^{i_k}(P^{i_k}) \\ (\mathbf{v}_1^{j_k})^T \mathbf{D}_2^{i_k} \\ (\mathbf{v}_1^{j_k})^T \mathbf{D}_3^{i_k} \end{bmatrix}, \quad \Psi_{q^{j_k}}^k = \begin{bmatrix} -\mathbf{L}^{j_k}(P^{j_k}) \\ (\mathbf{v}_2^{i_k})^T \mathbf{D}_1^{j_k} \\ (\mathbf{v}_3^{i_k})^T \mathbf{D}_1^{j_k} \end{bmatrix} \quad (54)$$

When formulating the constraint equations of the revolute joint k at the acceleration level, the constraint quadratic velocity vector that absorbs the terms that are quadratic in the generalized velocities is given by:

$$\mathbf{Q}_{d,\Psi}^k = \mathbf{Q}_{d,\Psi}^{i_k} + \mathbf{Q}_{d,\Psi}^{j_k} \quad (55)$$

where:

$$\begin{aligned} \mathbf{Q}_{d,\Psi}^{i_k} &= -\dot{\Psi}_{q^{i_k}}^k \dot{\mathbf{q}}^{i_k} \\ &= \begin{bmatrix} -\dot{\mathbf{L}}^{i_k}(P^{i_k}) \dot{\mathbf{q}}^{i_k} \\ -(\dot{\mathbf{v}}_1^{j_k})^T \mathbf{D}_2^{i_k} \dot{\mathbf{q}}^{i_k} - (\mathbf{v}_1^{j_k})^T \dot{\mathbf{D}}_2^{i_k} \dot{\mathbf{q}}^{i_k} \\ -(\dot{\mathbf{v}}_1^{j_k})^T \mathbf{D}_3^{i_k} \dot{\mathbf{q}}^{i_k} - (\mathbf{v}_1^{j_k})^T \dot{\mathbf{D}}_3^{i_k} \dot{\mathbf{q}}^{i_k} \end{bmatrix} \end{aligned} \quad (56)$$

and

$$\begin{aligned} \mathbf{Q}_{d,\Psi}^{j_k} &= -\dot{\Psi}_{q^{j_k}}^k \dot{\mathbf{q}}^{j_k} \\ &= \begin{bmatrix} \dot{\mathbf{L}}^{j_k}(P^{j_k}) \dot{\mathbf{q}}^{j_k} \\ -(\dot{\mathbf{v}}_2^{i_k})^T \mathbf{D}_1^{j_k} \dot{\mathbf{q}}^{j_k} - (\mathbf{v}_2^{i_k})^T \dot{\mathbf{D}}_1^{j_k} \dot{\mathbf{q}}^{j_k} \\ -(\dot{\mathbf{v}}_3^{i_k})^T \mathbf{D}_1^{j_k} \dot{\mathbf{q}}^{j_k} - (\mathbf{v}_3^{i_k})^T \dot{\mathbf{D}}_1^{j_k} \dot{\mathbf{q}}^{j_k} \end{bmatrix} \end{aligned} \quad (57)$$

Since the revolute joint is modeled by a set of scleronomic constraint equations, the partial derivative with respect to the time of the constraint vector associated with the revolute joint is the zero vector.

A generic prismatic joint k is described by $n_{C,\Psi}^k = 5$ algebraic equations. In the geometric description of a generic prismatic joint k , the unit vectors $\bar{\mathbf{v}}_1^{i_k}$ and $\bar{\mathbf{v}}_1^{j_k}$ define the direction vectors of the prismatic joint axis and are respectively expressed with respect to the rigid bodies i_k and j_k that form the kinematic pair k . For a prismatic joint k that connects the rigid bodies i_k and j_k of the multibody system, the following vector of extrinsic constraint equations can be assembled:

$$\Psi^k = \begin{bmatrix} (\mathbf{v}_2^{i_k})^T (\mathbf{r}^{i_k}(P^{i_k}) - \mathbf{r}^{j_k}(P^{j_k})) \\ (\mathbf{v}_3^{i_k})^T (\mathbf{r}^{i_k}(P^{i_k}) - \mathbf{r}^{j_k}(P^{j_k})) \\ (\mathbf{v}_1^{i_k})^T \mathbf{v}_2^{j_k} \\ (\mathbf{v}_1^{i_k})^T \mathbf{v}_3^{j_k} \\ (\mathbf{w}^{i_k})^T \mathbf{w}^{j_k} - d^{i_k,j_k} \end{bmatrix} \quad (58)$$

The Jacobian matrix of the constraint equations associated with the prismatic joint k can be written as:

$$\Psi_{q^k}^k = \begin{bmatrix} \Psi_{q^{i_k}}^k & \Psi_{q^{j_k}}^k \end{bmatrix} \quad (59)$$

where:

$$\Psi_{q^{i_k}}^k = \begin{bmatrix} (\mathbf{r}^{i_k,j_k}(P^{i_k}, P^{j_k}))^T \mathbf{D}_2^{i_k} + (\mathbf{v}_2^{i_k})^T \mathbf{L}^{i_k}(P^{i_k}) \\ (\mathbf{r}^{i_k,j_k}(P^{i_k}, P^{j_k}))^T \mathbf{D}_3^{i_k} + (\mathbf{v}_3^{i_k})^T \mathbf{L}^{i_k}(P^{i_k}) \\ (\mathbf{v}_2^{j_k})^T \mathbf{D}_1^{i_k} \\ (\mathbf{v}_3^{j_k})^T \mathbf{D}_1^{i_k} \\ (\mathbf{w}^{j_k})^T \mathbf{D}_w^{i_k} \end{bmatrix}, \quad \Psi_{q^{j_k}}^k = \begin{bmatrix} -(\mathbf{v}_2^{i_k})^T \mathbf{L}^{j_k}(P^{j_k}) \\ -(\mathbf{v}_3^{i_k})^T \mathbf{L}^{j_k}(P^{j_k}) \\ (\mathbf{v}_1^{i_k})^T \mathbf{D}_2^{j_k} \\ (\mathbf{v}_1^{i_k})^T \mathbf{D}_3^{j_k} \\ (\mathbf{w}^{i_k})^T \mathbf{D}_w^{j_k} \end{bmatrix} \quad (60)$$

being:

$$\mathbf{D}_w^{i_k} = a^{i_k} \mathbf{D}_1^{i_k} + b^{i_k} \mathbf{D}_2^{i_k} + c^{i_k} \mathbf{D}_3^{i_k} \quad (61)$$

and

$$\mathbf{D}_w^{j_k} = a^{j_k} \mathbf{D}_1^{j_k} + b^{j_k} \mathbf{D}_2^{j_k} + c^{j_k} \mathbf{D}_3^{j_k} \quad (62)$$

where $\mathbf{r}^{i_k,j_k}(P^{i_k}, P^{j_k}) = \mathbf{r}^{i_k}(P^{i_k}) - \mathbf{r}^{j_k}(P^{j_k})$. When formulating the constraint equations of the prismatic joint k at the acceleration level, the constraint quadratic velocity vector that absorbs the terms that are quadratic in the generalized velocities is given by:

$$\mathbf{Q}_{d,\Psi}^k = \mathbf{Q}_{d,\Psi}^{i_k} + \mathbf{Q}_{d,\Psi}^{j_k} \quad (63)$$



where:

$$\begin{aligned}
 \mathbf{Q}_{d,\Psi}^{i_k} &= -\dot{\Psi}_{\mathbf{q}^{i_k}}^k \dot{\mathbf{q}}^{i_k} \\
 &= \begin{bmatrix} -(\dot{\mathbf{r}}^{i_k,j_k}(P^{i_k}, P^{j_k}))^T \mathbf{D}_2^{i_k} \dot{\mathbf{q}}^{i_k} - (\mathbf{r}^{i_k,j_k}(P^{i_k}, P^{j_k}))^T \dot{\mathbf{D}}_2^{i_k} \dot{\mathbf{q}}^{i_k} \\ -(\dot{\mathbf{v}}_2^{i_k})^T \mathbf{L}^{i_k}(P^{i_k}) \dot{\mathbf{q}}^{i_k} - (\mathbf{v}_2^{i_k})^T \dot{\mathbf{L}}^{i_k}(P^{i_k}) \dot{\mathbf{q}}^{i_k} \\ -(\dot{\mathbf{r}}^{i_k,j_k}(P^{i_k}, P^{j_k}))^T \mathbf{D}_3^{i_k} \dot{\mathbf{q}}^{i_k} - (\mathbf{r}^{i_k,j_k}(P^{i_k}, P^{j_k}))^T \dot{\mathbf{D}}_3^{i_k} \dot{\mathbf{q}}^{i_k} \\ -(\dot{\mathbf{v}}_3^{i_k})^T \mathbf{L}^{i_k}(P^{i_k}) \dot{\mathbf{q}}^{i_k} - (\mathbf{v}_3^{i_k})^T \dot{\mathbf{L}}^{i_k}(P^{i_k}) \dot{\mathbf{q}}^{i_k} \\ -(\dot{\mathbf{v}}_2^{j_k})^T \mathbf{D}_1^{i_k} \dot{\mathbf{q}}^{i_k} - (\mathbf{v}_2^{j_k})^T \dot{\mathbf{D}}_1^{i_k} \dot{\mathbf{q}}^{i_k} \\ -(\dot{\mathbf{v}}_3^{j_k})^T \mathbf{D}_1^{i_k} \dot{\mathbf{q}}^{i_k} - (\mathbf{v}_3^{j_k})^T \dot{\mathbf{D}}_1^{i_k} \dot{\mathbf{q}}^{i_k} \\ -(\dot{\mathbf{w}}^{j_k})^T \mathbf{D}_w^{i_k} \dot{\mathbf{q}}^{i_k} - (\mathbf{w}^{j_k})^T \dot{\mathbf{D}}_w^{i_k} \dot{\mathbf{q}}^{i_k} \end{bmatrix} \tag{64}
 \end{aligned}$$

and

$$\begin{aligned}
 \mathbf{Q}_{d,\Psi}^{j_k} &= -\dot{\Psi}_{\mathbf{q}^{j_k}}^k \dot{\mathbf{q}}^{j_k} \\
 &= \begin{bmatrix} (\dot{\mathbf{v}}_2^{i_k})^T \mathbf{L}^{j_k}(P^{j_k}) \dot{\mathbf{q}}^{j_k} + (\mathbf{v}_2^{i_k})^T \dot{\mathbf{L}}^{j_k}(P^{j_k}) \dot{\mathbf{q}}^{j_k} \\ (\dot{\mathbf{v}}_3^{i_k})^T \mathbf{L}^{j_k}(P^{j_k}) \dot{\mathbf{q}}^{j_k} + (\mathbf{v}_3^{i_k})^T \dot{\mathbf{L}}^{j_k}(P^{j_k}) \dot{\mathbf{q}}^{j_k} \\ -(\dot{\mathbf{v}}_1^{i_k})^T \mathbf{D}_2^{j_k} \dot{\mathbf{q}}^{j_k} - (\mathbf{v}_1^{i_k})^T \dot{\mathbf{D}}_2^{j_k} \dot{\mathbf{q}}^{j_k} \\ -(\dot{\mathbf{v}}_1^{i_k})^T \mathbf{D}_3^{j_k} \dot{\mathbf{q}}^{j_k} - (\mathbf{v}_1^{i_k})^T \dot{\mathbf{D}}_3^{j_k} \dot{\mathbf{q}}^{j_k} \\ -(\dot{\mathbf{w}}^{i_k})^T \mathbf{D}_w^{j_k} \dot{\mathbf{q}}^{j_k} - (\mathbf{w}^{i_k})^T \dot{\mathbf{D}}_w^{j_k} \dot{\mathbf{q}}^{j_k} \end{bmatrix} \tag{65}
 \end{aligned}$$

Since the prismatic joint is modeled by a set of scleronomic constraint equations, the partial derivative with respect to the time of the constraint vector associated with the prismatic joint is the zero vector.

A generic planar joint k is described by $n_{c,\Psi}^k = 3$ algebraic equations. In the geometric description of a generic planar joint k , the unit vectors $\bar{\mathbf{v}}_1^{i_k}$ and $\bar{\mathbf{v}}_1^{j_k}$ define the direction vectors of the planar joint axis and are respectively expressed with respect to the rigid bodies i_k and j_k that form the kinematic pair k . For a planar joint k that connects the rigid bodies i_k and j_k of the multibody system, the following vector of extrinsic constraint equations can be assembled:

$$\Psi^k = \begin{bmatrix} (\mathbf{v}_1^{i_k})^T (\mathbf{r}^{i_k}(P^{i_k}) - \mathbf{r}^{j_k}(P^{j_k})) \\ (\mathbf{v}_2^{i_k})^T \mathbf{v}_1^{j_k} \\ (\mathbf{v}_3^{i_k})^T \mathbf{v}_1^{j_k} \end{bmatrix} \tag{66}$$

The Jacobian matrix of the constraint equations associated with the planar joint k can be written as:

$$\Psi_{\mathbf{q}^k}^k = \begin{bmatrix} \Psi_{\mathbf{q}^{i_k}}^k & \Psi_{\mathbf{q}^{j_k}}^k \end{bmatrix} \tag{67}$$

where:

$$\Psi_{\mathbf{q}^{i_k}}^k = \begin{bmatrix} (\mathbf{r}^{i_k,j_k}(P^{i_k}, P^{j_k}))^T \mathbf{D}_1^{i_k} + (\mathbf{v}_1^{i_k})^T \mathbf{L}^{i_k}(P^{i_k}) \\ (\mathbf{v}_1^{j_k})^T \mathbf{D}_2^{i_k} \\ (\mathbf{v}_1^{j_k})^T \mathbf{D}_3^{i_k} \end{bmatrix}, \quad \Psi_{\mathbf{q}^{j_k}}^k = \begin{bmatrix} -(\mathbf{v}_1^{i_k})^T \mathbf{L}^{j_k}(P^{j_k}) \\ (\mathbf{v}_2^{i_k})^T \mathbf{D}_1^{j_k} \\ (\mathbf{v}_3^{i_k})^T \mathbf{D}_1^{j_k} \end{bmatrix} \tag{68}$$

being $\mathbf{r}^{i_k,j_k}(P^{i_k}, P^{j_k}) = \mathbf{r}^{i_k}(P^{i_k}) - \mathbf{r}^{j_k}(P^{j_k})$. When formulating the constraint equations of the planar joint k at the acceleration level, the constraint quadratic velocity vector that absorbs the terms that are quadratic in the generalized velocities is given by:

$$\mathbf{Q}_{d,\Psi}^k = \mathbf{Q}_{d,\Psi}^{i_k} + \mathbf{Q}_{d,\Psi}^{j_k} \tag{69}$$

where:

$$\begin{aligned}
 \mathbf{Q}_{d,\Psi}^{i_k} &= -\dot{\Psi}_{\mathbf{q}^{i_k}}^k \dot{\mathbf{q}}^{i_k} \\
 &= \begin{bmatrix} -(\dot{\mathbf{r}}^{i_k,j_k}(P^{i_k}, P^{j_k}))^T \mathbf{D}_1^{i_k} \dot{\mathbf{q}}^{i_k} - (\mathbf{r}^{i_k,j_k}(P^{i_k}, P^{j_k}))^T \dot{\mathbf{D}}_1^{i_k} \dot{\mathbf{q}}^{i_k} \\ -(\dot{\mathbf{v}}_1^{i_k})^T \mathbf{L}^{i_k}(P^{i_k}) \dot{\mathbf{q}}^{i_k} - (\mathbf{v}_1^{i_k})^T \dot{\mathbf{L}}^{i_k}(P^{i_k}) \dot{\mathbf{q}}^{i_k} \\ -(\dot{\mathbf{v}}_1^{j_k})^T \mathbf{D}_2^{i_k} \dot{\mathbf{q}}^{i_k} - (\mathbf{v}_1^{j_k})^T \dot{\mathbf{D}}_2^{i_k} \dot{\mathbf{q}}^{i_k} \\ -(\dot{\mathbf{v}}_1^{j_k})^T \mathbf{D}_3^{i_k} \dot{\mathbf{q}}^{i_k} - (\mathbf{v}_1^{j_k})^T \dot{\mathbf{D}}_3^{i_k} \dot{\mathbf{q}}^{i_k} \end{bmatrix} \tag{70}
 \end{aligned}$$

and

$$\begin{aligned}
 \mathbf{Q}_{d,\Psi}^{j_k} &= -\dot{\Psi}_{\mathbf{q}^{j_k}}^k \dot{\mathbf{q}}^{j_k} \\
 &= \begin{bmatrix} (\dot{\mathbf{v}}_1^{i_k})^T \mathbf{L}^{j_k}(P^{j_k}) \dot{\mathbf{q}}^{j_k} + (\mathbf{v}_1^{i_k})^T \dot{\mathbf{L}}^{j_k}(P^{j_k}) \dot{\mathbf{q}}^{j_k} \\ -(\dot{\mathbf{v}}_2^{i_k})^T \mathbf{D}_1^{j_k} \dot{\mathbf{q}}^{j_k} - (\mathbf{v}_2^{i_k})^T \dot{\mathbf{D}}_1^{j_k} \dot{\mathbf{q}}^{j_k} \\ -(\dot{\mathbf{v}}_3^{i_k})^T \mathbf{D}_1^{j_k} \dot{\mathbf{q}}^{j_k} - (\mathbf{v}_3^{i_k})^T \dot{\mathbf{D}}_1^{j_k} \dot{\mathbf{q}}^{j_k} \end{bmatrix} \tag{71}
 \end{aligned}$$

Since the planar joint is modeled by a set of scleronomic constraint equations, the partial derivative with respect to the time of the constraint vector associated with the prismatic joint is the zero vector.



3. Controller Synthesis for Articulated Mechanical Systems

3.1 State-Space Representation of Controlled Multibody Systems

To properly design a controller for a given articulated mechanical system, it is necessary to develop an accurate mathematical model of the mechanical system to be controlled so that realistic predictions, based on numerical experiments, can be made about the performance of the desired controller operating on the original system. Depending on the nature of the system model, it is possible to differentiate between linear mechanical systems and nonlinear mechanical systems [80]. While linear mechanical systems mathematically represent simple dynamical systems that require standard control algorithms, nonlinear mechanical systems are complex systems that require nonstandard control algorithms. In particular, multibody mechanical systems, such as the case study that is the object of the present investigation, belong to the latter category. Therefore, the development of control algorithms that are suited for these dynamic systems is particularly challenging. For both linear and nonlinear dynamical systems, however, a fundamental preliminary step, to be carried out before focusing on the design of a controller, is the state-space representation of the equations of motion. This is because this simple coordinate transformation allows for readily performing dynamical simulations by using standard numerical integration methods.

By using a multibody formulation in redundant coordinates, it is possible to write the index-1 dynamic equations for nonlinear multibody systems in the configuration space as follows:

$$\begin{cases} M\ddot{q} = Q_b + Q_u - C_q^T \lambda \\ C_q \ddot{q} = Q_d \end{cases} \quad (72)$$

where Q_u is a vector of dimensions $n_q \times 1$ representing the generalized force vector of the control actions and is given by:

$$Q_u = B_a u \quad (73)$$

where n_u is the number of control inputs, u is a vector having dimensions $n_u \times 1$ containing the control actions, and B_a is a matrix of dimensions $n_q \times n_u$ denoting the actuator collocation matrix.

As shown above, one can readily make use of the augmented formulation for calculating at each instant of time both the generalized acceleration vector \ddot{q} and the Lagrange multiplier vector λ of the multibody system, which are necessary for performing the dynamic analysis. In this vein, for conveniently evaluating the performance of the control system, it is necessary to transform the dynamical model of the multibody system under study from a representation in the configuration space to a representation in the state space. In general, the system behavior changes with time, and the information about its evolution can be captured by the rate-of-change variables within a system or in combinations of these variables and their time derivatives. In this respect, a set of system variables that describe the condition of the dynamical system at any instant in time are used to identify a state space model. These new variables are known as the state variables of the dynamical system [15]. Typically, the dimension of the set of state variables is equal to $n_z = 2n_q$. These state variables describe the behavior of a given dynamical and, for a multibody mechanical system, can be expressed as follows:

$$z = \begin{bmatrix} z_1 \\ z_2 \end{bmatrix} = \begin{bmatrix} q \\ \dot{q} \end{bmatrix} \quad (74)$$

where z is the system state vector having dimensions $n_z \times 1$ that can be partitioned into two blocks of dimensions $n_q \times 1$ given by $z_1 = q$ and $z_2 = \dot{q}$. It follows that the equations of motion of a generic nonlinear multibody mechanical system can be written in the state space as:

$$\dot{z} = f \quad (75)$$

being:

$$f = \begin{bmatrix} f_1 \\ f_2 \end{bmatrix} = \begin{bmatrix} \dot{q} \\ \ddot{q} \end{bmatrix} \quad (76)$$

where f is the system state function having dimensions $n_z \times 1$ that can be partitioned into two blocks of dimensions $n_q \times 1$ given by $f_1 = \dot{q}$ and $f_2 = \ddot{q}$. The state-space representation of the equations of motion of a multibody mechanical system also simplifies their numerical solution since it allows for the use of standard numerical integration schemes in the computer implementation, such as the explicit Runge-Kutta methods or the explicit Adams-Bashforth methods.

3.2 Nonlinear Controller Design for Controlled Multibody Systems

From a mathematical perspective, when considering the formal structure of a control policy, there are two types of controllers possible: open-loop controllers and closed-loop controllers [80]. Open-loop controllers, also known as feedforward controllers, are defined independently of the current state of the dynamical system to be controlled. On the other hand, closed-loop controllers, also known as feedback controllers, are based on detecting the current state of the dynamical system. In a typical scenario, an open-loop or feedforward controller is aimed at guiding the mechanical system of interest from its initial configuration to a final configuration, which should be as close as possible to the desired one. Conversely, a closed-loop or feedback controller is meant for compensating as much as possible for the error of the final configuration achieved by the mechanical system when it is near to the desired one.

One drawback of feedforward controllers is that this class of control systems is not very robust because the control law does not depend on the actual fulfillment of the goals set for the controller since this verification can be done only by measuring the current state of the dynamical system. Feedback controllers are, in general, very robust because the control law depends on the current measurement of the system state and, therefore, it is possible to verify the actual achievement of the objectives set for the controller. In fact, when adopting a feedback control strategy, by properly using sensors capable of partially or totally capturing the time evolution of the system state, it is possible to measure the controlled variable and have an indication of whether or not the control system is working properly, whereas this is not the case when employing a pure feedforward control approach. However, the most effective and successful control strategies are generally formulated by combining a feedforward control approach and a feedback control technique.

Before start delving into the analysis of the mathematical structure of the simple but effective control systems suitable for multibody mechanical systems, it is convenient to focus on the specific control goals to be achieved by the control approach of the adaptive lifting table considered as the case study of this investigation. In the case study of this paper, to solve simultaneously three separate control problems, three control laws need to be devised. The first control problem to be solved deals with the gross motion control of the position of the platform. More specifically, starting from a set of operative conditions, the desired elevation of the adaptive lifting table must be obtained. This problem is solved by designing a first driving controller that serves for guiding



the motion in large of the platform. The second control problem to be solved concerns the fine motion control of the position of the platform. More precisely, the goal of this second controller is to monitor the position of the platform when reaching the desired elevation. This problem is solved by designing a second compensation controller aimed at correcting the position errors made by the first control system when approaching the desired set point and guiding the fine motion of the platform. The third and last control problem to be solved is relevant to the definition of a safety controller. This problem is solved by devising a start-and-stop controller for guaranteeing perimeter safety. This controller ensures that the operator stays sufficiently distanced from the machine during its movement, thereby preventing the risk of accidents.

The objective of a control system is to affect the dynamics of the multibody system of interest in order to achieve desirable dynamical behavior. More specifically, controlling a dynamical system means properly designing the time laws of the manipulable mechanical actions to obtain an advantageous dynamic behavior, which can be devised in advance by solving motion planning tasks. Depending on the nature of the dynamical system, the control actions that need to be applied to the system itself can be forces, torques, and moments, whereas the desired behavior can be formulated in terms of preassigned time laws for the positions, velocities, and generalized accelerations of the system.

Control systems typically have two goals: regulation and tracking. In a regulation problem, the system is controlled to maintain its output as close as possible to a certain set point. In a tracking problem, the system is controlled so that its output follows as precisely as possible a particular desired trajectory. The stabilization problem is a particular example of the regulation problem. In this case, a control system is intended to drive the system towards the rest configuration from any nonzero initial conditions. Thus, the desired set point of the regulation problem is the zero vector. Due to the nature of the problem to be solved, a special but very important class of control systems, namely state-feedback controllers [69], is considered in this investigation. In this type of control system, the control input is a function of the system states. Furthermore, an appropriate set of feedback parameters is introduced to construct the control actions, and the mathematical structure that defines the controller can be linear or nonlinear.

Among the category of feedback controllers, there are several advanced control techniques. One of the most simple and effective control strategies, which is very common in industrial engineering applications because of its versatility, is the Proportional-Integral-Derivative (PID) control method [15]. In combination with an inverse dynamics control approach, the PID control strategy is adopted in the present work for guiding the motion of the adaptive lifting platform employed in the paper as the case study [99]. In the definition of a PID controller, the control actions are formulated by considering the instant variations of the state variables of the dynamical system of interest. More specifically, the input of a general PID controller is the error function calculated by comparing the actual dynamical behavior and the desired time evolution of the dynamic system [100]. The current time evolution of the mechanical system is measured through the use of sensors, which must be properly collocated on the system, whereas the desired behavior assumed as the reference is determined in advance to satisfy the design goals of the control policy.

By denoting the total control action of a PID controller with the vector u of dimensions $n_u \times 1$, this vector can be written as the sum of three separate contributions. The first contribution is a vector of dimensions $n_u \times 1$ indicated as u_p that represents a term proportional to the error function. The second contribution is a vector of dimensions $n_u \times 1$ indicated as u_i that represents a term proportional to the integral over time of the error function. The third contribution is a vector of dimensions $n_u \times 1$ indicated as u_d that represents a term proportional to the derivative over time of the error function. Thus, the total vector of control actions can be expressed as:

$$u = u_p + u_i + u_d = -K_p e - K_i \bar{e} - K_d \dot{e} \tag{77}$$

being:

$$e = q - q_d, \quad \bar{e} = \int_0^t e d\tau, \quad \dot{e} = \frac{de}{dt} \tag{78}$$

where τ is a dummy time variable, q_d represents the desired configuration vector of the multibody mechanical system having dimensions $n_q \times 1$, while K_p , K_i , and K_d denote three coefficient matrices of dimensions $n_q \times n_q$ that respectively identify the proportional, integral, and derivative terms of the PID controller [101]. According to the control strategy mentioned before, the corresponding closed-loop control scheme is represented in Figure 3.

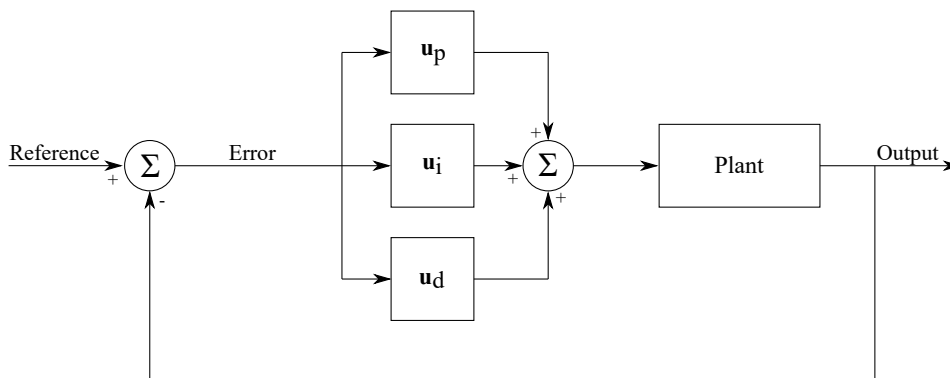


Fig. 3. PID controller scheme.

When used to solve the motion control problem of the mechanical system of interest, to achieve good performance of the control system, the coefficient matrices that specifically define the characteristics of a given PID controller must be properly tuned, and this is often a trial-and-error iterative process [80]. In general, the behavior summarized in Table 1 indicates how the overall performance of a generic PID control system varies when the control parameters are adjusted.

A preliminary calibration of the control parameters can be conveniently carried out by exploiting the Ziegler-Nichols method, which, however, must be subsequently modified and refined through an objective analysis of the performance resulting from dynamical simulations. This approach is a heuristic tuning technique developed by John G. Ziegler and Nathaniel B. Nichols in the 1940s to get a proper estimation of the numerical values of the controller parameters [102]. First, the gains denoted with K_i and K_p are initially set to zero. The proportional gain K_p is then increased until it reaches the ultimate gain referred to as K_u , at which point the output of the control loop begins to continually oscillate. Subsequently, by using the numerical values of K_u and the oscillation period T_u so found, the final gains are set as shown in Table 2.



Table 1. Effect of independent increase of each one of the PID parameters.

PARAMETER	RISE TIME	OVERSHOOT	SETTLING TIME	ASYMPTOTIC ERROR	STABILITY
K_p	Decreases	Increases	Minor Changes	Decreases	Improves
K_i	Decreases	Increases	Increases	Deleted	Improves
K_d	Increases	Decreases	Decreases	No Effect	Deteriorates

Table 2. Tuning the numerical values of the controller parameters according to the Ziegler-Nichols method.

CONTROL TYPE	K_p	K_i	K_d
P	$0.50K_u$		
PI	$0.45K_u$	$0.54K_u/T_u$	
PID	$0.60K_u$	$1.2K_u/T_u$	$3K_uT_u/40$

The main advantage of the Ziegler-Nichols method is that the online tuning requires no tuning parameters, making it simple to deploy and use in practice. However, the disadvantages are the process upsets that may occur during tuning, resulting in excessively aggressive parameters [103]. For example, the method does not work well when applied to time-delayed processes.

In conclusion, it is important to note that the PID control technique described before can be interpreted as a combination of feedforward plus feedback control methods. This is because, in general, the reference dynamical behavior utilized for the multibody system is an optimized time law, which results from the solution of the motion planning problem that must be carried out in advance.

4. SOLIDWORKS CAD Model

4.1 Design Constraints Identification

This section examines the design constraints imposed on the realization of the physical prototype of the adaptive lifting table and analyzes the various system components and mechanical parts that form the CAD assembly.

The main goal is to use the lifting table to load and empty a pallet up to a maximum weight of 1000 (kg). To materially achieve this goal, the lifter is actuated by a rack and pinion mechanism. The system will be able to reach a maximum height of 1 (m) since this reference height is the result of consolidated ergonomic studies [75]. This measure comes out of biomechanical evaluations that allow for achieving an optimal range of height of the work surface in manual work conditions, in which there is no flexion of the trunk and an appropriate angle rotation is considered for the shoulder. The reference height of the moving platform is selected by considering that the ideal height of the working platform for a female worker is 0.81 (m) when the height of the worker falls within the fifth percentile. Similarly, the ideal height of the working platform for a male worker is 1.12 (m) when the height of the worker falls within the ninety-fifth percentile. Remembering that the fifth percentile for the height parameter is the value relative to which only 5 % of the population considered has a lower height, and the ninety-fifth percentile is the value relative to which only 5 % of the population considered has a higher height, and that, on average, men are taller than women, given the greater presence of men in goods lifting jobs, a height of 1 (m) seemed to be the right compromise within the defined range 0.81 (m) - 1.12 (m). However, by exploiting the adaptive mechanism devised in this work, the height can be adjusted according to the actual height of the operator. In fact, the lifter is automated to ensure that the optimal height is reached and to guarantee a comfortable posture for the operator based on a stable working platform having a constant height. To do this, the height variation is necessarily inversely proportional to the load collocated on the platform.

In summary, the goal is to realize an empty working platform at an elevation of 1 (m), whereas a full platform with an assumed maximum load of 1000 (kg) at an elevation of 0 (m). Since the surface area of a pallet is about 0.96 (m²), the density expected from the goods will be around 1.04 (kg/dm³). In the case of working with different goods, thus of different densities from the one just defined, the lifter will still yield the desired behavior by changing the control parameters.

4.2 CAD Model Development

At this stage, it is possible to carry out the analysis and description of the main mechanical components that form the adaptive lifting table considered as the case study of this investigation. The CAD model of the lifter developed in this work is shown in Figure 4.

The main components of the adaptive pantograph mechanism are described below, whereas the design choices and the couplings are briefly outlined as well.

4.2.1 Structural Frame

The lower base has a standard shape (item 1 in Figure 4). In particular, it was designed according to construction needs with flanges and brackets properly inserted, whose fixing is guaranteed by welding. The stability of the basement, and, as a result, of the entire structure fastened to the ground, is guaranteed by large structural elements through screws, which are anchored to the concrete base endowed with proper dowels. The basement is designed to be placed below the floor level. By doing so, in correspondence with the closure of the scissor system, the upper base is tangent to the ground. The upper base, on the other hand, deviates from the standard configuration to allow an optimal force measurement of the load cells. This is done by inserting a tubular structure to which the arms are constrained and then placing a cover fixed exclusively to the cells (item 3 in Figure 4). Welded tubular connections were placed between the arms to guarantee synchronous movement (item 2 in Figure 4).

4.2.2 Mechanical Couplings

On the inner arms, welded pins were also inserted to provide the locking by interference with the outer arms, thereby ensuring a rest position corresponding to the minimum height (Figure 5).

The couplings between the inner arms, the outer arms, and the basements were achieved in the same way by using pivots, bushings, washers, and Seeger rings (Figure 5a). Given the short rotations that the arms perform, the use of bushings was chosen



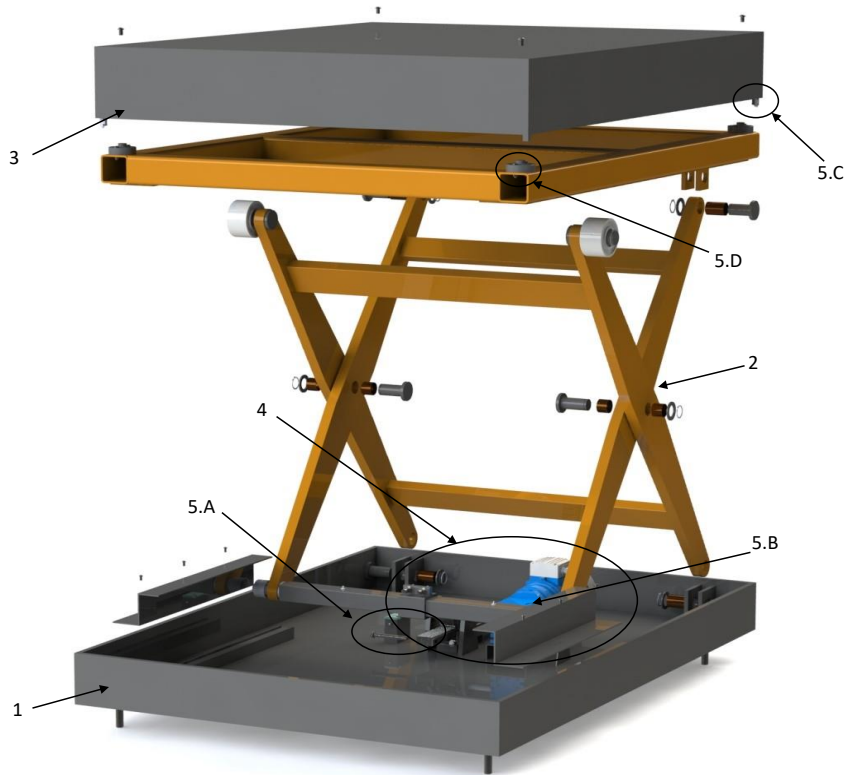
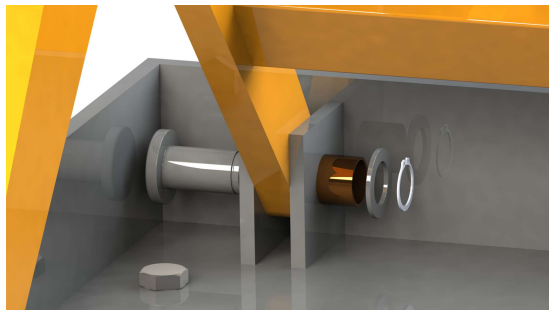
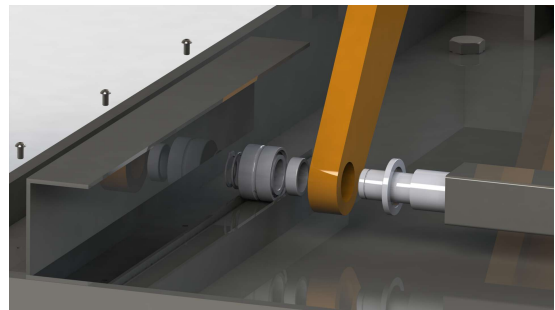


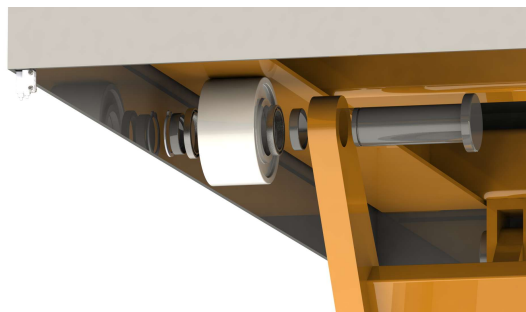
Fig. 4. CAD exploded view of the pantograph adaptive lifter mechanism with references to the various components. The body numbering is as follows: 1: Lower Base; 2: Arms; 3: Upper Base; 4: Electric Motor and Transmission; 5. A, 5. B, 5. C, and 5. D: Sensors.



(a) Revolute joint between the lower base and the outer arm.



(b) Revolute joint between the inner arm and the connecting rod.



(c) Revolute joint between the upper base and the inner arm.

Fig. 5. Mechanical joints disassembly.

because the use of bearings seemed exaggerated or not appropriate. The sliding of the connecting rod between the arms on the lower base is ensured by the use of a double row of roller bearings to obtain maximum resistance under radial loads (Figure 5b). The sliding of the outer arms with the upper basement is realized by using pins, a double row of bearings, and a Polytetrafluoroethylene (PTFE) wheel (Figure 5c).



4.2.3 Motor and Transmission

As far as the selection of the electric motor and the corresponding mechanical transmission is concerned, it is important to emphasize that one peculiarity of the adaptive mechanism developed in the present work is in the use of a rack and pinion mechanical transmission (item 4 in Figure 4). This solution is not very common in this field due to the long strokes and high loads applied to the platform. However, the mechanical system designed in this study was made as stable as possible with the introduction of proper guides and reinforcement brackets (Figure 6).

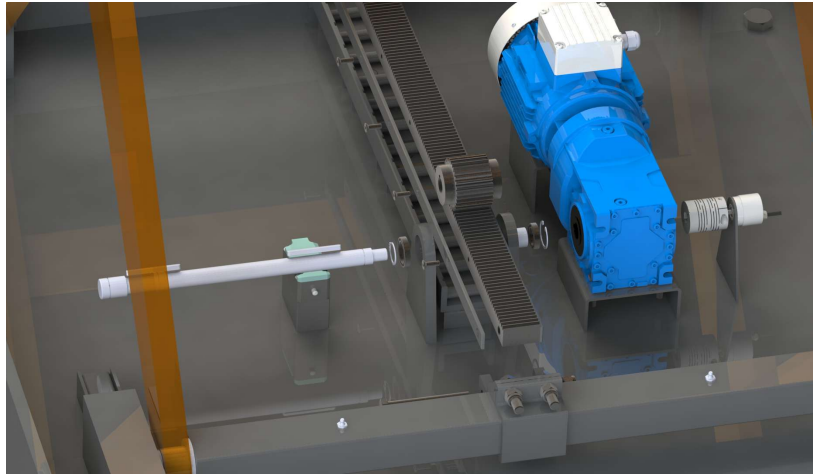


Fig. 6. Top view of the mechanical transmission disassembly.

The rack is constrained through brackets to the connecting rod and tightened by friction, using two bolts, to reinforcements with a square-shaped section, which runs along the entire connecting rod between the arms. The rack was also reinforced with brackets along its entire length and blocked with countersunk head screws in blind holes, whereas the motor and the gearbox were locked to the lower base. For the electric motor, a DC brushless motor was chosen, modulated with an inverter coupled to a reducer.

4.2.4 Electromechanical Sensors

A set of proprioceptive and exteroceptive sensors were considered in the design phase (Figure 7). These are a sensor for detecting the height of the scissor platform, one for measuring the weight of the packages and the adaptation to the desired height, and the last one for monitoring the perimeter security to stop the movement of the platform if there is interference in the closure of the lifter. For the measurement of the desired height (item 5.A in Figure 4), redundant sensors are planned to be installed. These are proximity sensor that provides the displacement of the connecting rod between the arms (Figure 7a). An absolute, non-incremental encoder is used to indicate the displacement of the rack (item 5.B in Figure 4), and this is done by measuring the rotation of the pinion (Figure 7b). Furthermore, in order to measure the weight of the packages between the upper basement and the cover (item 5.D in Figure 4), load cells are employed (Figure 7c). For the perimeter sensors (item 5.C in Figure 4), photocells or photoelectric sensors were installed and connected on the edge of the cover that blocks the system if any obstacle interferes with the signal between the transmitter and receiver (Figures 7d, 7e). To do this, however, eight photocells will be installed, two for each edge. To reduce the costs of these sensors, some appropriate reflectors were inserted in two diagonally opposite corners, thereby keeping only four sensors in the remaining two corners. All the mechanical components are fixed to welded flanges. The sensors are glued with screws and nuts, and the reflectors are strictly arranged at 45 (deg) for correct signal transmission.

5. SIMSCAPE MBD Model

5.1 Geometric Model Description

In this section, the adaptive mechanism considered as the case study of the paper is analyzed in detail in order to develop a multibody model by using SIMSCAPE MULTIBODY. The scissor lift table of interest for this research work is modeled as a multibody mechanical system composed of the following six rigid bodies: Lower Base (body $i = 0$), Inner Arm (body $i = 1$), Outer Arm (body $i = 2$), Connecting Rod (body $i = 3$), Roller (body $i = 4$), and Upper Base (body $i = 5$). Therefore, in the analytical formulation of the equations of motion, the mobile rigid bodies are five, where the number of rigid bodies is denoted with $N_b = 5$. To identify the configuration of each body without ambiguity, a set of generalized coordinates must be selected such that the location of an arbitrary point on the body can be described in terms of these generalized coordinates. For each rigid body, the number of these coordinates, called Lagrangian coordinates, is $n_b = n_d + n_p = 7$. This is because, in the SIMSCAPE MULTIBODY software, the set of Euler parameters, in number equal to $n_p = 4$, is employed to describe the three-dimensional pose of each body, whereas the displacement coordinates necessary for identifying the absolute position of the reference point of each body are in number simply equal to $n_d = d = 3$. Thus, the total number of generalized coordinates of the multibody mechanical system is indeed equal to $n_q = N_b n_b = 35$.

The generalized coordinates of the multibody system at hand, however, are not totally independent because of the presence of the mechanical joints that connect adjacent bodies. Consequently, the motion of each component in the multibody system is influenced by the motion of the others through the kinematic constraints, which restrict the displacement and velocity of each body. In order to understand and control the motion of the multibody system, a group of independent generalized coordinates defined as degrees of freedom can be identified. Each rigid body is connected to the other by a mechanical joint that is mathematically modeled as a kinematic constraint. A detailed discussion about the nature and the type of algebraic constraints necessary for modeling the adaptive scissor mechanism as a multibody mechanical system is provided below.



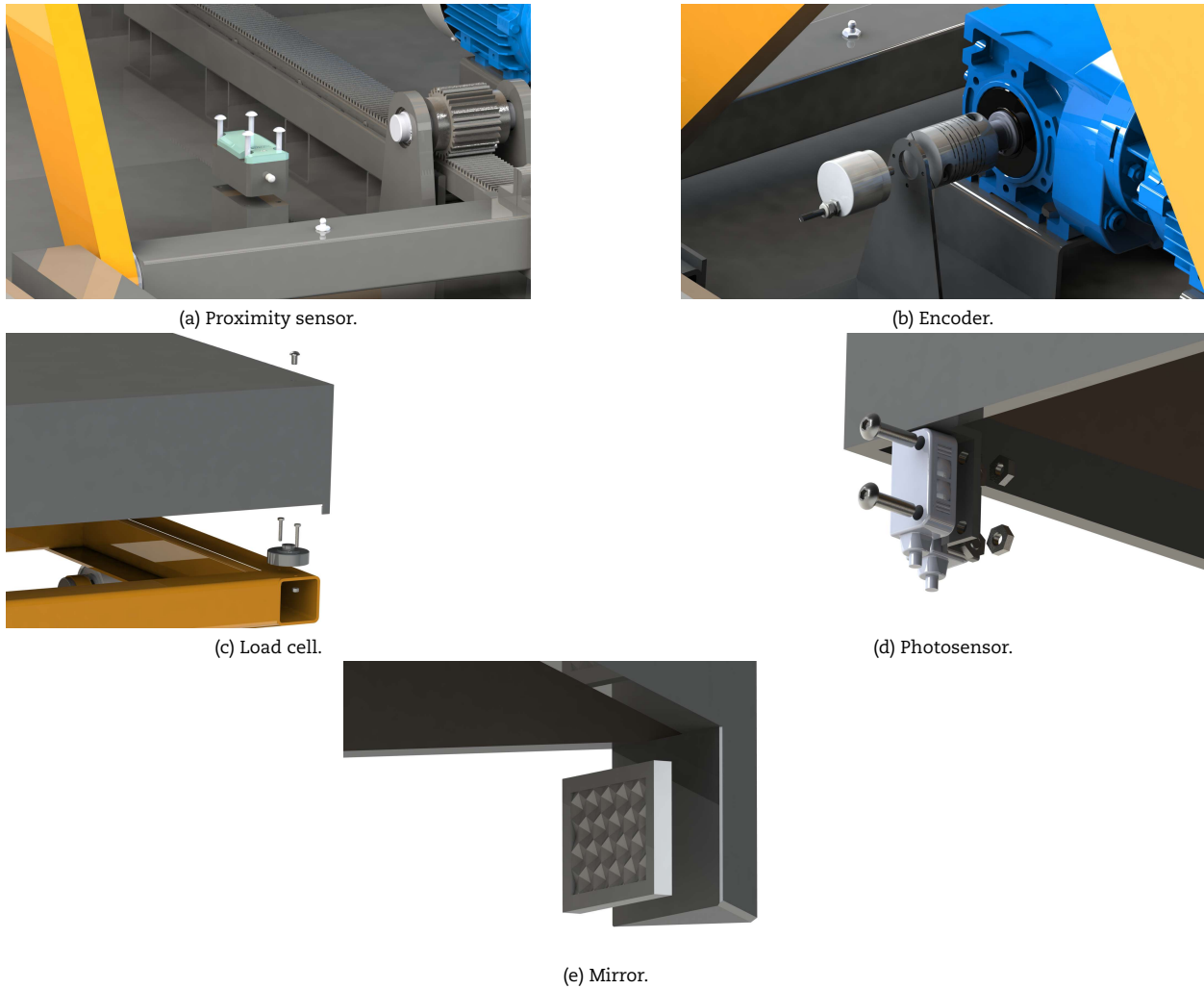


Fig. 7. Disassembled view of all the equipped sensors.

5.2 Mechanical Constraints Identification

A constraint is a massless mechanical device constructed in such a way as to limit the relative motion between the rigid bodies it connects [81]. Mechanical joints can be described mathematically by using a set of nonlinear algebraic constraint equations. Assuming that these constraint equations are linearly independent, each constraint equation indirectly defines a possible system motion since it directly formalizes the motions that are not permitted. In the analyzed multibody system, there are eight mechanical constraints and, therefore, the number of mechanical joints will be indicated by $N_c = 8$. The list of mechanical joints considered for the multibody system under study is provided below, where n_c^k denotes the number of algebraic equations associated with the generic kinematic constraint labeled with the integer k :

- Planar Joint 1 (Upper Base $i_k = 5 \sim$ Roller $j_k = 4$): $n_c^k = 3$.
- Planar Joint 2 (Lower Base $i_k = 0 \sim$ Upper Base $j_k = 5$): $n_c^k = 3$.
- Revolute Joint 1 (Inner Arm $i_k = 1 \sim$ Connecting Rod $j_k = 3$): $n_c^k = 5$.
- Revolute Joint 2 (Roller $i_k = 4 \sim$ Outer Arm $j_k = 2$): $n_c^k = 5$.
- Revolute Joint 3 (Lower Base $i_k = 0 \sim$ Outer Arm $j_k = 2$): $n_c^k = 5$.
- Revolute Joint 4 (Outer Arm $i_k = 2 \sim$ Inner Arm $j_k = 1$): $n_c^k = 5$.
- Revolute Joint 5 (Upper Base $i_k = 5 \sim$ Inner Arm $j_k = 1$): $n_c^k = 5$.
- Prismatic Joint (Connecting Rod $i_k = 3 \sim$ Lower Base $j_k = 0$): $n_c^k = 5$.

In the initial configuration of the lifting table assumed in the multibody model constructed by employing SIMSCAPE MULTIBODY, Table 3 shows the constraint types, the bodies interconnected by the kinematic pairs, and the position of the reference system connected to the base part of each constraint block.

In the geometric formulation of the kinematic joints, the absolute rotation axis of each revolute joint is the z-axis, the absolute axis orthogonal to Planar Joint 1 is the y-axis, the absolute axis orthogonal to Planar Joint 2 is the z-axis, and the absolute translation axis of the Prismatic Joint is the x-axis.

Considering the normalization conditions of each set of Euler parameters, the total number of intrinsic constraint equations is $n_{c,\Phi} = N_b = 5$. By inspecting the type and the number of kinematic constraints reported in Table 3, the total number of extrinsic



Table 3. Constraint positioning data in the SIMSCAPE MULTIBODY environment.

CONSTRAINT TYPE	BODIES CONNECTED BY THE CONSTRAINT	ABSOLUTE CONSTRAINT POSITION (mm)
Planar Joint 1	(Roller, Upper Base)	$\begin{bmatrix} -62.5 & 1322.0 & 0 \end{bmatrix}^T$
Planar Joint 2	(Lower Base, Upper Base)	$\begin{bmatrix} -62.5 & 1367.0 & 0 \end{bmatrix}^T$
Revolute Joint 1	(Inner Arm, Connecting Rod)	$\begin{bmatrix} 624.0 & 80.0 & -413.0 \end{bmatrix}^T$
Revolute Joint 2	(Roller, Outer Arm)	$\begin{bmatrix} 624.0 & 1267.0 & -443.0 \end{bmatrix}^T$
Revolute Joint 3	(Lower Base, Outer Arm)	$\begin{bmatrix} -765.0 & 80.0 & -542.0 \end{bmatrix}^T$
Revolute Joint 4	(Inner Arm, Outer Arm)	$\begin{bmatrix} -70.6 & 674.0 & -443.0 \end{bmatrix}^T$
Revolute Joint 5	(Upper Base, Inner Arm)	$\begin{bmatrix} -765.0 & 1267.0 & -413.0 \end{bmatrix}^T$
Prismatic Joint	(Connecting Rod, Lower Base)	$\begin{bmatrix} -105.0 & 94.0 & 22.5 \end{bmatrix}^T$

constraint equations is $n_{c,\Psi} = \sum_{k=1}^{N_c} n_c^k = 36$. As a result, the total number of algebraic constraint equations that appear in the multibody model is $n_c = n_{c,\Phi} + n_{c,\Psi} = 41$.

The thorough analysis of the kinematic constraints provided above has a twofold objective, that is, to construct an accurate multibody model of the adaptive lift table and to correctly identify the degrees of freedom of this system considered as the case study. It is, in fact, apparent that the lift mechanism has only one degree of freedom. Therefore, the mechanical joints forming the multibody model described before lead to a redundant set of algebraic equations. This can be readily proved through the following reasoning. In general, the number of system degrees of freedom is defined as the number of the system coordinates minus the number of independent constraint equations. For a multibody mechanical system endowed with n_q generalized coordinates and n_c independent constraint equations, the number of system degrees of freedom is given by $n_f = n_q - n_c$. For the rigid multibody system at hand, one obtains $n_f = -6$, which is obviously an incorrect result since the redundant constraint equations were not identified and discarded. This means that there are in total seven redundant constraint equations, where, for the sake of clarity, this number is denoted with n_r .

The list of redundant constraint equations associated with each mechanical joint is provided below, where n_r^k denotes the number of algebraic equations associated with the generic kinematic constraint labeled with the integer k :

- Planar Joint 1 (Upper Base $i_k = 5 \sim$ Roller $j_k = 4$): $n_r^k = 1$.
- Planar Joint 2 (Lower Base $i_k = 0 \sim$ Upper Base $j_k = 5$): $n_r^k = 3$.
- Revolute Joint 1 (Inner Arm $i_k = 1 \sim$ Connecting Rod $j_k = 3$): $n_r^k = 0$.
- Revolute Joint 2 (Roller $i_k = 4 \sim$ Outer Arm $j_k = 2$): $n_r^k = 0$.
- Revolute Joint 3 (Lower Base $i_k = 0 \sim$ Outer Arm $j_k = 2$): $n_r^k = 0$.
- Revolute Joint 4 (Outer Arm $i_k = 2 \sim$ Inner Arm $j_k = 1$): $n_r^k = 0$.
- Revolute Joint 5 (Upper Base $i_k = 5 \sim$ Inner Arm $j_k = 1$): $n_r^k = 0$.
- Prismatic Joint (Connecting Rod $i_k = 3 \sim$ Lower Base $j_k = 0$): $n_r^k = 3$.

The redundant constraint equations were identified by reasoning sequentially. The revolute joints do not create redundancies as each body is free to rotate around its own axis. The Prismatic Joint adds redundant constraint equations involving the rotations around the absolute x-axis and y-axis, as well as the translation along the absolute z-axis, which are already constrained by Revolute Joint 1. Planar Joint 1 adds redundant constraint equations involving the rotation around the absolute x-axis, already constrained by the presence of Revolute Joint 5 and Revolute Joint 2. The constraint equations added by Planar Joint 2 are instead redundant as they involve the rotations around the absolute x-axis and y-axis, as well as the translation along the absolute z-axis because of the presence of Revolute Joint 5. Consequently, the total number of redundant constraint equations is $n_r = \sum_{k=1}^{N_c} n_r^k = 7$, while the effective number of degrees of freedom $n_{f,e} = n_f + n_r = 1$. It is important to note that the inclusion of the Planar Joint 2 in the SIMSCAPE MBD model, despite its total redundancy from a kinematic viewpoint, is justified by the need to maintain a convenient reference for performing measurements in the computer implementation of the multibody model.

Finally, to complete the description of the multibody model implemented in the SIMSCAPE MULTIBODY software, the type and the number of external actions acting on the multibody system are the gravity force acting on each rigid body and the control forces acting on the Connecting Rod through the Prismatic Joint, being $N_e = N_b = 5$ the total number of external forces and $N_a = 1$ the total number of control actions.

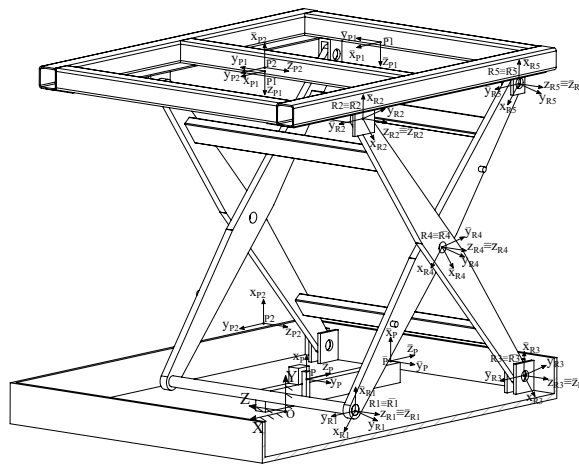


5.3 MBD Model Development

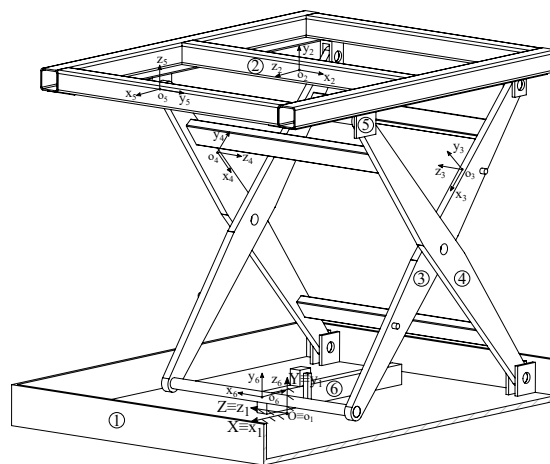
For constructing the multibody model in SIMSCAPE MULTIBODY starting from the geometric model originally developed in SOLIDWORKS, a general simplification was necessary because of the problems deriving from the computer simulation of a complex model having redundant constraints. To avoid approximation errors due to the numerical integration of an articulated dynamical model, the recognition of the kinematic constraints not useful for simulating the behavior of the multibody model was eluded, since this process also slows down the dynamical simulations. Despite the simplifications assumed for the multibody model, the same material properties as for the not simplified model were used to not affect the dynamic response of the dynamical system.

From a kinematic point of view, the main simplification made with respect to the SOLIDWORKS model is that the rack-and-pinion type transmission, and its corresponding block implemented in SIMSCAPE MULTIBODY, were replaced with a simplified transmission based on an equivalent prismatic joint. More specifically, between the base and the connecting rod of the multibody model developed using SIMSCAPE MULTIBODY, a prismatic joint was considered to guarantee only the translation between the surfaces of the connecting rod of the arms, which simulate those of the rack and the surfaces obtained on the base that simulates those of the pinion, so that the contact occurs on the nominal diameter or pitch diameter.

The MBD model used in SIMSCAPE MULTIBODY, properly simplified from the CAD model constructed in SOLIDWORKS, is reported in Figure 8.



(a) Position and orientation of the reference frames of the constraints in the initial configuration.



(b) Position and orientation of the CAD frame of each body in the initial configuration.

Fig. 8. Multibody model of the adaptive lifting table developed in the SIMSCAPE MULTIBODY environment. The overbar symbols in Figure 8a refer to reference systems that in the constraint blocks in SIMSCAPE MULTIBODY are connected to the follower port, the others to the base port. In Figure 8b, the body numbering is as follows: 1: Lower Base; 2: Upper Base; 3: Inner Arm; 4: Outer Arm; 5: Roller; 6: Connecting Rod.

During import from SOLIDWORKS, the CAD reference frame is self-generated by SIMSCAPE MULTIBODY and, therefore, it will be referred to as the CAD frame. In the computer simulations performed using SIMSCAPE MULTIBODY, the initial configuration considered for the multibody system at hand is that of maximum pantograph opening, that is, that of maximum lifting platform height.

The inertia properties of the rigid bodies used for modeling the mechanical components of the lifting mechanism are shown in Table 4, where the inertia matrices and the coordinates of the centroid reference system are both expressed with respect to the CAD



frames of each body.

Table 4. Geometric and inertial data of rigid bodies used in the SIMSCAPE MULTIBODY model.

BODY	BODY MASS (kg)	INERTIA MATRIX (kg × mm ²)	CENTROID LOCAL POSITION COORDINATES (mm)
Lower Base	$m = 402.0$	$I_{xx} = 6.038 \cdot 10^7$ $I_{yy} = 1.690 \cdot 10^8$ $I_{zz} = 1.097 \cdot 10^8$ $I_{xy} = I_{yx} = 6.441 \cdot 10^2$ $I_{xz} = I_{zx} = -8.244 \cdot 10^2$ $I_{yz} = I_{zy} = 1.426 \cdot 10^5$	$\bar{x} = -7.2$ $\bar{y} = 27.1$ $\bar{z} = 0$
Upper Base	$m = 84.0$	$I_{xx} = 2.097 \cdot 10^7$ $I_{yy} = 3.836 \cdot 10^7$ $I_{zz} = 1.759 \cdot 10^7$ $I_{xy} = I_{yx} = -1.124 \cdot 10^5$ $I_{xz} = I_{zx} = 3.470 \cdot 10^{-2}$ $I_{yz} = I_{zy} = -15.600$	$\bar{x} = 0$ $\bar{y} = 0$ $\bar{z} = 0$
Inner Arm	$m = 71.2$	$I_{xx} = 1.265 \cdot 10^7$ $I_{yy} = 2.303 \cdot 10^7$ $I_{zz} = 1.055 \cdot 10^7$ $I_{xy} = I_{yx} = 0$ $I_{xz} = I_{zx} = 0$ $I_{yz} = I_{zy} = 4.292 \cdot 10^5$	$\bar{x} = 259.0$ $\bar{y} = -86.4$ $\bar{z} = 428.0$
Outer Arm	$m = 79.6$	$I_{xx} = 1.495 \cdot 10^7$ $I_{yy} = 2.708 \cdot 10^7$ $I_{zz} = 1.231 \cdot 10^7$ $I_{xy} = I_{yx} = 0$ $I_{xz} = I_{zx} = 0$ $I_{yz} = I_{zy} = 5.025 \cdot 10^5$	$\bar{x} = -287.0$ $\bar{y} = -90.2$ $\bar{z} = 458.0$
Roller	$m = 3.3$	$I_{xx} = 3.348 \cdot 10^5$ $I_{yy} = 1.684 \cdot 10^3$ $I_{zz} = 3.348 \cdot 10^5$ $I_{xy} = I_{yx} = 0$ $I_{xz} = I_{zx} = 0$ $I_{yz} = I_{zy} = 0$	$\bar{x} = 0$ $\bar{y} = 0$ $\bar{z} = -483.0$
Connecting Rod	$m = 28.2$	$I_{xx} = 1.822 \cdot 10^6$ $I_{yy} = 2.380 \cdot 10^6$ $I_{zz} = 0.844 \cdot 10^5$ $I_{xy} = I_{yx} = 5.198 \cdot 10^4$ $I_{xz} = I_{zx} = 0$ $I_{yz} = I_{zy} = 0$	$\bar{x} = -265.7$ $\bar{y} = -16.1$ $\bar{z} = 0$

Table 5, on the other hand, shows the rotation matrices and the absolute position of the CAD reference frame with respect to the inertial reference frame.

In the initial modeling endeavor, the implementation of the multibody model performed by using SIMSCAPE MULTIBODY wanted to exactly reproduce the same type of mechanical transmission. However, once the conversion of the model was carried out, implementation issues were encountered in the simulation of the control phase, with the impossibility of inserting the initial conditions leading to unsatisfactory results. As shown in Table 6, despite the drawback, the first inverse dynamics analysis, with the use of the "Gear - Rack and Pinion" type constraint block in SIMSCAPE MULTIBODY, provided reliable results, which given the high fidelity of the model to reality.

The numerical results shown in Table 6 are similar to those of the simplified model, in which the implementation of the complete model was carried out. It must be emphasized that, despite this simplification, the torque values obtained before and after the simplification are equal, which demonstrates the correctness of the simplification carried out. This fact proves the reliability of the results obtained from the simplified multibody model, as reported in Table 6.



Table 5. Position and orientation vectors of the initial configuration of the rigid bodies in the SIMSCAPE MULTIBODY model.

BODY	CAD FRAME			CAD FRAME ABSOLUTE POSITION COORDINATES (mm)
	ROTATION MATRIX $A = \begin{bmatrix} \alpha & \beta & \gamma \end{bmatrix}$			
Lower Base	$\alpha = \begin{bmatrix} 1 & 0 & 0 \end{bmatrix}^T$	$\beta = \begin{bmatrix} 0 & 1 & 0 \end{bmatrix}^T$	$\gamma = \begin{bmatrix} 0 & 0 & 1 \end{bmatrix}^T$	$x = 0$ $y = 0$ $z = 0$
Upper Base	$\alpha = \begin{bmatrix} 0 & 0 & 1 \end{bmatrix}^T$	$\beta = \begin{bmatrix} 0 & 1 & 0 \end{bmatrix}^T$	$\gamma = \begin{bmatrix} 1 & 0 & 0 \end{bmatrix}^T$	$x = -63$ $y = 1367$ $z = 0$
Inner Arm	$\alpha = \begin{bmatrix} 0.569 & -0.822 & 0 \end{bmatrix}^T$	$\beta = \begin{bmatrix} 0.822 & 0.569 & 0 \end{bmatrix}^T$	$\gamma = \begin{bmatrix} 0 & 0 & 1 \end{bmatrix}^T$	$x = -510$ $y = 957$ $z = -428$
Outer Arm	$\alpha = \begin{bmatrix} -0.569 & -0.822 & 0 \end{bmatrix}^T$	$\beta = \begin{bmatrix} -0.822 & 0.569 & 0 \end{bmatrix}^T$	$\gamma = \begin{bmatrix} 0 & 0 & -1 \end{bmatrix}^T$	$x = -275$ $y = 957$ $z = 458$
Roller	$\alpha = \begin{bmatrix} 1 & 0 & 0 \end{bmatrix}^T$	$\beta = \begin{bmatrix} 0 & 0 & -1 \end{bmatrix}^T$	$\gamma = \begin{bmatrix} 0 & 1 & 0 \end{bmatrix}^T$	$x = -20$ $y = 1267$ $z = 483$
Connecting Rod	$\alpha = \begin{bmatrix} 0 & 0 & 1 \end{bmatrix}^T$	$\beta = \begin{bmatrix} 0 & 1 & 0 \end{bmatrix}^T$	$\gamma = \begin{bmatrix} -1 & 0 & 0 \end{bmatrix}^T$	$x = -20$ $y = 80$ $z = 0$

Table 6. Comparison table between the torque obtained by computer simulations using SIMSCAPE MULTIBODY on the rack and pinion mechanism and that obtained from the equivalent mechanism.

LOAD (kg)	TORQUE ON THE EQUIVALENT MEMBER (N × m)	TORQUE ON RACK AND PINION (N × m)	RELATIVE ERROR (%)
1000	0	0	0
750	855.9	858.3	0.28
500	368.8	369.4	0.16
250	148.9	149.1	0.13
0	37.9	38.0	0.26

6. Numerical Results and Discussion

6.1 General Approach Followed for Performing the Computer Simulations

This section deals with the final multibody models used for computer simulations and the results obtained through numerical experiments. Because a simulated object replaces the mechanical system that needs to be studied, simulation modeling represents a modern research technique. To acquire useful insights into the behavior of mechanical systems being studied, several numerical experiments can be quickly carried out with its virtual prototype and, therefore, it is practical to apply simulation modeling to resolve the given tasks. The information that can be extracted after performing the required computations is relevant for a variety of subsystems, especially for actuator selection and the subsequent control law definition. In addition, the CAD programs make it possible to choose the design parameters that have a direct impact on the dynamics of a three-dimensional model, such as mass, moments of inertia, and the location of the center of mass of each component.

Software like SOLIDWORKS, MATLAB, and SIMULINK can be used to simulate the motion and the degrees of freedom allowed for the articulated mechanical system analysis. In particular, a computational tool of the SIMULINK/MATLAB software suite, the SIMSCAPE MULTIBODY software-modeling tool, offers block simulation of complicated dynamic systems based on visually oriented programming techniques. The interaction between SIMSCAPE MULTIBODY and other SIMULINK/MATLAB library elements enhances simulation possibilities. For example, because the moment of inertia and the coordinates of each connected system part must be determined, modeling a dynamic system only with the use of SIMULINK or MATLAB can be challenging. To solve this issue,



MathWorks has developed a plugin software for exporting CAD models that builds dynamic models in the SIMSCAPE MULTIBODY environment from a three-dimensional model created in the SOLIDWORKS CAD system.

Some modeling programs can be difficult to use precisely because of the difficulty of creating and interpreting the structure of the mechanical system to be simulated. SIMSCAPE MULTIBODY, on the other hand, allows for the elimination of this issue through the design of a flowchart that recognizes and connects constraints to the various bodies by importing the 3D model from SOLIDWORKS. The conversion is based on the import function, which takes as its main input the file name of the multibody XML description. The data necessary to reconstruct the original model, or substantially approximate it if the model has unsupported constraints, is transferred to the SIMSCAPE MULTIBODY application via an XML file. The translation of the CAD model consists of two steps: export and import. The CAD assembly model is transformed into a set of STEP or STL part geometry files and a multi-part XML description file during the export process. The part description and geometry files are transformed into the SLX SIMSCAPE MULTIBODY model and the M-data file during the import process [104]. The model gets all the input parameters of the block from the data file.

It is also important to note that the synergy between the CAD environment of SOLIDWORKS and the simulation of SIMSCAPE MULTIBODY allows for analyzing the most complex mechanical systems since one of the most challenging aspects of the modeling process of articulated systems is the creation of the model itself and the connection of the various bodies through constraints and the consequent verification of the couplings. However, this work can be much easier on CAD software because they are optimized for this purpose.

6.2 Description of the Specific Problems Analyzed through Numerical Experiments

The lifting system considered as the case study of this investigation is at the minimum height when the load on it is maximum, namely 1000 (*kg*), up to the maximum height of 1 (*m*) when it is completely unloaded [105]. In the intermediate steps, the height reached by the lifter is a function of the load on the platform. More specifically, four load steps from 0 (*kg*) to 1000 (*kg*) were considered, equally spaced, and corresponding to four height steps from 1000 (*mm*) to 0 (*mm*). The various load steps analyzed through dynamical simulations are shown in Table 7.

Table 7. Platform height variation depending on the load.

LOAD (<i>kg</i>)	PLATFORM HEIGHT (<i>m</i>)
1000	0
750	0.25
500	0.50
250	0.75
0	1.00

For a single change in the load made in one step, and correspondingly in the elevation of the platform, four loading and unloading cases were considered. The results and parameters obtained for all load and elevation conditions described in Table 7 are discussed in detail below, thereby keeping in mind that the conclusions drawn from this analysis are also valid for all the other cases.

The four scenarios considered are the most onerous in terms of actuation forces and applied loads acting on the structure of the adaptive lifting mechanism. These are an impulsive load from 750 (*kg*) to 1000 (*kg*), a progressive load from 750 (*kg*) to 1000 (*kg*), an impulsive unload from 1000 (*kg*) to 750 (*kg*), and a progressive unload from 1000 (*kg*) to 750 (*kg*). The adjective 'impulsive' refers to the fact that the loading or unloading is done instantaneously of an aliquot of 250 (*kg*), while the adjective 'progressive' refers to the law of loading or unloading varying over time as an inclined ramp of 5 (*kg/s*) for a total of 250 kilograms in 50 seconds. Moreover, in the latter case corresponding to a progressive load insertion, the reference used for error calculation is constant. For example, in the case of loading from 750 (*kg*) to 1000 (*kg*), a ramp load law was used, as previously described, but a reference position of zero, corresponding to a zero height of the lift table, is assumed as the constant reference value to be reached.

The strategy that led to the definition of the numerical results for each case is discussed in detail as follows. The preliminary numerical solution of an inverse dynamics problem is necessary to determine a feedforward control action, serving as a guiding controller, that will be subsequently combined with a feedback control action, serving as a compensating controller, evaluated through the solution of a forward dynamics problem. First, the analysis of the laws of motion of the system starting from the evaluation of an inverse dynamics problem is represented by the block diagram shown in Figure 9.

The various heights to be reached were taken as reference and the corresponding displacement that the pinion made on the rack, namely the rack displacement, is measured in the CAD model. Imposing the corresponding displacement to the Prismatic Joint, the force to be applied to keep the desired height is measured in the SIMSCAPE MULTIBODY model. The results obtained from this analysis are then useful for solving the subsequent controlled dynamics problem. The measured rack displacements imposed on the Prismatic Joint as initial conditions are shown in Table 8.

Table 8. Initial condition on the equivalent transmission mechanism for the various load steps.

LOAD (<i>kg</i>)	TRANSMISSION INITIAL CONDITION (<i>mm</i>)
1000	0
750	57.4
500	167.5
250	346.9
0	643.9

As regards the problem of the forward dynamics analysis of the present multibody mechanical system, this process cleverly exploits the results obtained in the previous inverse dynamics analysis. A schematization of the model used for the forward analysis is shown in Figure 10.

The forward dynamics analysis is focused on the implementation of a PD feedback control system, which, by appropriately evaluating the error on the displacement of the Prismatic Joint, and, by tuning the controller, provides an effective controller based on a combination of a Feedforward Force (FF) and a Feedback Force (FB) [13]. By doing so, the control action applied to the multibody system will be:



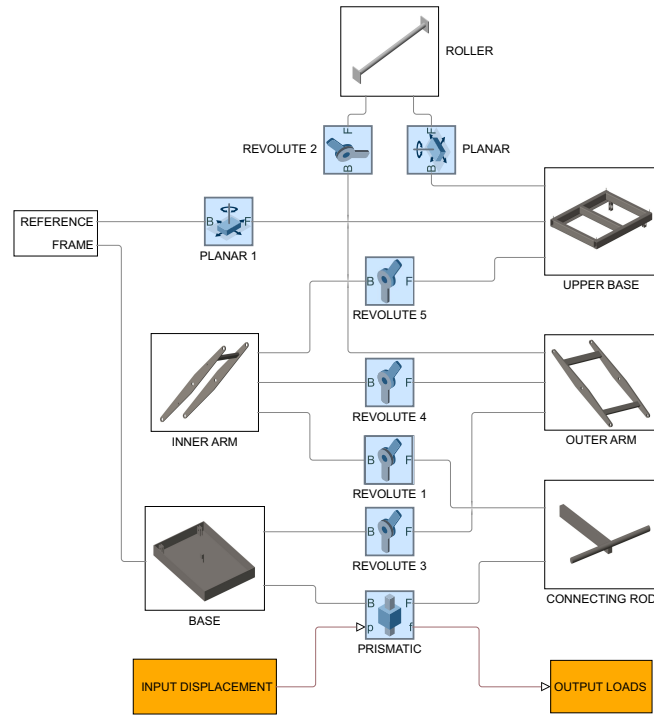


Fig. 9. Schematic of the SIMSCAPE MULTIBODY model assumed as the reference model for the inverse dynamics analysis.

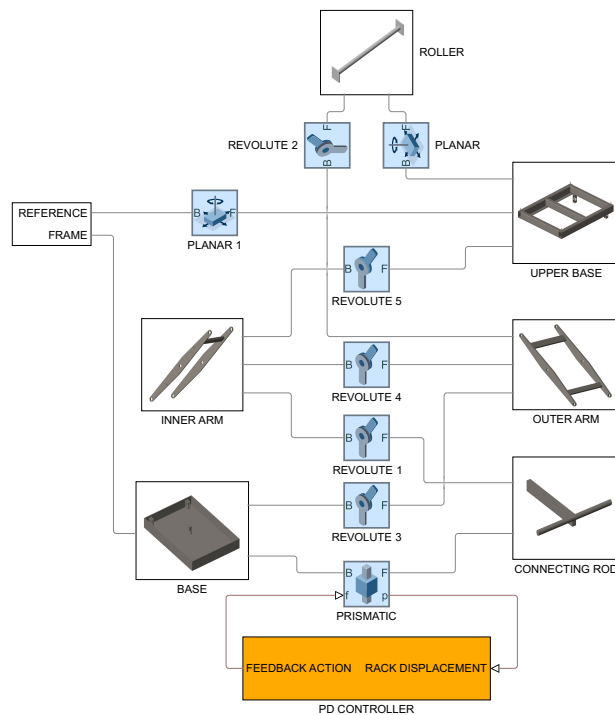


Fig. 10. Schematic of the SIMSCAPE MULTIBODY model assumed as the reference model for the forward dynamics analysis.

-subtracted from the force in FF in the load case, when the lift height decreases. The FF controller implemented, as well as the reference for the error calculation, will be the one corresponding to the height to be reached. Considering that the FF increases as the height of the lifter decreases, the FB force is subtracted, being this control action proportional to the error and its derivative;

+added to the force in FF in the unloading case, when the lift height increases. The FF controller implemented, as well as the reference for calculating the error, will be the one corresponding to the height to be reached. Considering that the FF decreases as the lift height increases, the FB force is added, being this control action proportional to the error and its derivative;

It is, therefore, clear that the height of the lifter, which will be increased or decreased by 0.25 (m) at each step, must depend on the height reached in the previous step since the force in FF and the initial conditions to be applied for a correct implementation vary according to it.



6.3 Results of the Dynamical Simulations

In this section, to assess the practical feasibility of the control actions devised in this work, as well as the structural integrity of the adaptive mechanism, the results obtained for the four case studies in the worst-case scenario are presented, corresponding to steps 750 (*kg*) - 1000 (*kg*) in the loading cases and 1000 (*kg*) - 750 (*kg*) in the unloading cases. In the two loading scenarios, the time history of the total control force acting on the lifter mechanism is the sum of the FF and FB contributions [15]. In the two unloading scenarios, on the other hand, the time history of the total control force acting on the lifter mechanism is the difference between the FF and FB contributions. The numerical results found in MATLAB through thorough numerical experiments concerning all the most relevant operative scenarios based on the SIMSCAPE multibody model developed in this investigation are reported and discussed in detail below.

6.3.1 Impulsive Loading Scenario

In the impulsive loading case, the time history of the lift height is shown in Figure 11, where Figure 11a represents the platform displacement and Figure 11b represents the platform velocity.

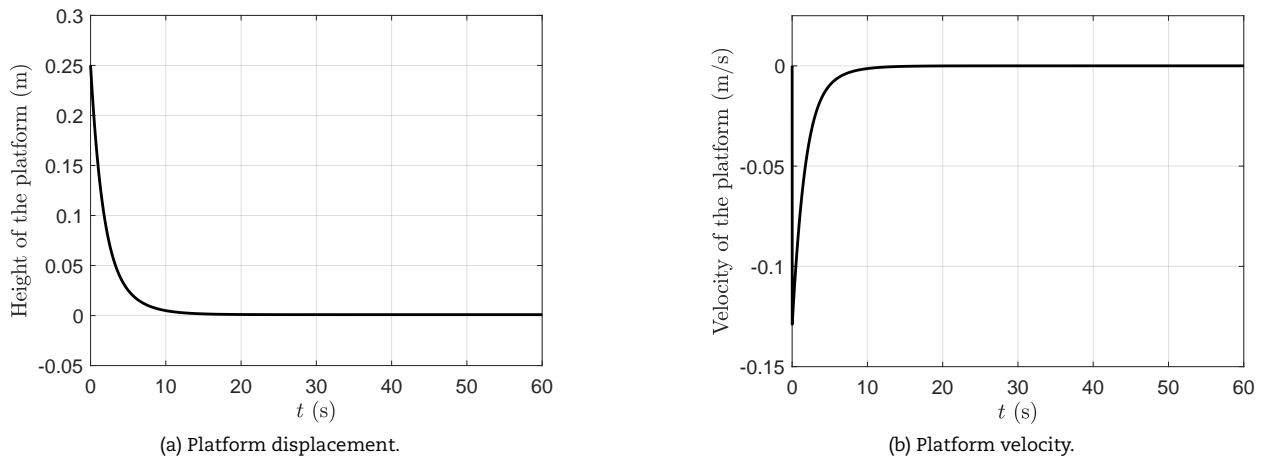


Fig. 11. Time evolution of the lift height displacement and velocity for the impulsive loading case.

As shown in Figure 12 concerning the impulsive loading case, the time history of the control force acting on the lifter mechanism is represented in Figure 12a, while the time history of the error of the height of the lifter with respect to the desired setpoint is represented in Figure 12b.

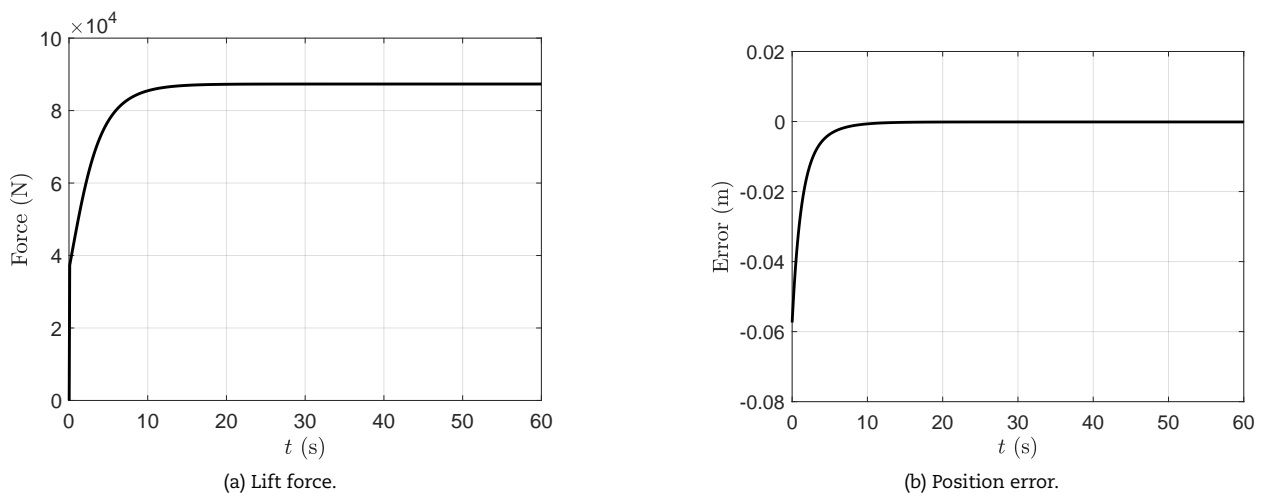


Fig. 12. Time evolution of the lift force and time evolution of the position error for the impulsive loading case.

The numerical results of the dynamical simulations shown in Figures 11 and 12 demonstrate the effectiveness of the proposed control strategy in the case of the impulsive loading scenario.

6.3.2 Progressive Loading Scenario

In the progressive loading case, the time history of the lift height is shown in Figure 13, where Figure 13a represents the platform displacement and Figure 13b represents the platform velocity.



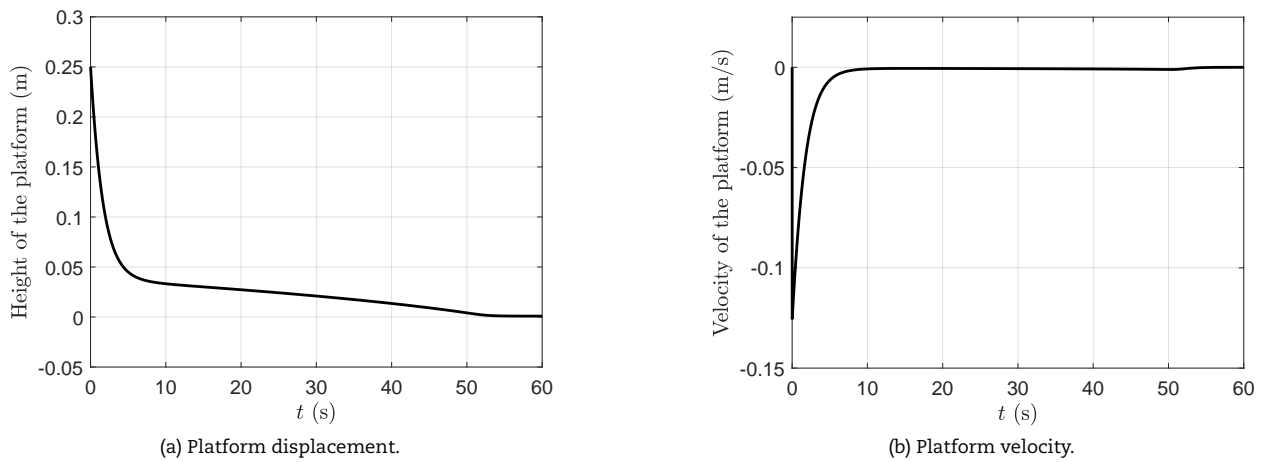


Fig. 13. Time evolution of the lift height displacement and velocity for the progressive loading case.

As shown in Figure 14 concerning the progressive loading case, the time history of the control force acting on the lifter mechanism is represented in Figure 14a, while the time history of the error of the height of the lifter with respect to the desired setpoint is represented in Figure 14b.

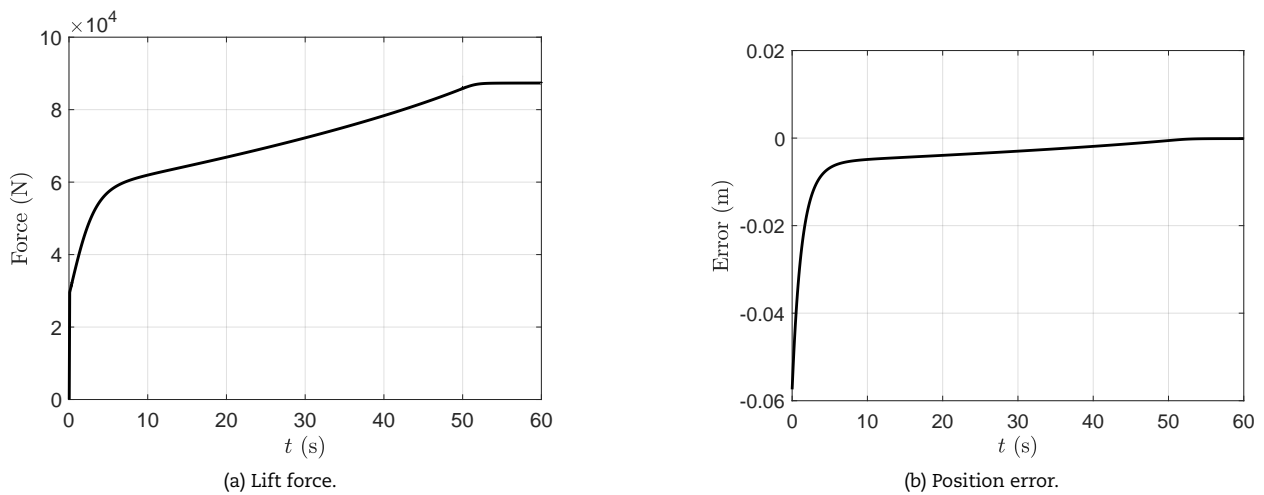


Fig. 14. Time evolution of the lift force and time evolution of the position error for the progressive loading case.

The numerical results of the dynamical simulations shown in Figures 13 and 14 demonstrate the effectiveness of the proposed control strategy in the case of the progressive loading scenario.

6.3.3 Impulsive Unloading Scenario

In the impulsive unloading case, the time history of the lift height is shown in Figure 15, where Figure 15a represents the platform displacement and Figure 15b represents the platform velocity.

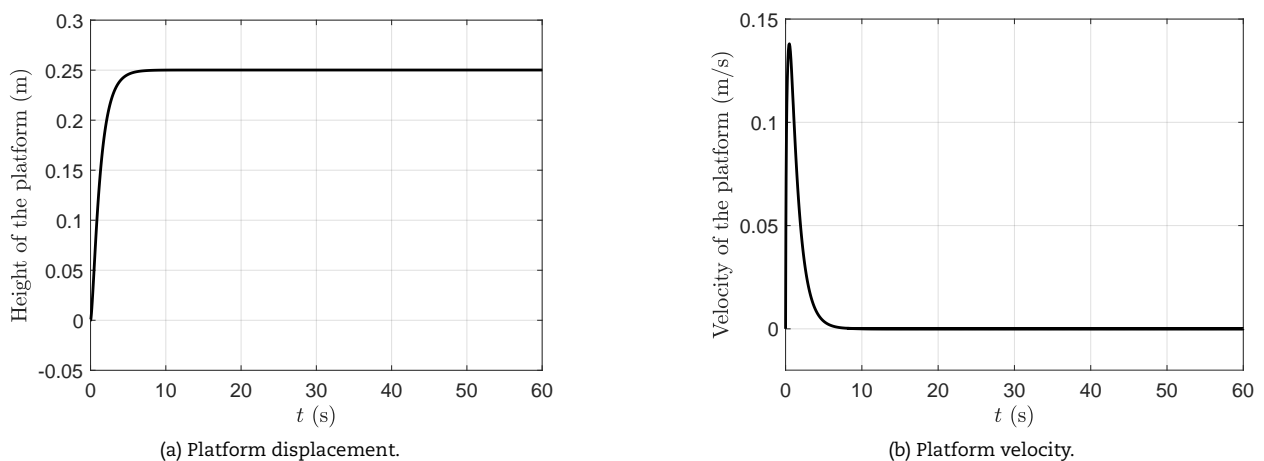


Fig. 15. Time evolution of the lift height displacement and velocity for the impulsive unloading case.



As shown in Figure 16 concerning the impulsive unloading case, the time history of the control force acting on the lifter mechanism is represented in Figure 16a, while the time history of the error of the height of the lifter with respect to the desired setpoint is represented in Figure 16b.

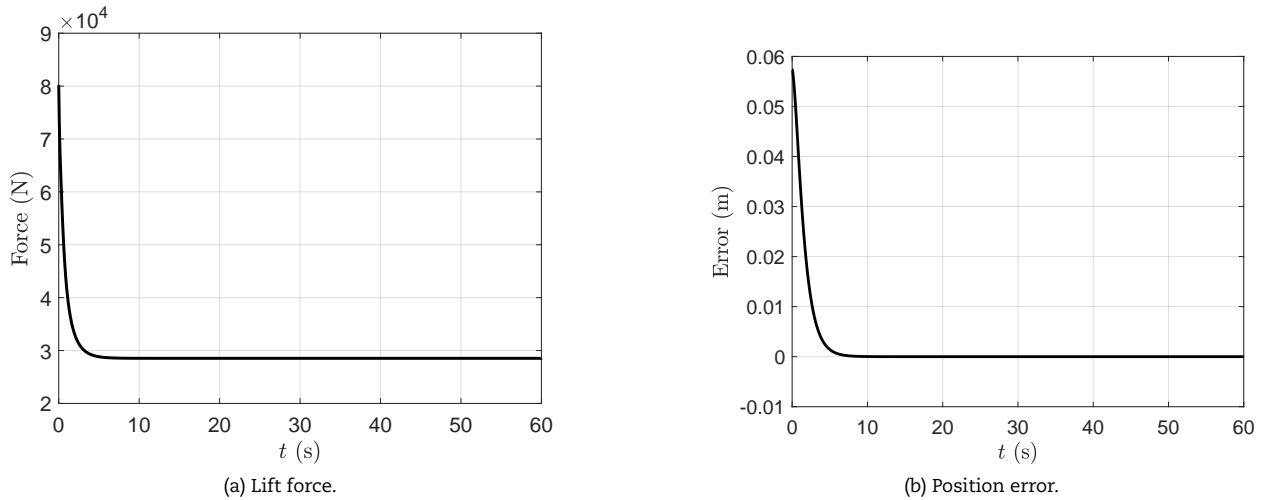


Fig. 16. Time evolution of the lift force and time evolution of the position error for the impulsive unloading case.

The numerical results of the dynamical simulations shown in Figures 15 and 16 demonstrate the effectiveness of the proposed control strategy in the case of the impulsive unloading scenario.

6.3.4 Progressive Unloading Scenario

In the progressive unloading case, the time history of the lift height is shown in Figure 17, where Figure 17a represents the platform displacement and Figure 17b represents the platform velocity.

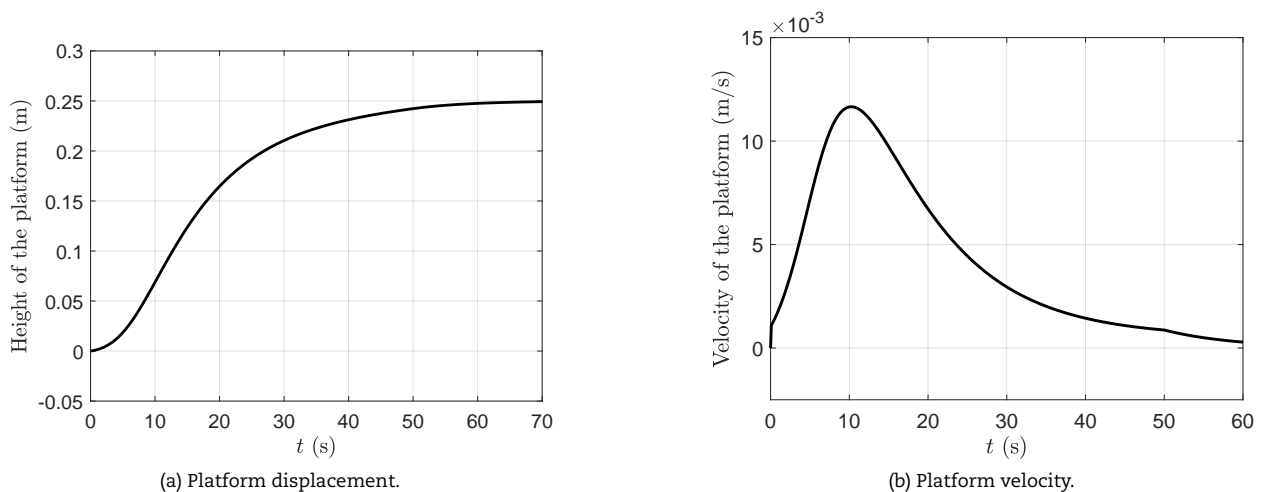


Fig. 17. Time evolution of the lift height displacement and velocity for the progressive unloading case.

As shown in Figure 18 concerning the progressive unloading case, the time history of the control force acting on the lifter mechanism is represented in Figure 18a, while the time history of the error of the height of the lifter with respect to the desired setpoint is represented in Figure 18b.



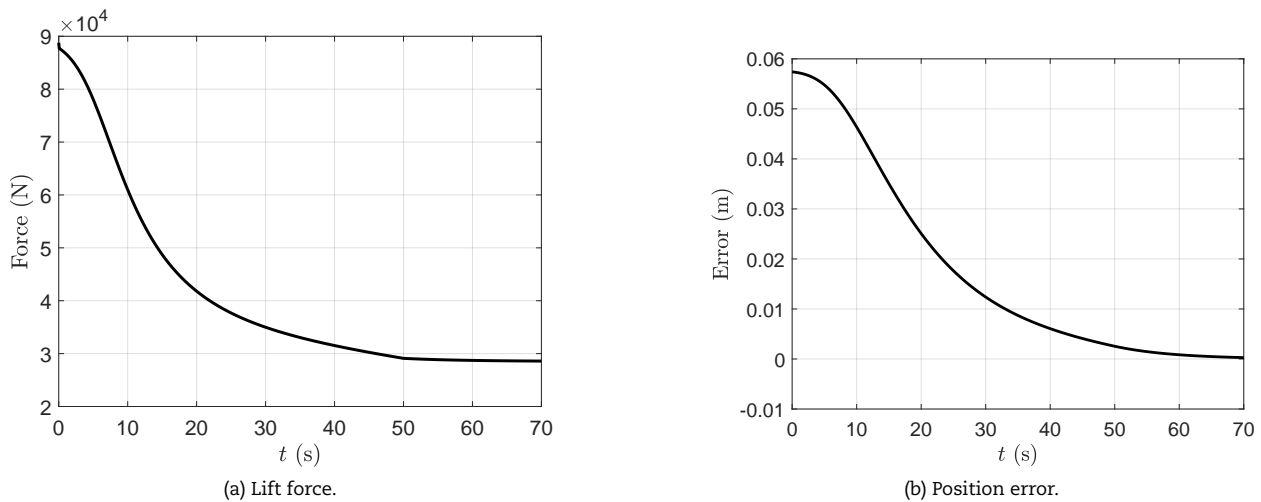


Fig. 18. Time evolution of the lift force and time evolution of the position error for the progressive unloading case.

The numerical results of the dynamical simulations shown in Figures 17 and 18 demonstrate the effectiveness of the proposed control strategy in the case of the progressive unloading scenario.

6.4 Final Remarks

A brief discussion on the quality of the numerical results found through numerical experiments is proposed herein.

To facilitate understanding of the results obtained in all the scenarios analyzed in the paper, the load curves as a function of time are shown in Figure 19 for each case. In Figure 19, the solid line colored black refers to the impulsive loading law, the dashed line colored black refers to the progressive loading law, the solid line colored orange refers to the impulsive unloading law, and the dashed line colored orange refers to the progressive unloading law.

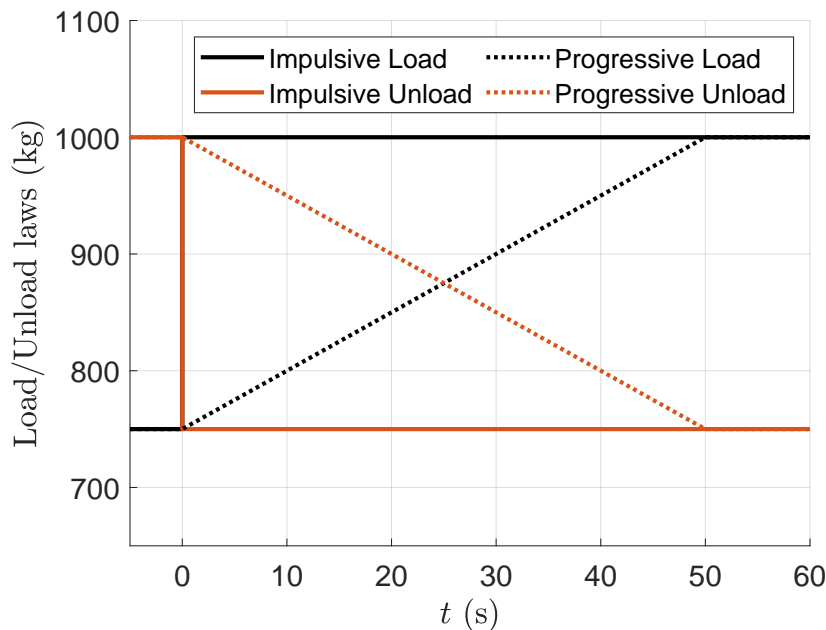


Fig. 19. Time evolution of the lifted load for all the operative scenarios analyzed in the paper.

By comparing Figure 19 with Figures 11, 13, 15, and 17, an analogy can be seen between the load laws and the time evolution of the platform displacement and velocity. Specifically, in all the impulsive cases, the settling time is low and in line with the impulsive loading laws. In all the progressive cases, on the other hand, the settling time is higher due to the progressive loading laws.

Regarding the platform height in the cases of impulsive loading and unloading scenarios, shown respectively in Figure 11 and Figure 15, it can be seen that reaching the desired setpoint value occurs in about 10 seconds in both cases. For safety and ergonomic reasons, this is deemed an appropriate time to travel 0.25 meters. On the other hand, in the cases of progressive loading and unloading scenarios, shown respectively in Figure 13 and Figure 17, the time evolution of the platform height is much slower. However, this is assumed to be in line with a gradually increasing/decreasing loading process. In all cases, the desired height is achieved smoothly and with a zero tangent or, equivalently, with a sufficiently low velocity.

Regarding the total control force, when the load increases, by observing Figure 12a and from Figure 14a, an asymptotic trend is found at the value of FF corresponding to the weight of 1000 (kg) given in Table 10, corresponding to the value of control force suitable for holding the platform at the altitude of 0 meters. When the load decreases, on the other hand, by observing Figure 16a and from Figure 18a, an asymptotic trend is found at the value of FF corresponding to the weight of 750 (kg) given in Table 10, corresponding to the value of control force suitable for holding the platform at the altitude of 0.25 (m).

The error, evaluated on the prismatic joint, as expected, has an opposite trend to the lift height. In all cases, the error achieves



zero value, thereby demonstrating the correct functioning of the control system devised in this investigation. When estimating the power required to satisfy the loading/unloading laws found, referring to the heaviest conditions, i.e., those of impulsive cargo loading, from 750 (*kg*) to 1000 (*kg*), it is advisable to use a motor with a power rating of at least 1.6 (*kW*).

The calibration of the control parameters for the various case studies was done empirically starting from an estimate carried out with a semi-empirical criterion such as Ziegler-Nichols, to indicate the order of magnitude. Then, the parameters were calibrated for the individual case. The final refined sets of control parameters found in this work are shown in Table 9.

Table 9. Feedback control parameters employed for all the loading and unloading scenarios considered in the numerical experiments.

IMPULSIVE UNLOADING (<i>kg</i>)	K_p (<i>kN/m</i>)	K_d (<i>kN × s/m</i>)
1000-750	900	800
750-500	400	500
500-250	400	400
250-0	400	400
IMPULSIVE LOADING (<i>kg</i>)	K_p (<i>kN/m</i>)	K_d (<i>kN × s/m</i>)
0-250	400	400
250-500	400	500
500-750	900	800
750-1000	5500	6200
PROGRESSIVE UNLOADING (<i>kg</i>)	K_p (<i>kN/m</i>)	K_d (<i>kN × s/m</i>)
1000-750	1050	7500
750-500	165	700
500-250	55	400
250-0	45	650
PROGRESSIVE LOADING (<i>kg</i>)	K_p (<i>kN/m</i>)	K_d (<i>kN × s/m</i>)
0-250	400	400
250-500	400	500
500-750	900	800
750-1000	5500	6200

The proportional-derivative control parameters reported in Table 9 were designed and refined through numerical experiments to guarantee a smooth and sufficiently slow set of laws of motion. In particular, a proportional-derivative controller was chosen for the architecture of the control system, thereby omitting the integral term that is generally needed to cancel the asymptotic error. However, in virtue of the presence of a feedforward control action, the feedback control law of this type allowed for the cancellation of the error and the achievement of the desired height of the lifting platform. The results obtained in the inverse dynamic analysis regarding the feedforward action for both loading and unloading cases are summarized in Table 10. In Table 10, the control torque was calculated from the control force, previously obtained through computer simulations, by multiplying the force magnitude by the nominal radius of the rack and pinion mechanical transmission.

Table 10. Feedforward control forces and torques employed for all the loading and unloading scenarios considered in the numerical experiments.

UNLOADING (<i>kg</i>)	DISPLACEMENT (<i>m</i>)	FORCE (<i>N</i>)	TORQUE (<i>N × m</i>)
1000	0	-	-
750	0.25	28530	855.90
500	0.50	12290	368.80
250	0.75	4964	148.90
0	1.00	1264	37.91
LOADING (<i>kg</i>)	DISPLACEMENT (<i>m</i>)	FORCE (<i>N</i>)	TORQUE (<i>N × m</i>)
0	1.00	1264	37.91
250	0.75	4964	148.90
500	0.50	12290	368.80
750	0.25	28530	855.90
1000	0	87760	2633

As far as the practical realization of the control system that guides the motion of the adaptive platform is concerned, a Programmable Logic Controller (PLC), equipped with Input/Output (I/O) functionalities, is needed. Through the input functions, the board receives signals collected from external sensors such as load cells, proximity sensors, encoders, and safety photoelectric sensors. The behavior of the whole adaptive system will vary according to the values of the signals coming from the sensors, which are elaborated by the control logic, as well as considering the operations determined by the program running at that moment and as a result of the interaction with the operator. The output signal is then sent to an inverter that will drive the actuator, such as a DC brushless motor, in the desired behavior to adjust the height of the lifting table. The practical implementation by using, for instance, a PLC or a modern microcontroller for realizing the control laws devised in this investigation will be the object of future research works.



7. Summary, Conclusions, and Future Work

The main goal of this work is to systematically perform the computer-aided design, the multibody dynamic analysis, and the proportional-derivative control synthesis of an adaptive mechanism serving as a lifting table. For this purpose, the paper describes first the methodological approach, the fundamental analytical methods, and the numerical techniques thoroughly used in this research work. Subsequently, the paper reports the process of the virtual model development and the presentation of the results found through numerical experiments obtained in this research study.

In this work, the fundamental steps concerning the development of a virtual prototype of a smart mechanism serving as an adaptive lifting table are illustrated. For this purpose, the computational tools of computer-aided design, analysis, and control are employed in an integrated framework, which revolves around the use of the Multibody System Dynamics (MBD) approach to the analysis of articulated mechanical systems. Due to continuous studies and the high level of development of Computer-Aided Design (CAD) systems, full-scale models and experiments can be reduced to the minimum or, eventually, eliminated. Consequently, the mechanism designer must be aware of the kinematic and dynamic properties of the designed mechanism in order to predict how it will operate in real-world situations. Therefore, the scope of the paper fits in a seamless manner in the unified context of computer-aided design, multibody dynamics, and nonlinear control, which represent the main areas of interest for the research endeavors of the authors.

The main focus of this investigation is to devise a new solution for the redesign of an existing mechanism that is aimed at satisfying the safety and ergonomic needs of human operators in an industrial context. In particular, this paper starts with a study of the disorders and hazards that an operator may contract in the workplace if appropriate ergonomic conditions are not met, especially with regard to lifting and manual handling of goods, all aggravated by the repetitiveness of the operation. As mentioned before, one possible solution for the issue addressed in this study is the development of an adaptive mechanism. The solution in most of the cases found in engineering applications is, indeed, the use of lifting platforms with self-adaptive behavior. In this vein, the goal of automatically adapting the height of the lift table analyzed in this work is to limit the bending, stress, and strain on the trunk of the human operator as much as possible. More specifically, an intelligent control based on a proportional-derivative error logic was conceived in this work, thereby adapting the lift height according to the weight detected on the platform. For example, an increase in weight implies more goods on the platform. Consequently, one needs to adjust the height of the platform to keep the workspace plane at a constant height. Therefore, this is the main idea behind the concept of the adaptive mechanism designed and tested in this investigation.

In this paper, the development of a virtual prototype of an adapting lift table is presented. To this end, a detailed full-size three-dimensional CAD model was developed first by using SOLIDWORKS. The virtual prototype of the mechanical system of interest was designed in such a way as to allow for a one-meter change in elevation. In the construction of the CAD model in a virtual environment, special care was devoted to the assembly/disassembly of the mechanical components that form the adaptive mechanism, as well as to the collocation of the sensors necessary for the proper operation of the machine. Subsequently, a multibody model composed of only rigid bodies was developed considering the CAD model of the lifting platform. To achieve this goal, adopting first some necessary simplifications for the sake of easier computer implementation, a multibody mechanical model having the same geometric characteristics as the original CAD model was imported into the SIMSCAPE MULTIBODY software based on the MATLAB environment. By doing so, several dynamical simulations were performed on the simplified multibody model, which allowed for a convenient determination of the control parameters necessary to guide the self-adaptive lifting mechanism in the different scenarios considered in this investigation. The dynamic behavior of the controlled lift platform in all the cases considered in this work was extensively illustrated in the paper, and the corresponding laws of motion for the principal mechanical components were shown. Therefore, the numerical results presented in the manuscript demonstrate the effectiveness of the control system synthesized in this study.

The research work carried out in this investigation fits into all engineering fields where the task of frequently lifting heavy goods is common. In summary, this study presents an interesting solution to the hazards to which human operators are subjected in industrial workplaces. However, in the next research works, several interesting tracks for future investigations could be followed. Although limited by the number of cases, as well as by the constraints in height and weight that were taken into consideration, the systematic analysis and design methodology utilized in this paper is totally applicable to other different case studies. In this direction, the main insights for the continuation and deepening of the work already done are projected, thereby considering a constant lift height other than 1 (m), a load greater or less than 1000 (kg), and the volume/density of the goods different from that considered in the paper. In this respect, it is important to note that considering the three variables mentioned above, only two are independent of each other. Additionally, taking into account alternative load laws that differ from those considered in this work is also of utmost importance for the implementation of the proposed design to other engineering applications found in the industrial field. For instance, by evaluating the weight measured by the load cells serving as force sensors, special algorithms could also be devised to automatically determine the proper loading/unloading time laws that the human operator could potentially adopt, and, in comparison with those already implemented in the controller, perform the one that best fits the detected weight. These issues will be addressed in future investigations. Future research work will be also focused on the Integration of Computer-Aided Design and Analysis (I-CAD-A) for the development of nonlinear control systems suitable for articulated mechanical systems.

Author Contributions

This research paper was principally devised and developed by the first author (Carmine Maria Pappalardo). Great support in the development of the paper was provided by the second and third authors (Timoteo Magaldi and Lorenzo Masucci). The detailed review carried out by the fourth and fifth authors (Rosario La Regina and Alessandro Naddeo) considerably improved the quality of the work. The manuscript was written with the contribution of all authors. All authors discussed the results, reviewed the methodology, and approved the final version of the manuscript.

Acknowledgments

Not applicable.

Conflict of Interest

The authors declared no potential conflicts of interest with respect to the research, authorship, and publication of this article.



Funding

The authors received no financial support for the research, authorship, and publication of this article.

Data Availability Statements

The datasets generated and/or analyzed during the current study are available from the corresponding author on reasonable request.

References

- [1] Gu, S., Chen, J., Tian, Q., An implicit asynchronous variational integrator for flexible multibody dynamics, *Computer Methods in Applied Mechanics and Engineering*, 2022, 401, 115660.
- [2] Wang, K., Tian, Q., A nonsmooth method for spatial frictional contact dynamics of flexible multibody systems with large deformation, *International Journal for Numerical Methods in Engineering*, 2023, 124(3), 752–779.
- [3] Shabana, A.A., Integration of computer-aided design and analysis: application to multibody vehicle systems, *International Journal of Vehicle Performance*, 2019, 5(3), 300–327.
- [4] Bettiga, J., Boschetti, G., Frade, B.R., González, F., Piva, G., Richiedei, D., Trevisani, A., Numerical and experimental investigation on the synthesis of extended kalman filters for cable-driven parallel robots modeled through daes, *Multibody System Dynamics*, 2023, 1–30.
- [5] Cammarata, A., Lacagnina, M., Sinatra, R., Closed-form solutions for the inverse kinematics of the agile eye with constraint errors on the revolute joint axes, 2016 IEEE/RSJ International Conference on Intelligent Robots and Systems (IROS), IEEE, 317–322.
- [6] Villecco, F., Pellegrino, A., Entropic measure of epistemic uncertainties in multibody system models by axiomatic design, *Entropy*, 2017, 19(7), 291.
- [7] Liguori, A., Formato, A., Cattani, P., Villecco, F., Sizing the actuators for a dragon fly prototype, *Journal of Applied and Computational Mechanics*, 2023.
- [8] Pappalardo, C.M., Guida, D., Dynamic analysis and control design of kinematically-driven multibody mechanical systems., *Engineering Letters*, 2020, 28(4).
- [9] De Simone, M.C., Veneziano, S., Guida, D., Design of a non-back-drivable screw jack mechanism for the hitch lifting arms of electric-powered tractors, *Actuators*, vol. 11, Multidisciplinary Digital Publishing Institute, 358.
- [10] Cammarata, A., Sinatra, R., Maddio, P., A two-step algorithm for the dynamic reduction of flexible mechanisms, *Mechanism Design for Robotics: Proceedings of the 4th IFToMM Symposium on Mechanism Design for Robotics*, Springer, 25–32.
- [11] Huang, Z., Xi, F., Huang, T., Dai, J.S., Sinatra, R., Lower-mobility parallel robots: theory and applications, 2010.
- [12] Pappalardo, C.M., Lok, S.I., Malgaca, L., Guida, D., Experimental modal analysis of a single-link flexible robotic manipulator with curved geometry using applied system identification methods, *Mechanical Systems and Signal Processing*, 2023, 200, 110629.
- [13] Borase, R.P., Maghade, D., Sondkar, S., Pawar, S., A review of pid control, tuning methods and applications, *International Journal of Dynamics and Control*, 2021, 9(2), 818–827.
- [14] Villecco, F., Pellegrino, A., Evaluation of uncertainties in the design process of complex mechanical systems, *Entropy*, 2017, 19(9), 475.
- [15] Johnson, M.A., Moradi, M.H., PID control, Springer, 2005.
- [16] De Simone, M.C., Rivera, Z., Guida, D., Finite element analysis on squeal-noise in railway applications, *FME Transactions*, 2018, 46(1), 93–100.
- [17] Borisov, A., Bosov, A., Miller, G., Optimal stabilization of linear stochastic system with statistically uncertain piecewise constant drift, *Mathematics*, 2022, 10(2), 184.
- [18] Quatrano, A., De, S., Rivera, Z., Guida, D., Development and implementation of a control system for a retrofitted cnc machine by using arduino, *FME Transactions*, 2017, 45(4), 565–571.
- [19] Lee, C., Liu, X., Liu, Y., Zhang, L., Optimal control of a time-varying double-ended production queueing model, *Stochastic Systems*, 2021, 11(2), 140–173.
- [20] Ditzler, G., Roveri, M., Alippi, C., Polikar, R., Learning in nonstationary environments: A survey, *IEEE Computational Intelligence Magazine*, 2015, 10(4), 12–25.
- [21] Citarella, R., Armentani, E., Caputo, F., Naddeo, A., Fem and bem analysis of a human mandible with added temporomandibular joints, *The Open Mechanical Engineering Journal*, 2012, 6(1).
- [22] Cappetti, N., Naddeo, A., Naddeo, F., Solitro, G., Finite elements/taguchi method based procedure for the identification of the geometrical parameters significantly affecting the biomechanical behavior of a lumbar disc, *Computer methods in biomechanics and biomedical engineering*, 2016, 19(12), 1278–1285.
- [23] Tasora, A., Mangoni, D., Fusai, D., Multibody simulation of contacts between arbitrary meshes of cad quality: recent results, open problems and possible developments.
- [24] Benatti, S., Tasora, A., Mangoni, D., Training a four legged robot via deep reinforcement learning and multibody simulation, *Multibody Dynamics 2019: Proceedings of the 9th ECCOMAS Thematic Conference on Multibody Dynamics*, Springer, 391–398.
- [25] Huston, R., *Multibody dynamics—modeling and analysis methods*, 1991.
- [26] Orzechowski, G., Fraczek, J., Integration of the equations of motion of multibody systems using absolute nodal coordinate formulation, *acta mechanica et automatica*, 2012, 6(2), 75–83.
- [27] Patel, M., Orzechowski, G., Tian, Q., Shabana, A.A., A new multibody system approach for tire modeling using ancf finite elements, *Proceedings of the Institution of Mechanical Engineers, Part K: Journal of Multi-body Dynamics*, 2016, 230(1), 69–84.
- [28] Barbagallo, R., Sequenzia, G., Oliveri, S., Cammarata, A., Dynamics of a high-performance motorcycle by an advanced multibody/control co-simulation, *Proceedings of the Institution of Mechanical Engineers, Part K: Journal of Multi-body Dynamics*, 2016, 230(2), 207–221.
- [29] Tanev, T., Cammarata, A., Marano, D., Sinatra, R., Elastostatic model of a new hybrid minimally-invasive-surgery robot, *The 14th IFToMM World Congress, Taipei, Taiwan*.
- [30] Muscat, M., Cammarata, A., Maddio, P.D., Sinatra, R., Design and development of a towfish to monitor marine pollution, *Euro-Mediterranean Journal for Environmental Integration*, 2018, 3(1), 1–12.
- [31] Cammarata, A., Sinatra, R., Maddio, P.D., Static condensation method for the reduced dynamic modeling of mechanisms and structures, *Archive of Applied Mechanics*, 2019, 89, 2033–2051.
- [32] Flores, P., Ambrósio, J., Claro, J.P., Lankarani, H.M., *Kinematics and dynamics of multibody systems with imperfect joints: models and case studies*, vol. 34, Springer Science & Business Media, 2008.
- [33] Jain, A., *Robot and multibody dynamics: analysis and algorithms*, Springer Science & Business Media, 2010.
- [34] Shi, M., Rong, B., Liang, J., Zhao, W., Pan, H., Dynamics analysis and vibration suppression of a spatial rigid-flexible link manipulator based on transfer matrix method of multibody system, *Nonlinear Dynamics*, 2023, 111(2), 1139–1159.
- [35] Li, Y., Yang, Y., Li, M., Liu, Y., Huang, Y., Dynamics analysis and wear prediction of rigid-flexible coupling deployable solar array system with clearance joints considering solid lubrication, *Mechanical Systems and Signal Processing*, 2022, 162, 108059.
- [36] De Simone, M.C., Guida, D., Control design for an under-actuated uav model, *FME Transactions*, 2018, 46(4), 443–452.
- [37] Ziegler, J.G., Nichols, N.B., et al., Optimum settings for automatic controllers, *trans. ASME*, 1942, 64(11).
- [38] Senatore, A., Pisaturo, M., Sharifzadeh, M., Real time identification of automotive dry clutch frictional characteristics using trust region methods, *Proceedings of the 23rd Conference of the Italian Association of Theoretical and Applied Mechanics, Salerno, Italy*, 4–7.
- [39] Sharifzadeh, M., Farnam, A., Senatore, A., Timpone, F., Akbari, A., Delay-dependent criteria for robust dynamic stability control of articulated vehicles, *International Conference on Robotics in Alpe-Adria Danube Region*, Springer, 424–432.
- [40] Palomba, I., Richiedei, D., Trevisani, A., Kinematic state estimation for rigid-link multibody systems by means of nonlinear constraint equations, *Multibody System Dynamics*, 2017, 40(1), 1–22.
- [41] Palomba, I., Richiedei, D., Trevisani, A., Two-stage approach to state and force estimation in rigid-link multibody systems, *Multibody System Dynamics*, 2017, 39(1), 115–134.





- [42] Strano, S., Terzo, M., Accurate state estimation for a hydraulic actuator via a sdre nonlinear filter, *Mechanical Systems and Signal Processing*, 2016, 75, 576–588.
- [43] Strano, S., Terzo, M., A sdre-based tracking control for a hydraulic actuation system, *Mechanical Systems and Signal Processing*, 2015, 60, 715–726.
- [44] Strano, S., Terzo, M., Actuator dynamics compensation for real-time hybrid simulation: an adaptive approach by means of a nonlinear estimator, *Nonlinear Dynamics*, 2016, 85(4), 2353–2368.
- [45] Russo, R., Strano, S., Terzo, M., Enhancement of vehicle dynamics via an innovative magnetorheological fluid limited slip differential, *Mechanical Systems and Signal Processing*, 2016, 70, 1193–1208.
- [46] Fister, D., Fister Jr, I., Fister, I., Safaric, R., Parameter tuning of pid controller with reactive nature-inspired algorithms, *Robotics and Autonomous Systems*, 2016, 84, 64–75.
- [47] Zhai, R., Xiao, P., Zhang, R., Ju, J., In-wheel motor control system used by four-wheel drive electric vehicle based on whale optimization algorithm-proportional-integral-derivative control, *Advances in Mechanical Engineering*, 2022, 14(6), 16878132221104574.
- [48] Pappalardo, C.M., Guida, D., Control of nonlinear vibrations using the adjoint method, *Meccanica*, 2017, 52, 2503–2526.
- [49] Pappalardo, C.M., Guida, D., Adjoint-based optimization procedure for active vibration control of nonlinear mechanical systems, *Journal of Dynamic Systems, Measurement, and Control*, 2017, 139(8).
- [50] Momin, G.G., Hatti, R., Dalvi, K., Bargi, F., Devare, R., Design, manufacturing & analysis of hydraulic scissor lift, *International Journal of Engineering Research and General Science*, 2015, 3(2), 733–740.
- [51] Ismael, O.Y., Almaged, M., Mahmood, A., et al., Quantitative design analysis of an electric scissor lift, *American Academic Scientific Research Journal for Engineering, Technology, and Sciences*, 2019, 59(1), 128–141.
- [52] Hongyu, T., Ziyi, Z., Design and simulation based on pro/e for a hydraulic lift platform in scissors type, *Procedia Engineering*, 2011, 16, 772–781.
- [53] Akgün, Y., Gantes, C.J., Sobek, W., Korkmaz, K., Kalochairitis, K., A novel adaptive spatial scissor-hinge structural mechanism for convertible roofs, *Engineering Structures*, 2011, 33(4), 1365–1376.
- [54] Liu, T., Sun, J., Simulative calculation and optimal design of scissor lifting mechanism, 2009 Chinese Control and Decision Conference, IEEE, 2009–2082.
- [55] Olenin, G., Design of hydraulic scissors lifting platform, 2016.
- [56] Li, B., Wang, S.M., Yuan, R., Xue, X.Z., Zhi, C.J., Dynamic characteristics of planar linear array deployable structure based on scissor-like element with joint clearance using a new mixed contact force model, *Proceedings of the Institution of Mechanical Engineers, Part C: Journal of Mechanical Engineering Science*, 2016, 230(18), 3161–3174.
- [57] Spengler, D.M., Bigos, S.J., Martin, N.A., Zeh, J., Fisher, L., Nachemson, A., Back injuries in industry: A retrospective study: I. overview and cost analysis, *Spine*, 1986, 11(3), 241–245.
- [58] Marras, W.S., Lavender, S.A., Leurgans, S.E., Rajulu, S.L., Allread, S.W.G., Fathallah, F.A., Ferguson, S.A., The role of dynamic three-dimensional trunk motion in occupationally-related, *Spine*, 1993, 18(5), 617–628.
- [59] Chaffin, D.B., Manual materials handling and the biomechanical basis for prevention of low-back pain in industry—an overview, *American Industrial Hygiene Association Journal*, 1987, 48(12), 989–996.
- [60] Naddeo, A., Cappetti, N., Califano, R., Vallone, M., Manual assembly workstation redesign based on a new quantitative method for postural comfort evaluation, *Applied Mechanics and Mechanical Engineering IV*, vol. 459 of *Applied Mechanics and Materials*, Trans Tech Publications Ltd, 368–379.
- [61] Naddeo, A., Califano, R., Vallone, M., Cicalese, A., Coccaro, C., Marcone, F., Shullazi, E., The effect of spine discomfort on the overall postural (dis)comfort, *Applied Ergonomics*, 2019, 74, 194 – 205.
- [62] Naddeo, A., Apicella, M., Galluzzi, D., Comfort-driven design of car interiors: A method to trace iso-comfort surfaces for positioning the dashboard commands, *SAE Technical Papers*, 2015, 2015-April(April).
- [63] Shrivastava, N., Pande, A., Lele, J., Kampassi, K., Embedded control system for self adjusting scissor lift, 2018 Fourth International Conference on Computing Communication Control and Automation (ICCCUBEA), IEEE, 1–5.
- [64] Trapanese, S., Naddeo, A., Cappetti, N., A preventive evaluation of perceived postural comfort in car-cockpit design: Differences between the postural approach and the accurate muscular simulation under different load conditions in the case of steering-wheel usage, *SAE Technical Papers*, 2016, 2016-April(April).
- [65] Naddeo, A., Califano, R., Vink, P., The effect of posture, pressure and load distribution on (dis)comfort perceived by students seated on school chairs, *International Journal on Interactive Design and Manufacturing*, 2018, 12(4), 1179 – 1188.
- [66] Mohan, S., Zech, W.C., Characteristics of worker accidents on nysdot construction projects, *Journal of Safety Research*, 2005, 36(4), 353–360.
- [67] Ramsey, T., Davis, K.G., Kotowski, S.E., Anderson, V.P., Waters, T., Reduction of spinal loads through adjustable interventions at the origin and destination of palletizing tasks, *Human factors*, 2014, 56(7), 1222–1234.
- [68] Udwadia, F.E., Kalaba, R.E., *Analytical dynamics*, 1996.
- [69] Juang, J.N., Phan, M.Q., *Identification and control of mechanical systems*, Cambridge University Press, 2001.
- [70] Rani, D., Agarwal, N., Tirth, V., Design and fabrication of hydraulic scissor lift, *MIT International Journal of Mechanical Engineering*, 2015, 5(2), 81–87.
- [71] Stuart-Buttle, C., A case study of factors influencing the effectiveness of scissor lifts for box palletizing, *American Industrial Hygiene Association Journal*, 1995, 56(11), 1127–1132.
- [72] Pope, M.H., Goh, K.L., Magnusson, M.L., et al., Spine ergonomics, *Annual review of biomedical engineering*, 2002, 4(1), 49–68.
- [73] Pappalardo, C.M., Del Giudice, M., Oliva, E.B., Stieven, L., Naddeo, A., Computer-aided design, multibody dynamic modeling, and motion control analysis of a quadcopter system for delivery applications, *Machines*, 2023, 11(4), 464.
- [74] Cammarata, A., Pappalardo, C.M., On the use of component mode synthesis methods for the model reduction of flexible multibody systems within the floating frame of reference formulation, *Mechanical Systems and Signal Processing*, 2020, 142, 106745.
- [75] Ulin, S.S., Armstrong, T.J., Radwin, R.G., Use of computer aided drafting for analysis and control of posture in manual work, *Applied Ergonomics*, 1990, 21(2), 143–151.
- [76] Flores, P., *Concepts and formulations for spatial multibody dynamics*, Springer, 2015.
- [77] Pappalardo, C.M., Vece, A., Galdi, D., Guida, D., Developing a reciprocating mechanism for the emergency implementation of a mechanical pulmonary ventilator using an integrated cad-mbd procedure, *FME Transactions*, 2022, 50(2), 238–247.
- [78] De Simone, M.C., Rivera, Z., Guida, D., A new semi-active suspension system for racing vehicles, *FME Transactions*, 2017, 45(4), 578–584.
- [79] De Simone, M.C., Guida, D., Identification and control of a unmanned ground vehicle by using arduino, *UPB Sci. Bull. Ser. D*, 2018, 80, 141–154.
- [80] Visioli, A., *Practical PID control*, Springer Science & Business Media, 2006.
- [81] Pappalardo, C.M., A natural absolute coordinate formulation for the kinematic and dynamic analysis of rigid multibody systems, *Nonlinear Dynamics*, 2015, 81, 1841–1869.
- [82] Nikravesh, P.E., *Planar multibody dynamics: formulation, programming with MATLAB®, and applications*, CRC press, 2018.
- [83] De Jalon, J.G., Bayo, E., *Kinematic and dynamic simulation of multibody systems: the real-time challenge*, Springer Science & Business Media, 2012.
- [84] Pappalardo, C.M., La Regina, R., Guida, D., Multibody modeling and nonlinear control of a pantograph scissor lift mechanism, *Journal of Applied and Computational Mechanics*, 2023, 9(1), 129–167.
- [85] Yu, X., Zwölfer, A., Mikkola, A., An efficient, floating-frame-of-reference-based recursive formulation to model planar flexible multibody applications, *Journal of Sound and Vibration*, 2023, 547, 117542.
- [86] Gaull, A., A rigorous proof for the equivalence of the projective newton-euler equations and the lagrange equations of second kind for spatial rigid multibody systems, *Multibody System Dynamics*, 2019, 45(1), 87–103.
- [87] Lynch, K.M., Park, F.C., *Modern robotics*, Cambridge University Press, 2017.
- [88] Wehage, K.T., Wehage, R.A., Ravani, B., Generalized coordinate partitioning for complex mechanisms based on kinematic substructuring, *Mechanism and Machine Theory*, 2015, 92, 464–483.
- [89] Bauchau, O.A., Laulusa, A., Review of contemporary approaches for constraint enforcement in multibody systems, *Journal of Computational and Nonlinear Dynamics*, 2008, 3(1).
- [90] Eich-Soellner, E., Führer, C., *Numerical methods in multibody dynamics*, vol. 45, Springer, 1998.





- [91] Shabana, A.A., Dynamics of multibody systems, Cambridge university press, 2020.
- [92] Haug, E.J., Multibody dynamics on differentiable manifolds, Journal of Computational and Nonlinear Dynamics, 2021, 16(4), 041003.
- [93] Laulusa, A., Bauchau, O.A., Review of classical approaches for constraint enforcement in multibody systems, 2008.
- [94] Shabana, A.A., Computational dynamics, John Wiley & Sons, 2009.
- [95] Zhao, X.M., Chen, Y.H., Zhao, H., Dong, F.F., Udwadia–kalaba equation for constrained mechanical systems: formulation and applications, Chinese journal of mechanical engineering, 2018, 31(1), 1–14.
- [96] Enferadi, J., Jafari, K., A kane's based algorithm for closed-form dynamic analysis of a new design of a 3rss-s spherical parallel manipulator, Multibody System Dynamics, 2020, 49, 377–394.
- [97] Flannery, M.R., D'alembert–lagrange analytical dynamics for nonholonomic systems, Journal of Mathematical physics, 2011, 52(3).
- [98] Mariti, L., Belfiore, N.P., Pennestri, E., Valentini, P.P., Comparison of solution strategies for multibody dynamics equations, International Journal for Numerical Methods in Engineering, 2011, 88(7), 637–656.
- [99] Cheli, F., Diana, G., Advanced dynamics of mechanical systems, vol. 2020, Springer, 2015.
- [100] King, M., Process control: a practical approach, John Wiley & Sons, 2016.
- [101] Almageed, M., Khather, S.I., Abdulla, A.I., Design of a discrete pid controller based on identification data for a simscape buck boost converter model, International Journal of Power Electronics and Drive Systems, 2019, 10(4), 1797.
- [102] Patel, V.V., Ziegler-nichols tuning method: Understanding the pid controller, Resonance, 2020, 25(10), 1385–1397.
- [103] Åström, K.J., Hägglund, T., Revisiting the ziegler–nichols step response method for pid control, Journal of process control, 2004, 14(6), 635–650.
- [104] Mishchenko, E., Mishchenko, V., Exploring the cad model of the manipulator using cad translation and simscape multibody, E3S Web of Conferences, vol. 279, EDP Sciences, 03014.
- [105] Alexandrov, A.G., Palenov, M.V., Adaptive pid controllers: State of the art and development prospects, Automation and remote control, 2014, 75(2), 188–199.


ORCID iD

Carmine Maria Pappalardo  <https://orcid.org/0000-0003-3763-7104>

Timoteo Magaldi  <https://orcid.org/0009-0002-1955-2158>

Lorenzo Masucci  <https://orcid.org/0009-0007-7116-6103>

Rosario La Regina  <https://orcid.org/0000-0003-4934-5678>

Alessandro Naddeo  <https://orcid.org/0000-0001-7728-4046>



© 2024 Shahid Chamran University of Ahvaz, Ahvaz, Iran. This article is an open access article distributed under the terms and conditions of the Creative Commons Attribution-NonCommercial 4.0 International (CC BY-NC 4.0 license) (<http://creativecommons.org/licenses/by-nc/4.0/>)

How to cite this article: Carmine Maria Pappalardo, Timoteo Magaldi, Lorenzo Masucci, Rosario La Regina, Alessandro Naddeo. Virtual Prototyping, Multibody Dynamics, and Control Design of an Adaptive Lift Table for Material Handling, J. Appl. Comput. Mech., xx(x), 2024, 1-35. <https://doi.org/10.22055/jacm.2024.45269.4342>

Publisher's Note Shahid Chamran University of Ahvaz remains neutral with regard to jurisdictional claims in published maps and institutional affiliations.

